JULY 1972

MDC G2968

SIMULATION OF A FLEXIBLE SPINNING VEHICLE

Final Report

CR-123789

MCDONNELL DOUGLAS ASTRONAUTICS COMPANY

MCDONNELL DOUGLAS CORPORATION

MCDONNELL DOUGLAS

SIMULATION OF A FLEXIBLE SPINNING VEHICLE

Final Report

JULY 1972

MDC G2968

PREPARED BY

W. A. BEAUDRY
GUIDANCE AND ADVANCE
FLIGHT MECHANICS DEPARTMENT

MCDONNELL DOUGLAS ASTRONAUTICS COMPANY-WEST

5301 Bolsa Avenue, Huntington Beach, CA 92647

C

FOREWORD

This report was prepared by McDonnell Douglas Astronautics Company (MDAC), under National Aeronautics and Space Administration Contract No. NAS8-26700. It covers work conducted from 3 May 1971 to 2 July 1972.

CONTENTS

FIGURES

Section 1
INTRODUCTION

This report presents the results of an experimental investigation of the controlled and uncontrolled dynamical behavior of a rotating or artificial-gravity space station including flexible-body effects. A dynamically scaled model was supported by a spherical air bearing which provided a nearly moment-free environment. Reaction jet systems were provided for spin-up and spin-down and for damping of wobble motion. Two single-gimbal gyros were arranged as a control-moment gyro wobble damping system. Remotely controllable movable masses were provided to simulate mass-shift disturbances such as arise from crew motions. An active mass-balance wobble damping system which acted to minimize the wobble motions induced by crew motions was also installed. Flexible-body effects were provided by a pair of inertia augmentation booms. Inertia augmentation booms are contemplated for use on rotating space stations to cause the spin axis moment of inertia to be the largest of the three moments of inertia as is necessary to assure gyroscopic stability. Test runs were made with each of the control systems with the booms locked (rigid body) and unlocked (flexible body).

Section 2
DESCRIPTION OF SIMULATION SYSTEM

Figure 2-1 shows the general arrangement of the flexible spinning vehicle simulation model. Disk-shaped weights mounted on threaded rods visible at the right end of the model (a similar set is at the left end) provide means for adjustment of the static and dynamic (principal axis alignment) balance. The pedestal of the air bearing support is visible beneath the model. The model is floated on a film of air beneath a 0.254m (10 in.) diameter beryllium sphere. One of the two inertia augmentation booms may be seen protruding from an opening in the front side of the model. Figure 2-2 shows the booms vibrating. The gas supply (nitrogen) for the reaction jet system (RCS) is stored in two gas bottles symmetrically located on the centerline of the model and ball to preserve the static balance as gas is used. To the right of the boom arm on the front of the model are the pressure gages and pressure regulator of the RCS. The jets are visible on brackets at the right end of the model, a similar set (not visible) is located at the left end.

The square box on top of the model near the left end provides mounting for the two control moment gyros (CMG's) of the CMG wobble damping system. The assembly of electronic circuit cards of the control system is in the box on the top of the model toward the right end. To the right of this are mounted the solenoid valves of the RCS .

The disturbance mass system is composed of two masses on vertical guide rods located at diagonally opposite corners of the model. The two masses are connected by a cable which is wrapped around and fastened to the pulley of a dc servomotor. On command from a potentiometer on the control panel, the servomotor will rotate to the commanded angle causing the two masses to move equally and in opposite directions generating a product of inertia disturbance. The active mass balance wobble damper system is also

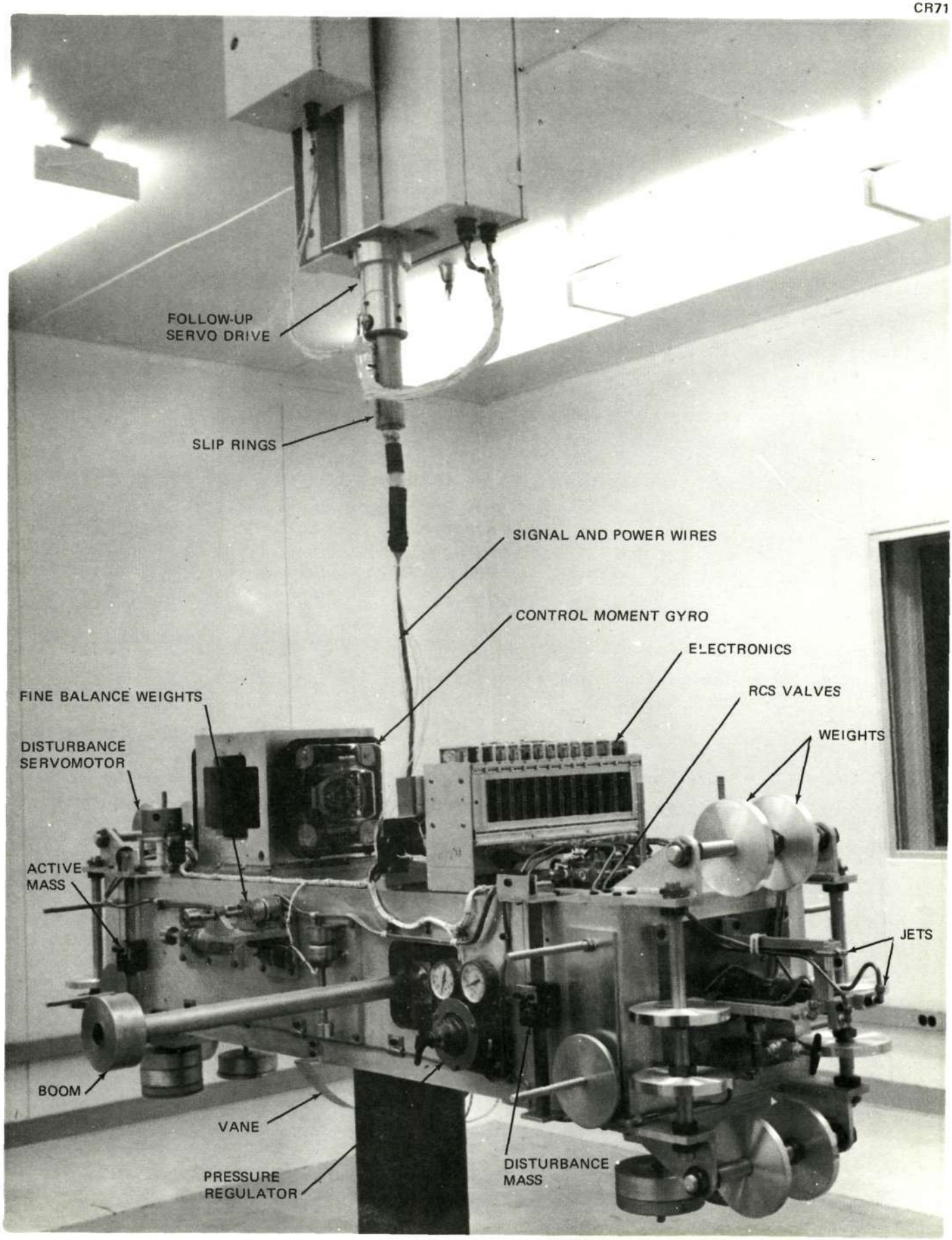

Figure 2-1. Flexible Vehicle Simulator Model

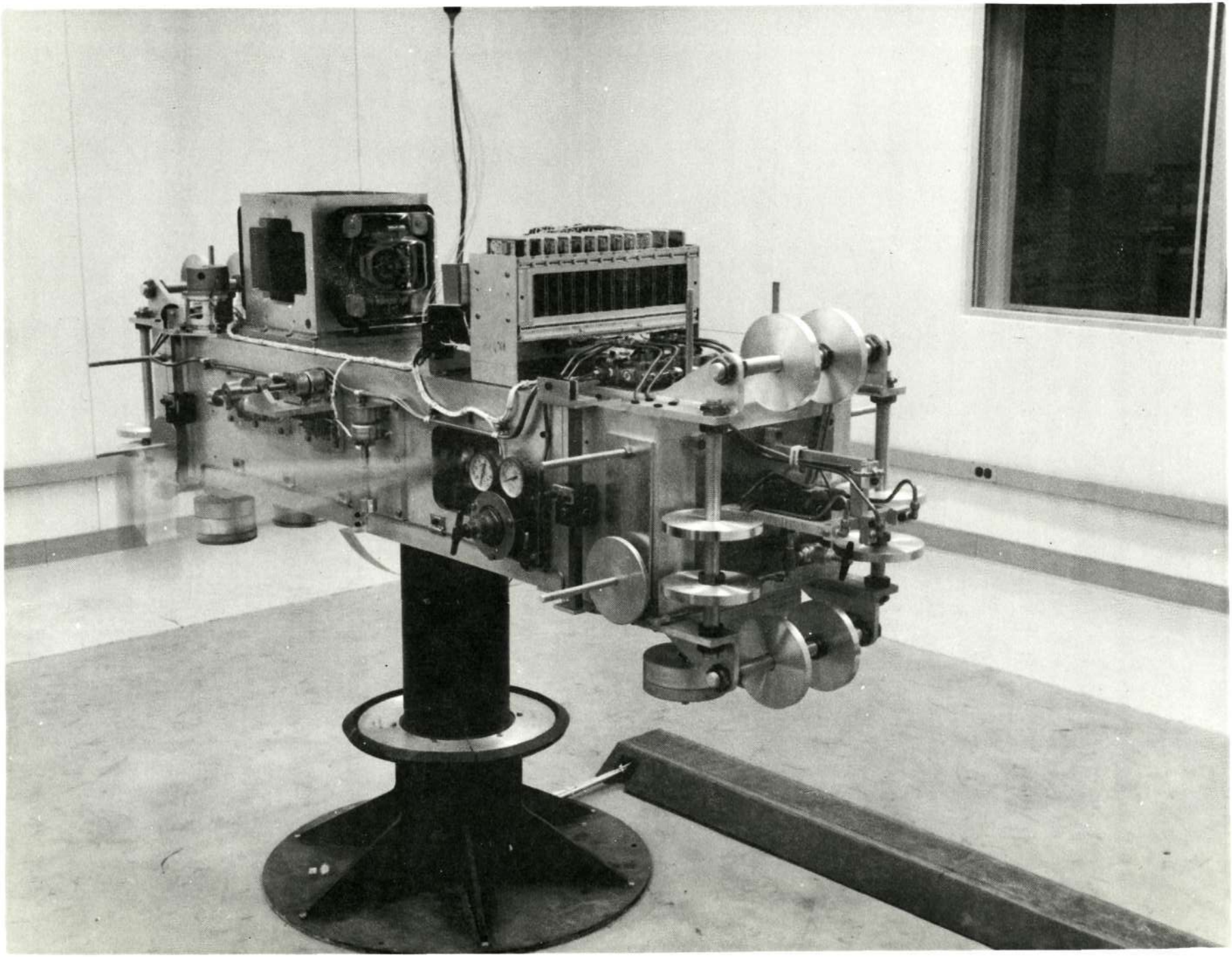

Figure 2-2. Boom Mechanism

composed of two vertically guided masses connected by a cable and moved by a servomotor. The active mass balance system position is commanded to be proportional to the sensed angular velocity about the long (Y) axis of the model and thus acts to minimize the product of inertia disturbance. To the right of the pressure regulator in Figure 2-1 is a vertical square guide for one of the two disturbance masses. A similar guide rod and mass may be seen near the left end of the model and is one of the two masses of the active mass balance system. Figure 2-3 is a close-up view of one of the two active mass balance wobble damper weights and its guide rod. The weights have ball bushings to minimize friction. Above the rod is the servo-drive assembly of the disturbance mass system. A similar drive system, not visible but directly behind on the opposite side of the model, drives the active mass balance system.

Figure 2-4 is a close-up of the body axis angular velocity sensor assembly, composed of three orthogonally mounted rate gyros and located on the rear side of the model.

Figure 2-5 is an overall view of the inertia augmentation boom assembly prior to mounting in the model. The positions of the tip masses can be changed to provide different moments of inertia. Figure 2-6 is a close-up of the mechanism. The band at the top constrains the booms to vibrate in the antisymmetric mode. The springs at the bottom can be adjusted to obtain various boom vibration frequencies. A potentiometer on one pivot provides a readout of the boom angle.

The signal and power-wire follow-up servo is shown in Figure 2-1. Immediately below the junction box attached to the ceiling of the insulated room in which the model is located is the follow-up servomotor which drives the attached slip ring assembly in synchronism with the spin of the table. The follow-up servosystem functions in a rate command mode with the rate command updated once per revolution based on a comparison of the time difference with which two light beams are broken. The upper light beam is in the servomotor housing and is broken once per revolution by a vane attached to

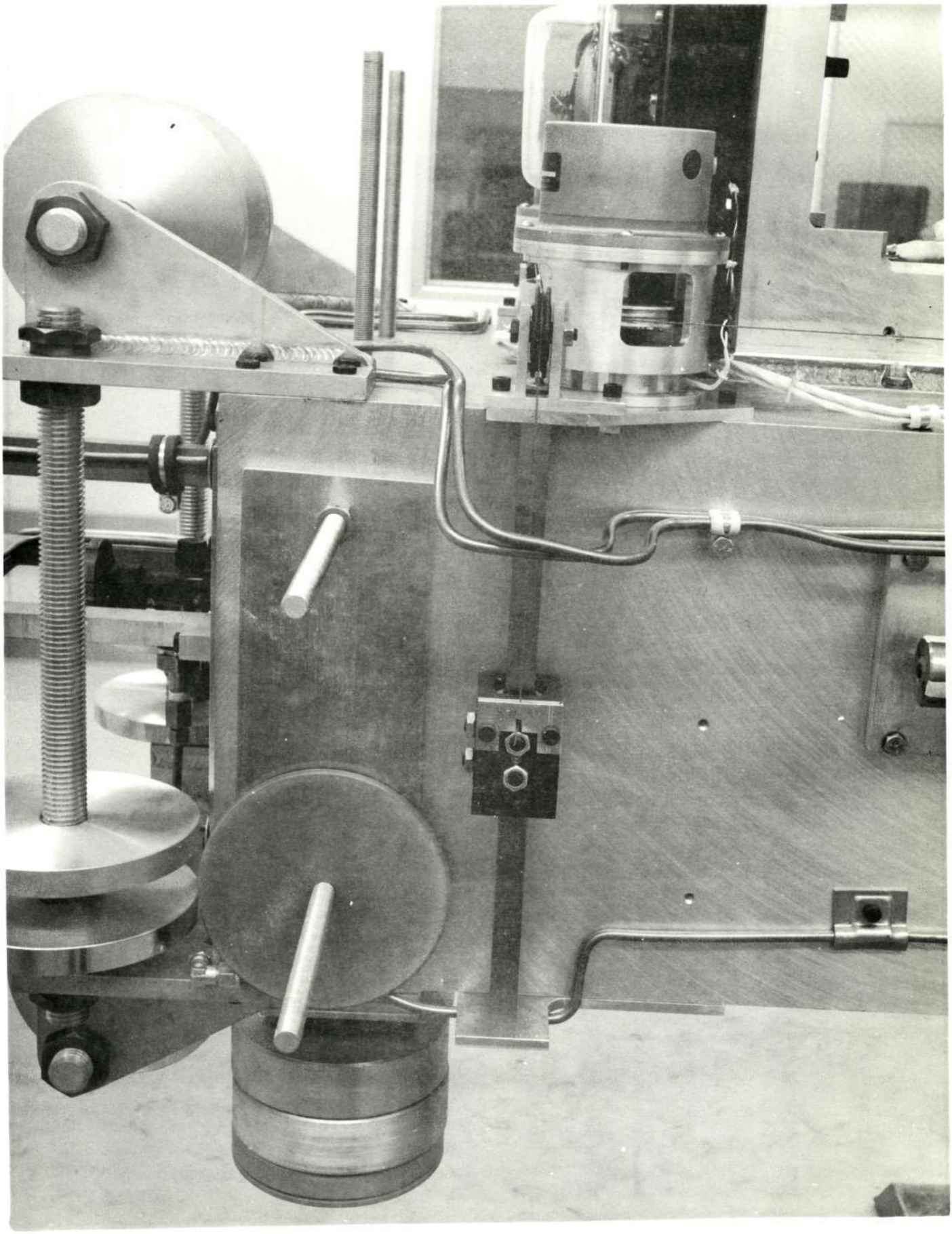

Figure 2-3. Close-up of Mass Balance Wobble Damper Weight

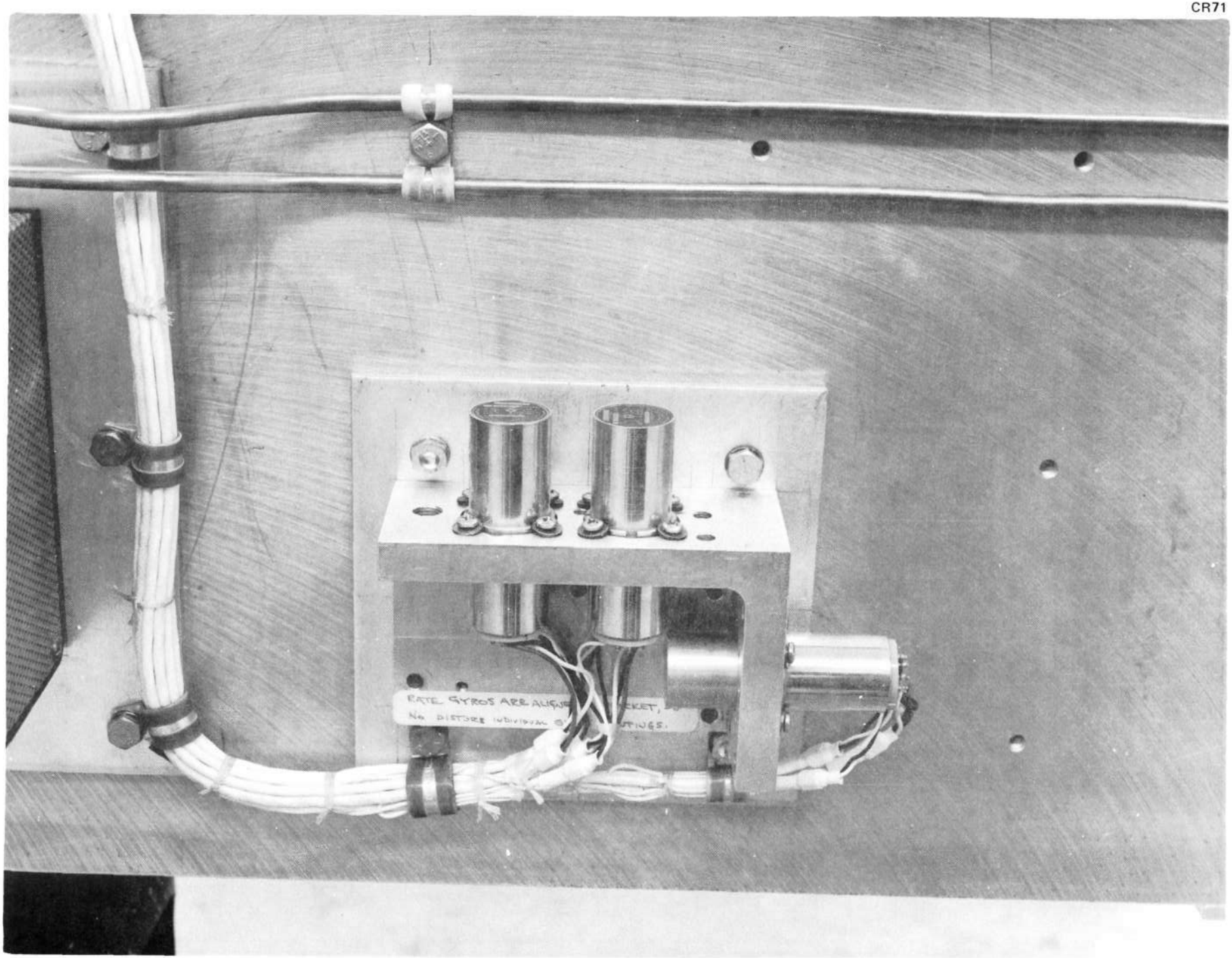

Figure 2-4. Close-up of Body Axis Angular Velocity Sensor Assembly

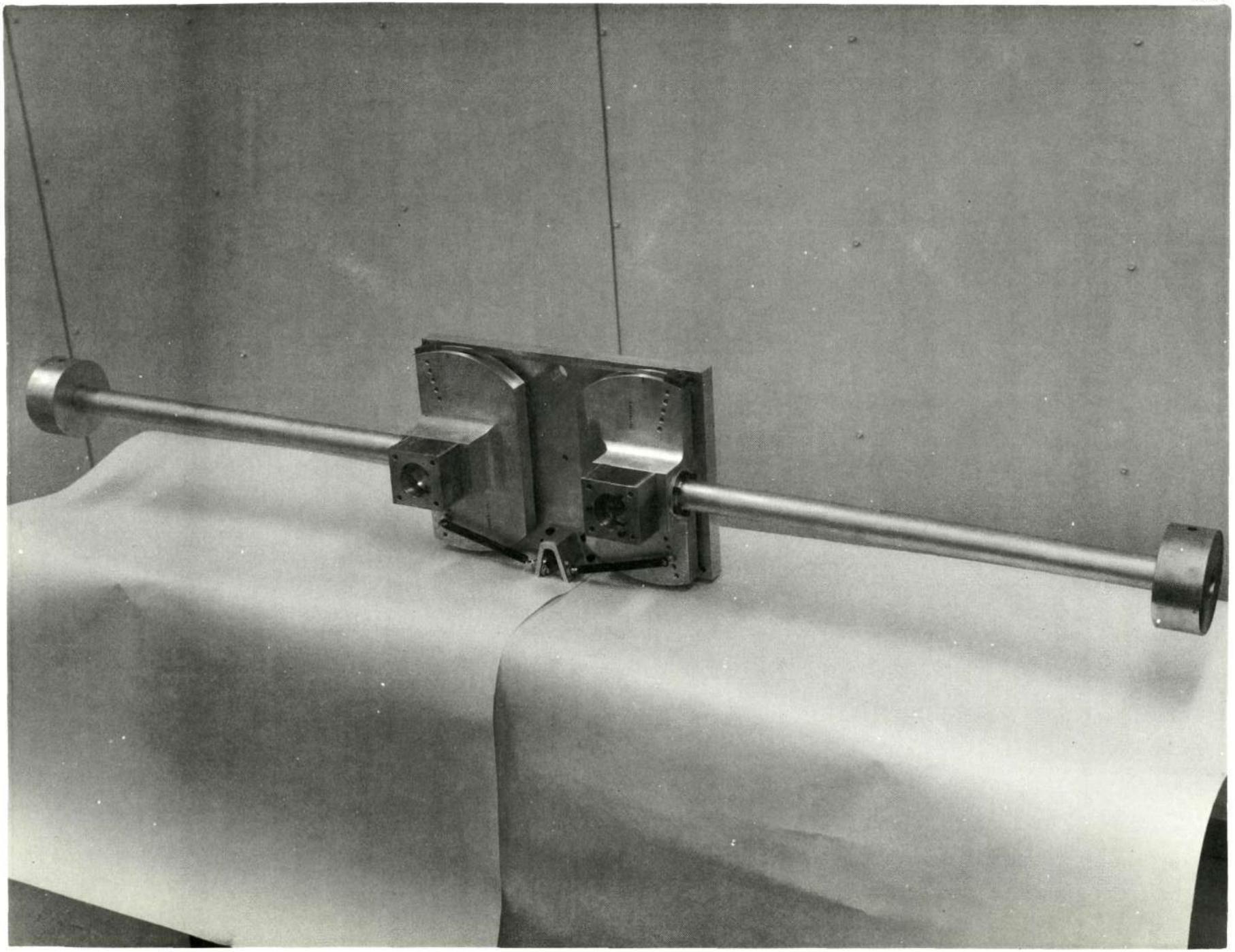

Figure 2-5. Inertia Augmentation Boom Assembly

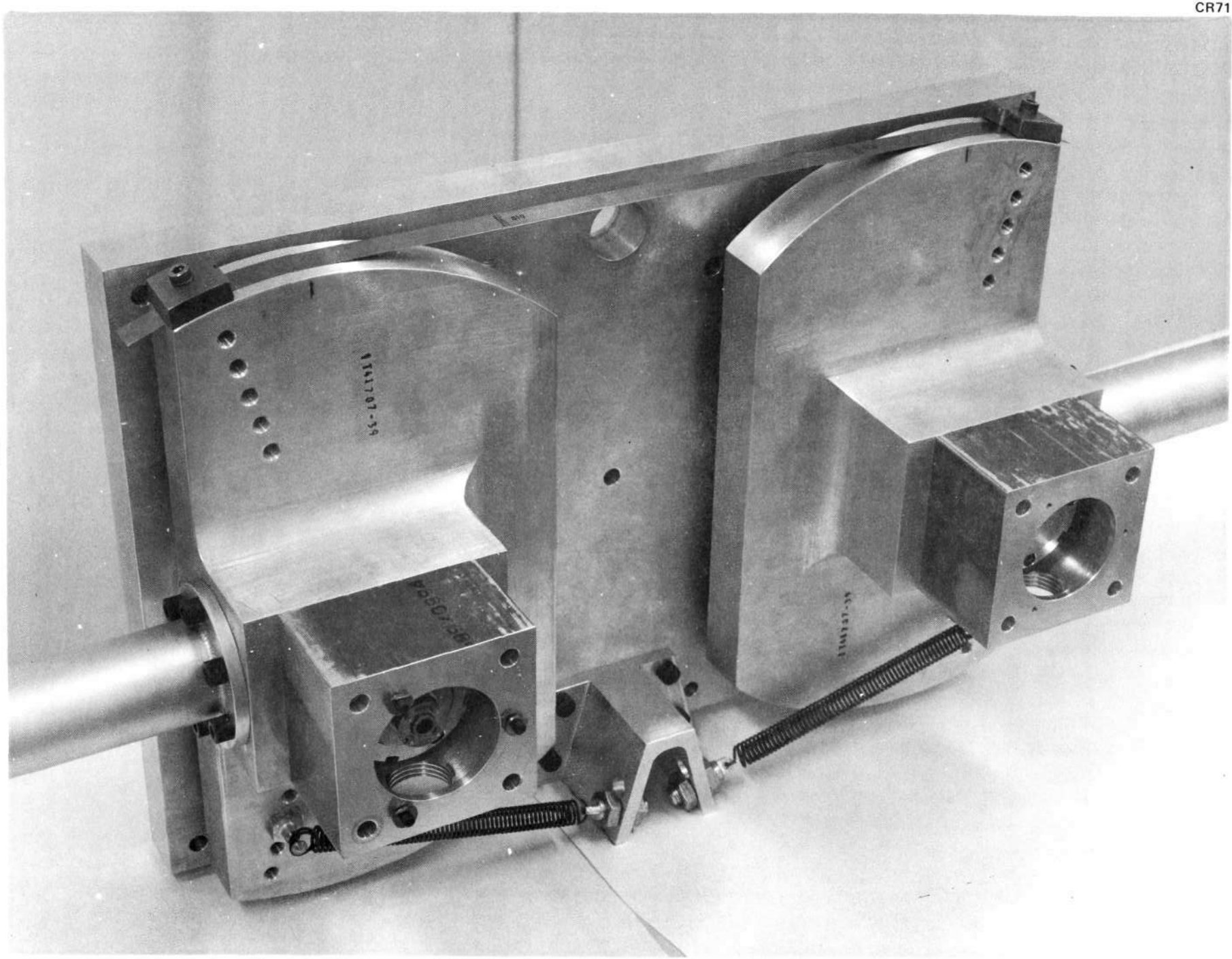

Fi[2-6. [up o[tia A[ntati[oom [bly [

the motor-shaft, and is sensed by a silicon photosensor. The other light beam is interrupted once per revolution by a vane attached to the bottom of the table.

Figure 2-7 shows the coordinate system used throughout this report. The model body axes, X, Y, and Z, are related to inertial axes, X_I, Y_I, and Z_I, by the Euler angles, β_1, β_2, and β_3. Equation (2-1) gives the transformation from body axis rates, ω_X, ω_Y, and ω_Z, to Euler angle rates, $\dot{\beta}_1$, $\dot{\beta}_2$, and $\dot{\beta}_3$. The rate signals from the body axis rate sensor assembly are fed to an analog computer which performs the transformation to Euler angle rates and subsequent integration to yield the Euler angles:

EULER ANGLE TRANSFORMATION

$$\begin{bmatrix} \dot{\beta}_1 \\ \dot{\beta}_2 \\ \dot{\beta}_3 \end{bmatrix} = \begin{bmatrix} \frac{C\beta_3}{C\beta_2} & -\frac{S\beta_3}{C\beta_2} & 0 \\ S\beta_3 & C\beta_3 & 0 \\ -\frac{C\beta_3\, S\beta_2}{C\beta_2} & \frac{S\beta_2\, C\beta_3}{C\beta_2} & 1 \end{bmatrix} \begin{bmatrix} \omega_X \\ \omega_Y \\ \omega_Z \end{bmatrix} \qquad (2\text{-}1)$$

CR71

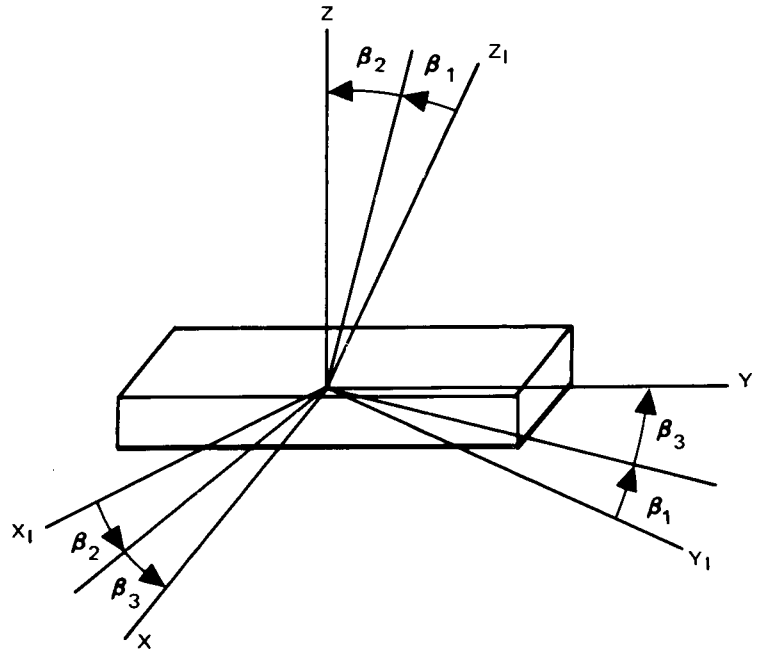

Figure 2-7. Model Coordinate System

2.1 FLEXIBLE BOOMS

The equations of motion of the spinning vehicle with flexible booms are derived in Appendix A (Equations A-39, A-41 and A-42). It is also shown in the appendix that the hinged booms have the same dynamical behavior (natural frequency and variation of frequency with spin angular velocity) as tip masses supported by cantilever beam structural members. The equations can be diagrammed as shown in Figure 2-8. At the frequency range of interest, the nutation frequency squared is approximately $\gamma^2 \cong 0.01$ rad^2/sec^2, much less than the spinning boom natural squared $\omega_S^2 \cong 2.8$ rad^2/sec^2; therefore, Figure 2-8 can be approximated by Figure 2-9 which in turn can be manipulated into Figure 2-10. The spinning vehicle with flexible booms can therefore be approximated by a spinning rigid vehicle with I_Z and I_Y replaced by I'_Z and I'_Y wherein the boom inertia contribution is reduced by a factor depending on boom flexibility and spin speed. Based on the approximation of Figure 2-10, the nutation frequency of the flexible vehicle is given by

$$\gamma = \left[\frac{(I'_Z - I_X)(I_Z - I_Y)}{I_X I'_Y}\right]^{1/2} \Omega \qquad (2\text{-}2)$$

Figure 2-10 is convenient for investigating the controlled characteristics of the system.

It will be noted in Figure 2-1 that the centerline of the booms is displaced from the center of the air bearing ball along the Y axis a distance R_Y which differs from the assumptions of Appendix A. It may be shown that the model still behaves according to the equations of motion of Appendix A provided that $2mR_Y^2$ is added to I_X and I_Z, the moments of inertia of the rigid center body. This has been done in the reported results.

CR71

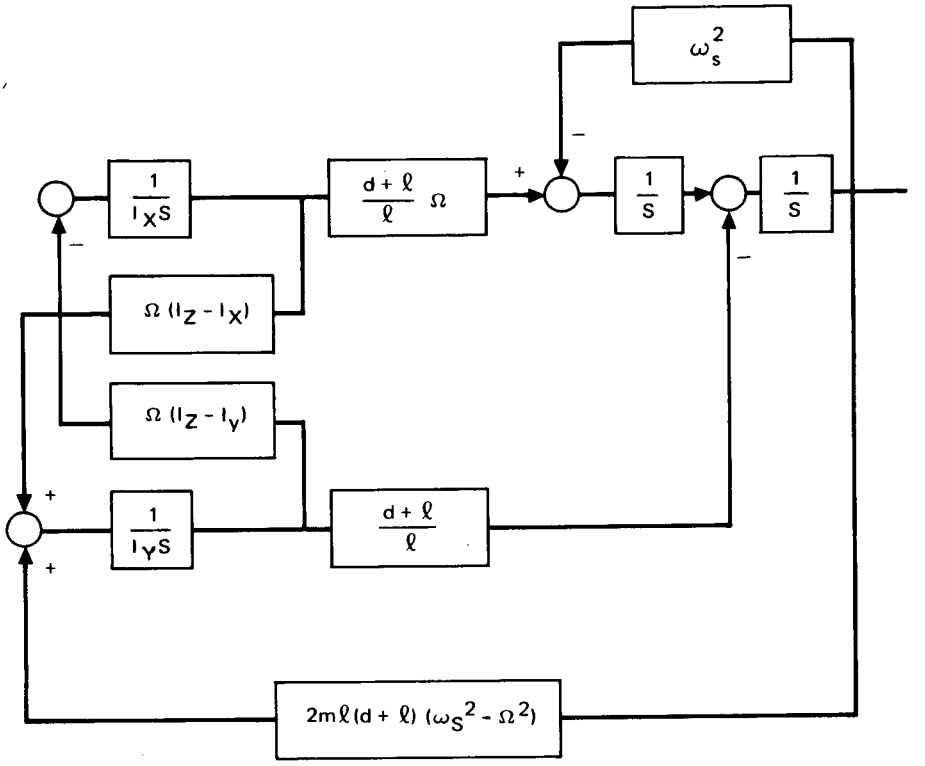

Figure 2-8. Flexible Boom Equation Diagram

CR71

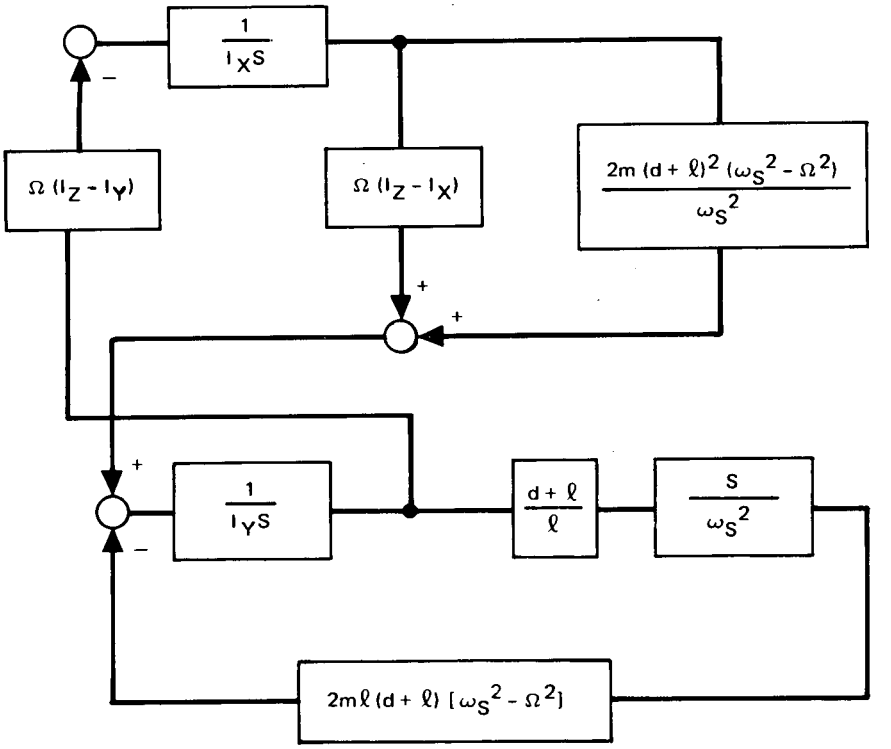

Figure 2-9. Approximate Equation Diagram for Flexible Boom

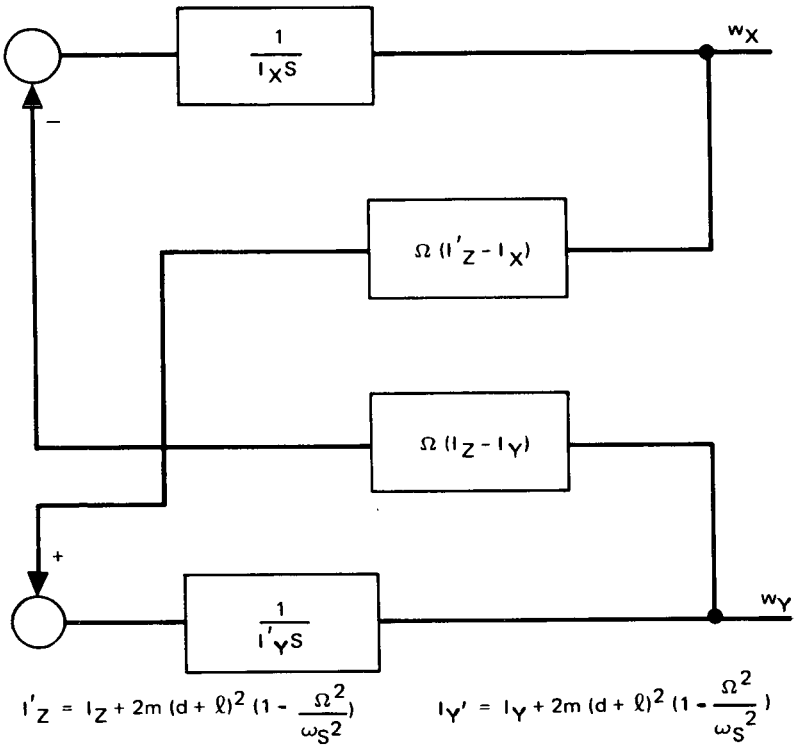

Figure 2-10. Manipulation of Flexible Boom Equations

2.2 CMG WOBBLE DAMPING

The CMG wobble damper on the simulation model is composed of two single-gimbal CMG (SGCMG) which have their gimbal axes parallel with the table spin axis (Figure 2-11). The gimbals are driven so that the gimbal angle of one CMG is the negative of the gimbal angle of the other CMG.

The torques acting on the transverse axes due to the CMG's are

$$T_X = H_1 \dot{\alpha}_1 S\alpha_1 - \omega_Z H_1 S\alpha_1 + H_2 \dot{\alpha}_2 S\alpha_2 + \omega_Z H_2 S\alpha_2 \qquad (2\text{-}3)$$

$$T_Y = H_1 \dot{\alpha}_1 C\alpha_1 + \omega_Z H_1 C\alpha_1 - H_2 \dot{\alpha}_2 C\alpha_2 - \omega_Z H_2 C\alpha_2 \qquad (2\text{-}4)$$

$$T_Z = \omega_X H_1 S\alpha_1 - \omega_Y H_1 C\alpha_1 - \omega_X H_2 S\alpha_2 + \omega_Y H_2 C\alpha_2 \qquad (2\text{-}5)$$

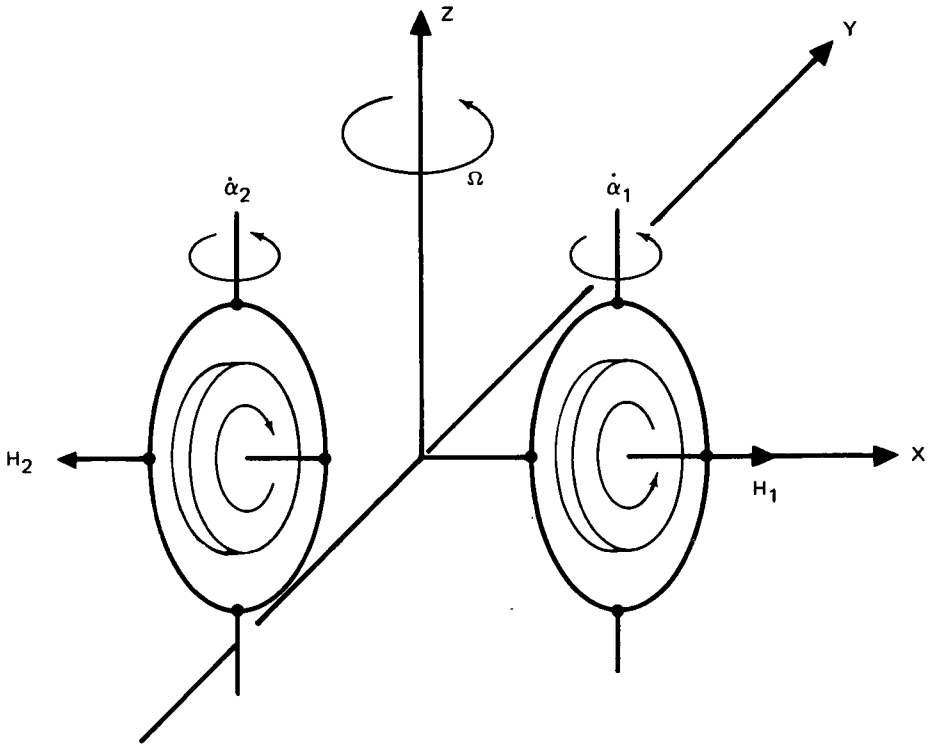

Figure 2-11. Twin CMG Wobble Damper

A block diagram of the wobble-damping control system is shown in Figure 2-12 where $\omega_Z \approx \Omega$ = constant. The gimbal angle control law is

$$\alpha_{1c} = -\alpha_{2c} = -K\omega_Y \tag{2-6}$$

A tracking loop (K_{TR} is the tracking loop gain) is included to maintain the relationship

$$\alpha_1 = -\alpha_2 = \alpha \tag{2-7}$$

Substituting this relationship into the torque equations and letting $H_1 = H_2 = H$ yields

$$T_X \approx -2H\Omega S\alpha \tag{2-8}$$

$$T_Y \approx 2H\dot{\alpha}S\alpha \tag{2-9}$$

$$T_Z = -2H\omega_X S\alpha \tag{2-10}$$

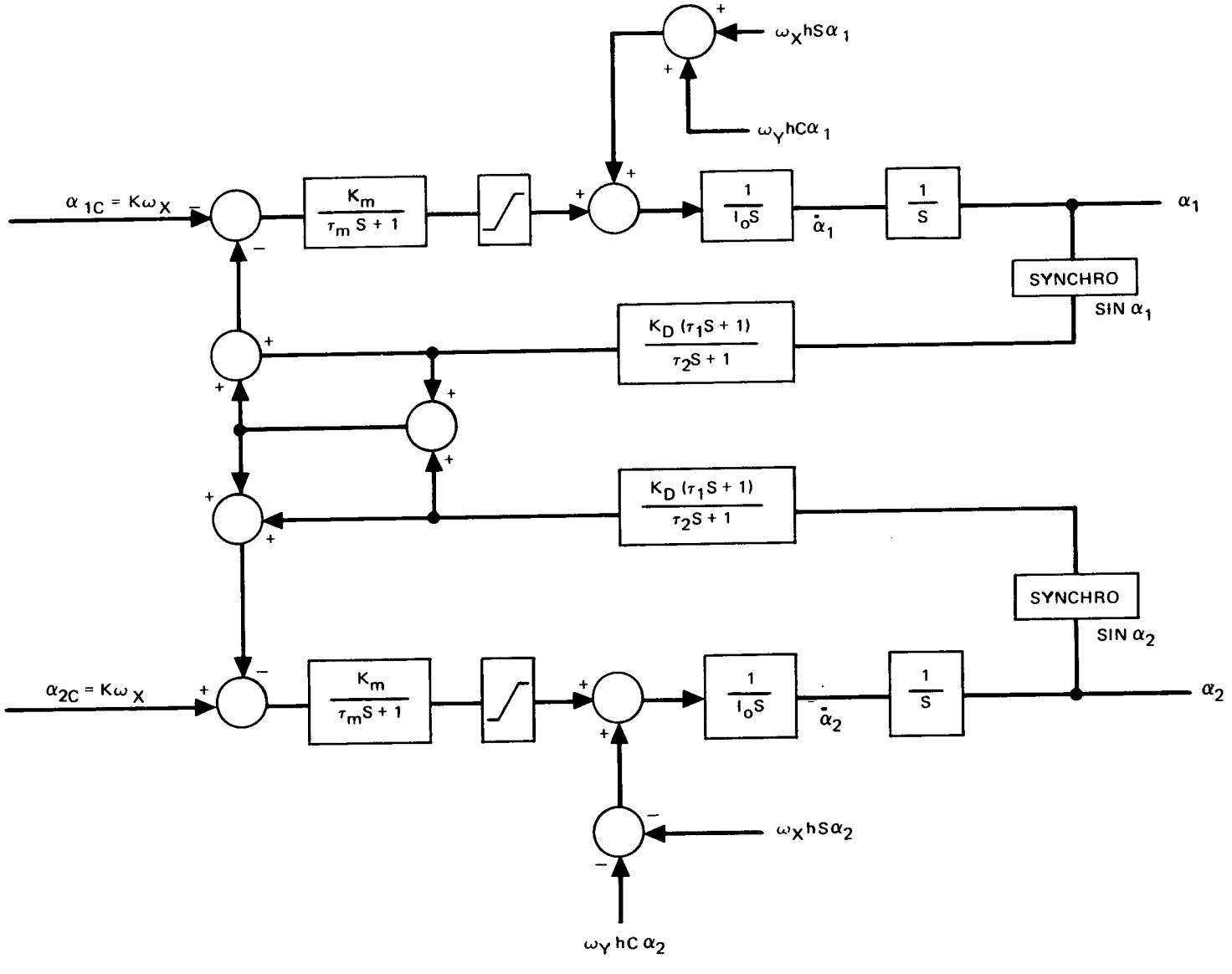

Figure 2-12. CMG Gimbal Servo Drivers

If we assume small gimbal angles ($C\alpha \approx 1$, $S\alpha \approx \alpha$), the system equations can be linearized and conventional control analyses can be applied.

Figure 2-13 is a simplified block diagram of the wobble damper. The gimbal angle control loop will have a much higher bandwidth than the rest of the system; therefore, if we assume that $\alpha = \alpha_c$, the simplified system equations are

$$I_X \dot{\omega}_X + (I_Z - I_Y)\Omega\,\omega_Y + 2H\Omega\alpha = 0 \qquad (2\text{-}11)$$

$$I_Y \dot{\omega}_Y + (I_X - I_Z)\,\Omega\,\omega_X - 2H\dot{\alpha} = 0 \qquad (2\text{-}12)$$

The characteristic equation is

$$S^2 + 2HK\Omega\left(\frac{B}{I_Y} + \frac{1}{I_X}\right) S + \frac{(I_Z - I_Y)(I_Z - I_X)\Omega^2}{I_X I_Y} = 0 \qquad (2\text{-}13)$$

CR71

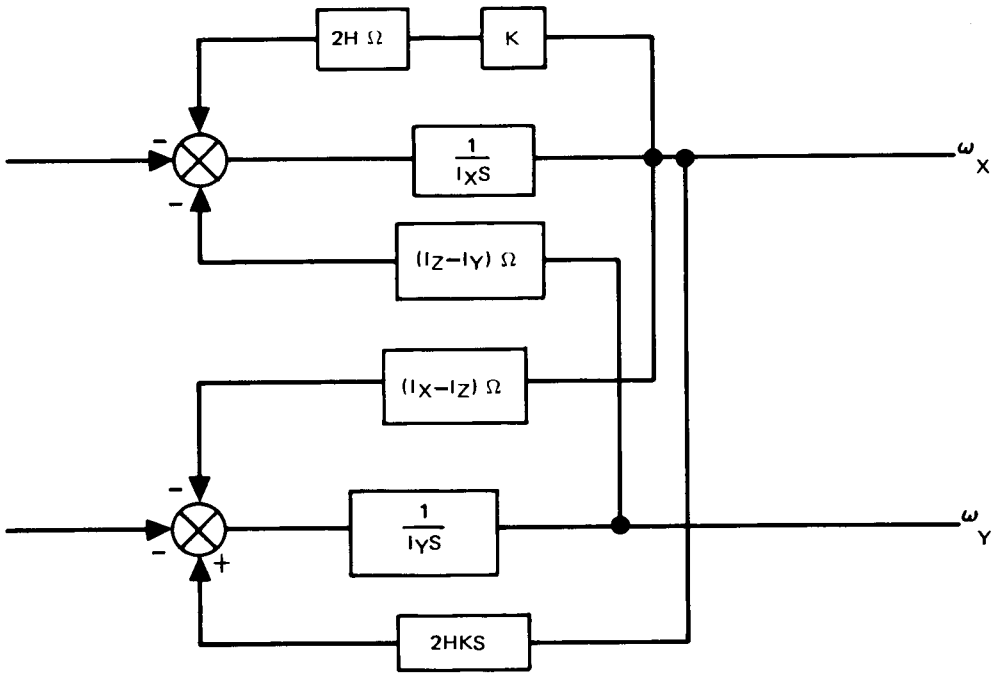

Figure 2-13. Simplified CMG Wobble Damper

The damping factor is

$$\zeta = \frac{K H \Omega}{\gamma}\left(\frac{B}{I_Y} + \frac{1}{I_X}\right) \tag{2-14}$$

and nutation frequency is

$$\gamma = \Omega \left[\frac{(I_Z - I_Y)(I_Z - I_X)}{I_X I_Y}\right]^{1/2} \tag{2-15}$$

The influence of the flexible booms may be determined by using the reduced moments of inertia I'_Z and I'_Y in the above equations. Since both γ and I_Y are reduced from the rigid body values in this case, increased damping is to be expected with flexible booms.

2.3 ACTIVE MASS BALANCE WOBBLE DAMPING CONTROL SYSTEM

The theory and computed results of operation of an active mass-balance control system are fully presented in Reference 1.* The principle of operation is to move a mass parallel to the Z axis an amount proportional to ω_Y thus generating an $I_{XZ}(t)$ product of inertia which acts to damp the wobble motion including that due to mass shifts. The main equation of Reference 1 is reproduced here for completeness.

$$\ddot{\omega}_Y + \frac{Cm_c |r_X|}{I_Y} \Omega^2 \omega_Y + (a + \delta a)\, b\Omega^2 \dot{\omega}_Y = -b\Omega^3 \frac{I_{YZ}(0)}{I_X} \tag{2-16}$$

where m_c is the control mass, r_X and r_Y are the position components of the control mass guides, and C is the gain constant in the commanded position of the control mass

*Reference 1. D. W. Childs. A Movable-Mass Attitude-Stabilization System for Artificial-g Space Stations. Journal of Spacecraft and Rockets, Vol. 8, No. 8, August 1971.

$$a = \frac{I_Z - I_Y}{I_X} = B \text{ of this report} \tag{2-17}$$

$$b = \frac{I_Z - I_X}{I_Y} = -A \text{ of this report} \tag{2-18}$$

$$\lambda = (ab)^{1/2} \tag{2-19}$$

$I_{YZ}(0)$ is the product of inertia disturbance arising from a mass shift such as crew motion. The term δa which increases the wobble natural frequency is not significant. The ratio of effective damping to critical damping is given by

$$\zeta = \frac{C m_c |r_X| \Omega}{2 I_Y \lambda} \tag{2-20}$$

The influence of flexible booms may be examined by use of the reduced values of I_Z and I_Y and since they are smaller than for a rigid body, indicate that increased damping would be obtained.

The model wobble damping system is composed of two movable masses located at diagonally opposite corners of the model. The two masses are connected by a cable and operated by a dc torquemotor so that they move in equal and opposite directions thus preserving the model static balance. It may be shown that the attitude equations of motion are identical with those of Reference 1 provided that the control mass, m_c, is understood to include both model masses.

2.4 REACTION JET SYSTEM

The reaction jet system located in the air bearing table has two functions:

A. To spin up and spin down the table (about Z axis).

B. To provide wobble damping during spinup and spindown (about X axis).

To accomplish these functions a two-axis rejection jet system with four pairs of nozzles is used. Functionally, the jets on the Z axis operate independently from the jets on the X axis.

2.4.1 Spin-up System

The spin-up system is shown in Figure 2-14. Upon command, the gas jets are turned on and are left on until the desired spin rate is reached. During the course of a run, air drag on the table acts against the table spin. When the rate decreases below the commanded rate, the jets are activated to keep the spin rate within a given tolerance of the nominal. This is accomplished by putting a dead zone in the reaction jets as shown in the figure. To spin down the table, the command, ω_{ZC}, is set equal to zero.

2.4.2 Reaction-Jet Wobble Damping

During spin-up or spin-down, it is not convenient to use the CMG's for wobble damping. The X-axis reaction jet system is used for wobble damping during these times. This system can also be manually commanded by

CR71

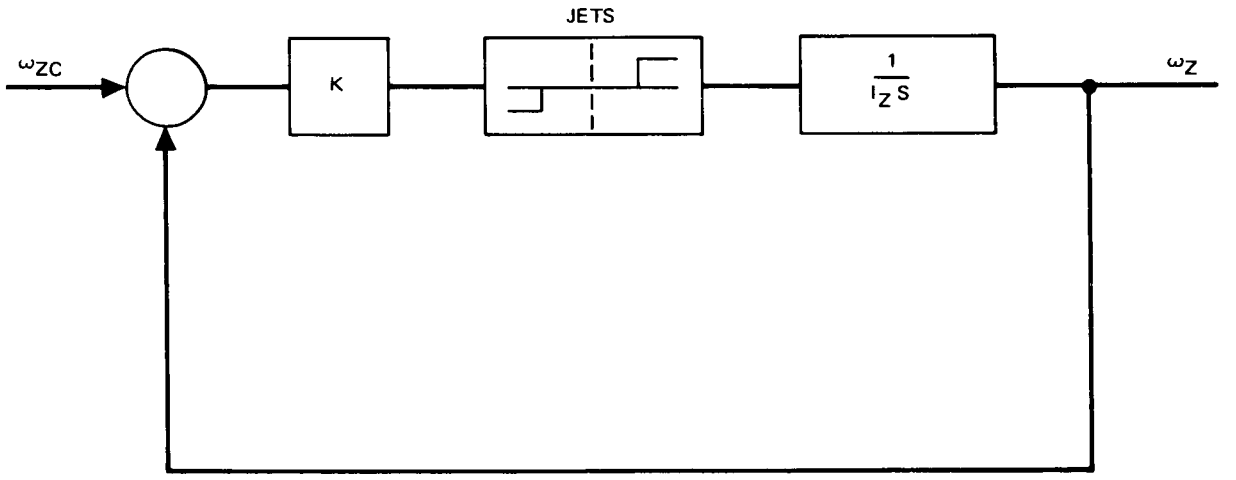

Figure 2-14. Spin-Up System

means of a switch on the control console to introduce initial conditions or disturbances about the X axis.

A block diagram of the system is shown in Figure 2-15.

2.4.3 Reaction Jet Control System Hardware

The system, as shown schematically in Figure 2-16, consists of four pairs of cold gas (nitrogen) reaction jets. The reaction jets are driven by two solenoid valves which are controlled by the spinup/wobble-control logic.

The nitrogen is carried in two symmetrically located tanks (to reduce any cg shift due to mass expulsion). The volume of the tanks is approximately 400 $in.^3$. This sizing of the tanks allows a number of simulation runs to be conducted before recharging is required.

Each of the jets is 0.66 mm (0.026 in.) in diameter and develops a thrust of 0.059 N (0.013 lb) when the supply pressure is 17.24 N/cm^2 (25 psi). The

CR71

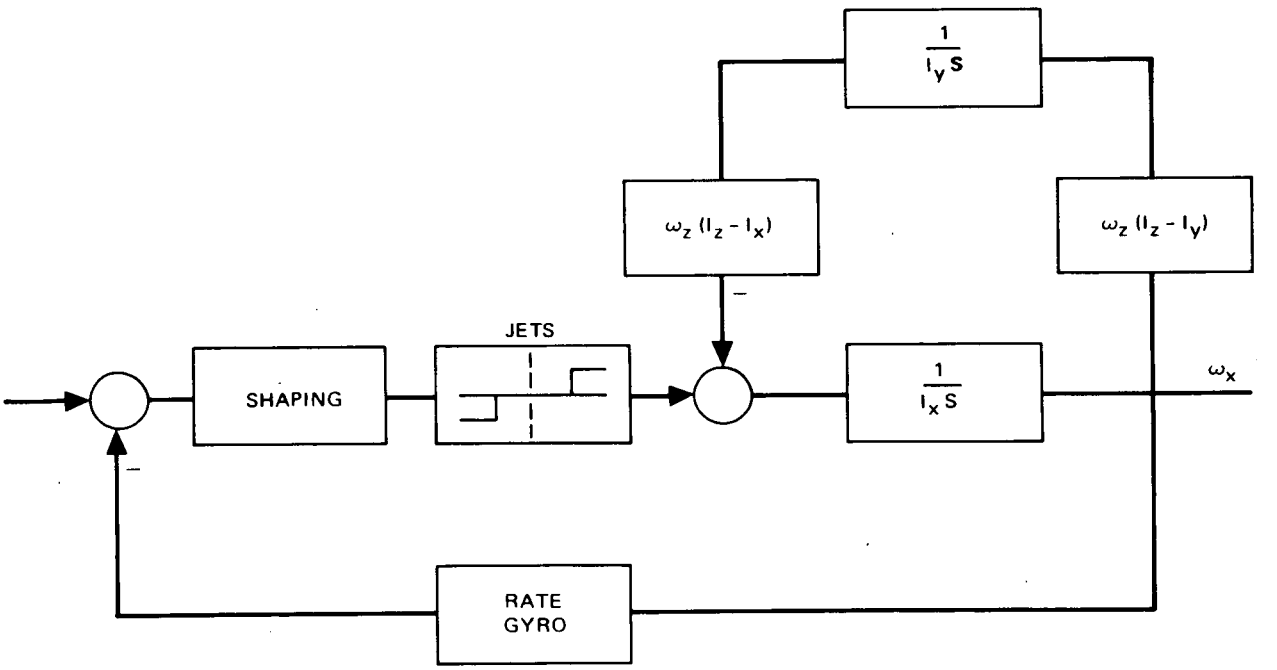

Figure 2-15. Reaction Jet Wobble Damper

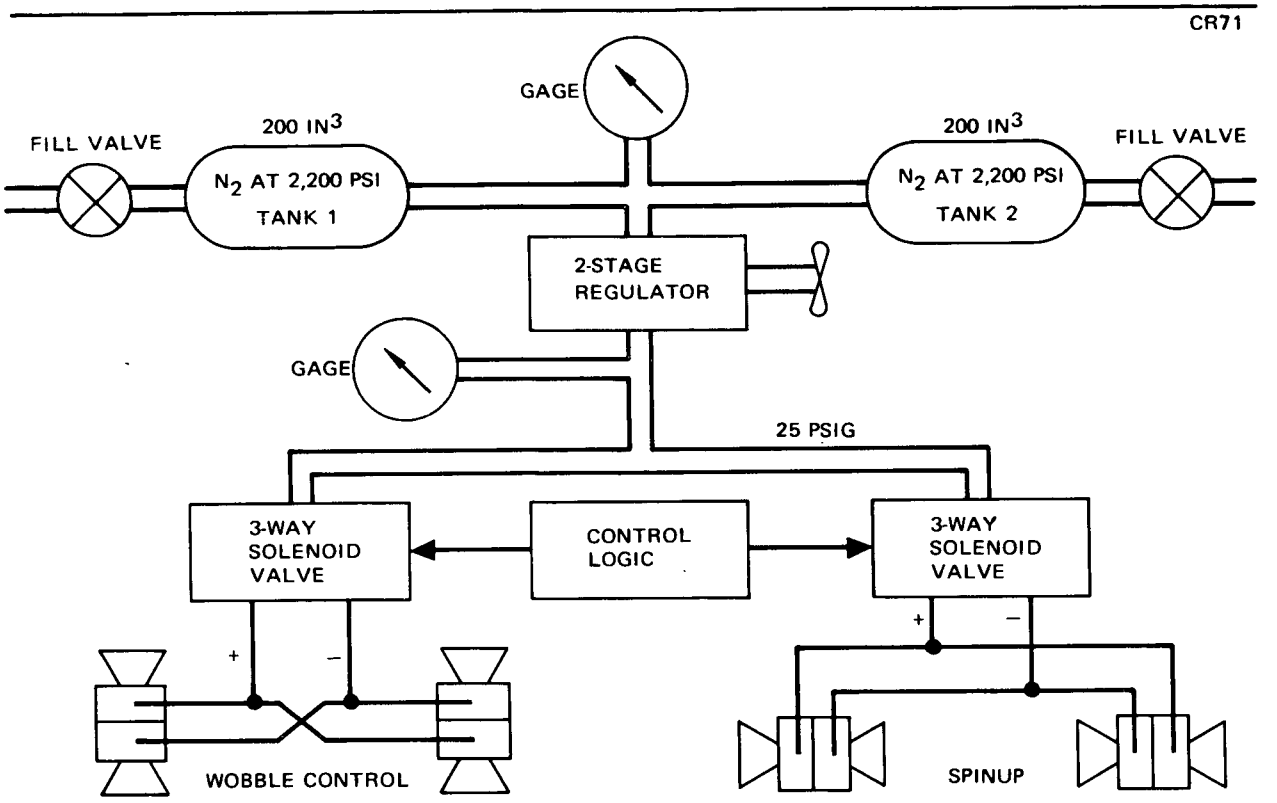

Figure 2-16. Schematic Diagram – Reaction Jet System for Spin-Up and Wobble Control

distance between jets is 2.286 m (6.94 ft). The pair of on-jets develop a moment of 0.124 N m (0.091 ft/lb) at this pressure. The spin up jets accelerate the model to a speed of 0.63 rad/sec (6 rpm) in approximately 20 min. The wobble damper dead zone was set at ±0.00524 rad/sec (0.3 deg/sec).

Section 3
SIMULATION RESULTS

Two model configurations with slightly different parameters were used in the simulation runs. The experimentally determined parameters for the two configurations were the following:

Center Body

	Configuration 1	Configuration 2
I_X	148.46 kg m^2 (111.16 slug ft^2)	148.16 kg m^2 (111.16 slug ft^2)
I_Y	22.70 kg m^2 (17.0 slug ft^2)	22.90 kg m^2 (17.15 slug ft^2)
I_Z	144.10 kg m^2 (107.90 slug ft^2)	144.20 kg m^2 (107.97 slug ft^2)
$I_X - I_Z$	4.354 kg m^2 (3.26 slug ft^2)	4.260 kg m^2 (3.19 slug ft^2)

For both configurations the boom parameters were

$$2I_B = 5.107 \text{ Kg } m^2 \text{ (3.824 slug } ft^2\text{)}$$

$$\omega_B = 1.636 \text{ rad/sec (0.260 cps)}$$

$$\frac{d+\ell}{\ell} = 1.2115$$

$$R = 0.9929$$

$$R\omega s^2 = 2.658 + 1.2115\ \Omega^2$$

The rigid body parameters are obtained by adding $2I_B$ to the I_Z and I_Y values for the center body.

3.1 RIGID BODY SPIN-UP AND SPIN-DOWN

Large angular excursions can occur during the low spin portion of a run since the system does not have a nonspinning attitude control system. To prevent excessive attitude excursions due to the spin-up jet misalignment, the wobble-damping jets, which provide torques about the X axis, were operated manually by means of a toggle switch on the control console to minimize the attitude excursions until spin speed is built up sufficiently to allow control by the RCS wobble damping system.

In this run the model was spun up and down with the booms locked (rigid body). At time zero, the spin-up jets were turned on and attitude was controlled manually as described above.

At 568 sec when the speed was 0.489 rad/sec (28 deg/sec 4.67 rpm), control was turned over to the RCS wobble damper which allowed ω_X to move to the edge of the RCS dead zone 0.0052 rad/sec (0.3 deg/sec) and remain there. At 926 sec, the speed had reached the set speed of 0.62 rad/sec (35.6 deg/sec). At 1,100 sec the RCS wobble damper was turned off and the spin-up jets allowed to maintain a constant speed while the steady-state nutation motion was observed. The nutation period observed of 68.4 sec is in excellent agreement with that calculated from the experimentally determined rigid-body parameters (68.0 sec). The offset from zero on ω_X indicates a significant I_{XZ} dynamic imbalance on this run. At 1,428 sec, the spin-up jets were turned off and the model allowed to spin down under air resistance. At 1,453 sec, the RCS wobble damper was turned on again and damped the oscillation to the edge of its dead zone in about half a cycle (43 sec). The length of this run precludes inclusion in this report; however, Figure 3-1 shows the constant speed and RCS wobble damping portion of this run from time 1,113 to 1,513 sec.

Figure 3-1 has ω_Z as the spin rate on channel 1, the scale is 0.035 rad/sec (2 deg/sec) per division, and the time scale is 1 sec per division. ω_X and ω_Y are on channels 2 and 3, with scales of 0.0017 rad/sec (0.1 deg/sec) per division. Channels 4–5 and 6 are not in use on this run; however, Channel 4 is the boom channel. The boom is locked in place (rigid body). The signals

FOLDOUT FRAME 1

FOLDOUT FRAME 2

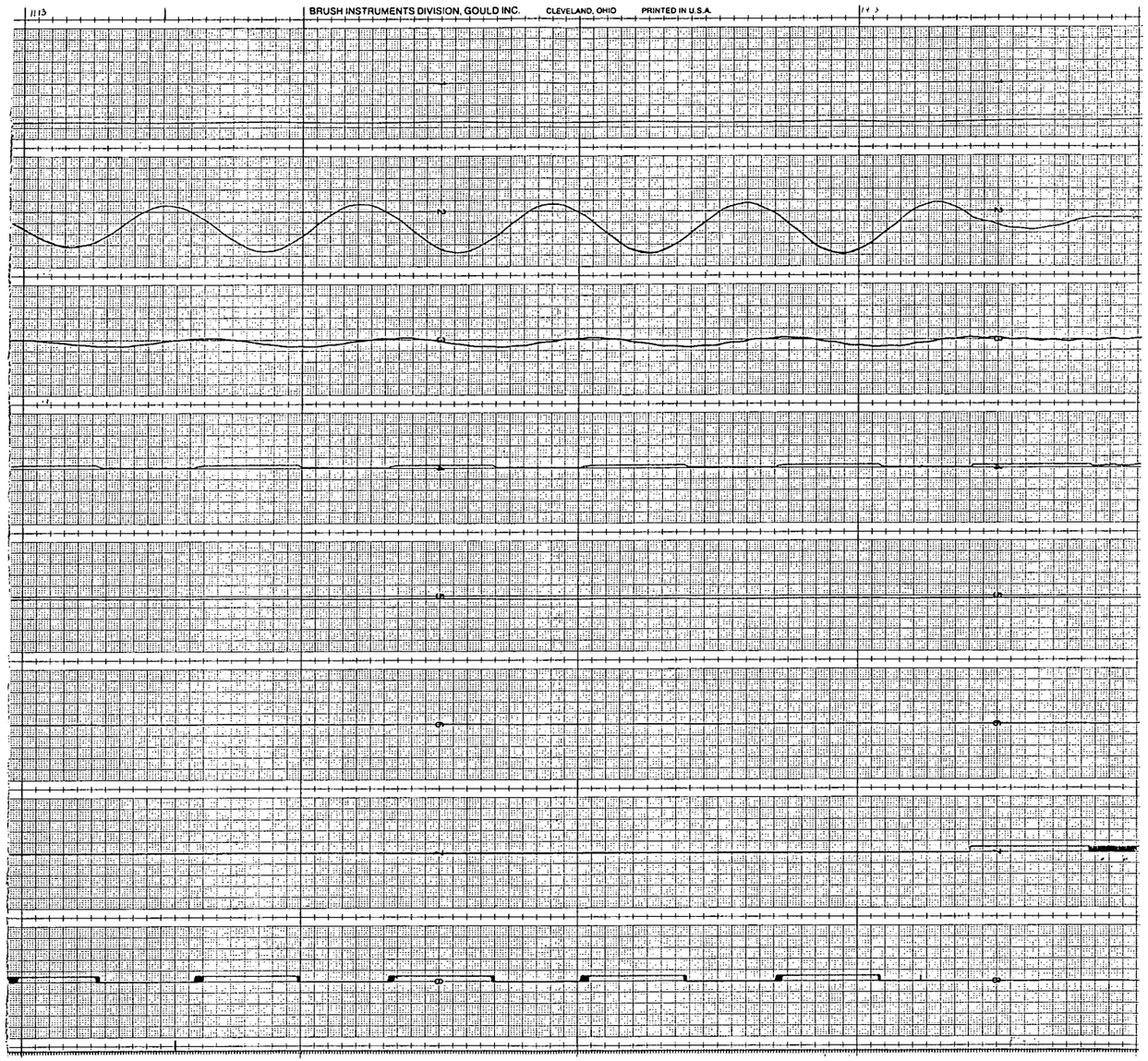

Figure 3-1. Rigid Body Spin-up and Down

observed are due to electrical noise coupling from the RCS jet firing. Channel 7 indicates the operation of the wobble damper jets which produces torques about the X axis. Channel 8 indicates the firings of the spin-up jets. Figure 3-2 shows the Euler angles during the corresponding time period. ω_X, ω_Y and ω_Z are repeated on channels 1, 2, and 3 to provide a common reference. The scales are 0.0035 rad/sec (0.2 deg/sec) per division on 1 and 2 and 0.035 rad/sec (2 deg/sec) per division on channel 3. Channels 4, 5 and 6 present the Euler angles with scales of 0.035 rad (2 deg) per division. The Euler angles are generated by an analog computer and the zero reference is the position of the spin axis when the computer is switched into operation.

3.2 FLEXIBLE VEHICLE

For this run the flexible booms were unlocked. The spin-up thrustors were turned on and the model was spun up with manual attitude control using the X axis RCS thrustors to limit attitude excursions during the low-speed portion of spin-up (Figure 3-3) ω_X and the boom angle steadily diverged from zero. Attitude control was turned over to the RCS wobble damper which remained steadily on. At a spin speed of 0.59 rad/sec (34 deg/sec) an attempt to return the attitude of the spin axis more nearly to the vertical caused the model to hit the angle stops which limit motion about the X and Y axes to ±15 degrees. After some large perturbations, the model recovered from this and exhibited the motion shown. It was evident that a significant negative product of inertia disturbance was present. The active and disturbance masses were commanded to move approximately 5 cm (2in.) from null position in a direction to relieve the product of inertia disturbance. The RCS wobble damper and the spin-up thrustors were turned on and the spin was increased to 0.587 rad/s (33.6 deg/s). The divergence of ω_X and boom angle observed in the earlier portion of the run reappeared but much less strongly. In this run, the nutation period is approximately the same as the rigid body nutation period (75 sec). This surprising result is believed to be due to friction in the boom pivots. It will be noted that the boom frequently appears to move in jumps of about one division (0.05 deg) as might be caused by slip-stick friction.

Additional runs were made with the model being spun-up to various speeds and released. This is referred to as caged spin-up. The model was then

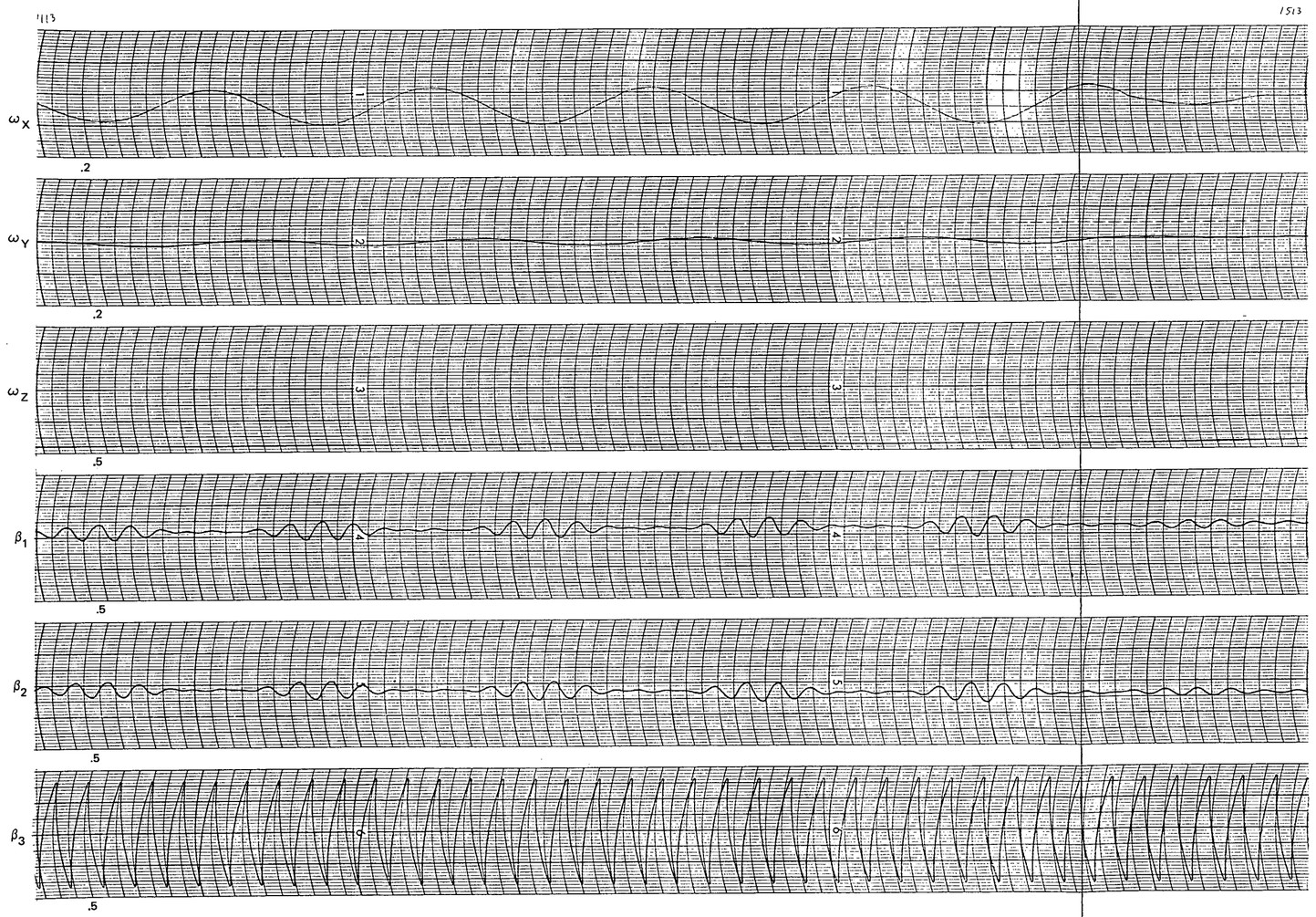

Figure 3-2. Rigid Body Spin-Up and Down Euler Angles

FOLDOUT FRAME 1

FOLDOUT FRAME 2

FOLDOUT FRAME 3

CR71

SCALES	CHANNELS	1	2	3	4	5	6	7	8
SCALES DEGREES PER DIV.		2 DEG/S	0.2 DEG/S	0.2 DEG/S	0.05 DEG	AM	DM	XRCS	ZRCS

TIME SCALE 2 SEC PER DIVISION

Figure 3-3. Flexible Body Spin-Up Run

allowed to coast so that the free motion could be observed unperturbed by the RCS system. Figure 3-4 shows the result of a spin-up and release at a spin of 0.64 rad/sec (36.8 deg/sec). ω_X and the boom angle immediately diverged indicating that the stability boundary has been approached in good agreement with the calculated value. (Stability factor = 1.0 at Ω = 0.69 rad/sec, 39.4 deg/sec.)

Figure 3-5 shows the result of a spin-up and release at 0.59 rad/sec (34 deg/sec). A significant boom oscillation was excited, indicating operation not far from the stability boundary. Again the nutation period is close to that of the rigid body. The jerky movement of the booms is again evident.

Figure 3-6 is the record from a spin-up and release at 0.51 rad/sec (29.1 deg/sec). A relatively small boom amplitude is excited indicating operation relatively far from the stability boundary.

3.3 ACTIVE MASS BALANCE WOBBLE DAMPER

Figure 3-7 gives simulation results obtained with the active mass balance system with the booms locked (rigid body). The model was spun up to 0.626 rad/sec (36 deg/sec) and released and the free motion observed for about one cycle. The ω_X offset from zero indicated a negative I_{XZ} product of inertia. The wobble damper damped the oscillation in about one cycle. The disturbance mass was then commanded to move 0.6 inch in a direction to relieve the product of inertia, again the active mass system damped the motion in one cycle, although the spin had decreased considerably. The broad ω_Y trace is due to a low-amplitude, high-frequency oscillation of the active masses. It does not show in the active mass trace because the signal has been put through a low-pass filter with a break frequency of 20 rad/sec. The locked boom structural frequency appeared to be participating in this and is possibly related to the natural frequency of the cable connecting the two masses. It is possible that additional low-pass filtering on the input signal ω_Y could eliminate the low-amplitude oscillation.

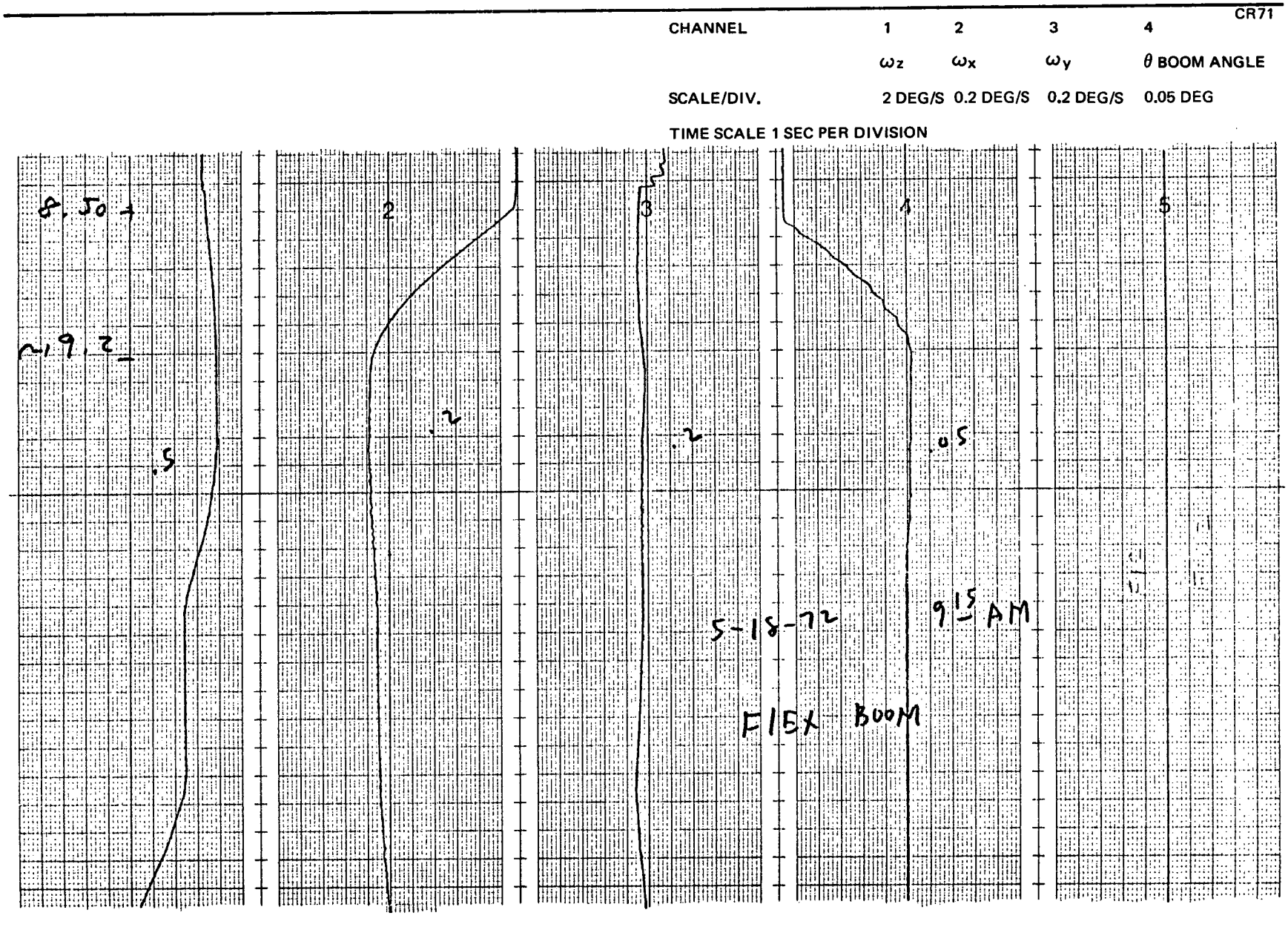

Figure 3-4. Caged Spin-Up to 0.64 Rad/Sec (36.8 deg/sec)

CHANNEL	1	2	3	4	5	6	7	8
	ω_z	ω_x	ω_y	θ			XRCS	ZRCS
SCALE/DIVISION	2 DEG	0.2 DEG	0.2 DEG	0.05 DEG				

TIME SCALE 1 SEC/DIV

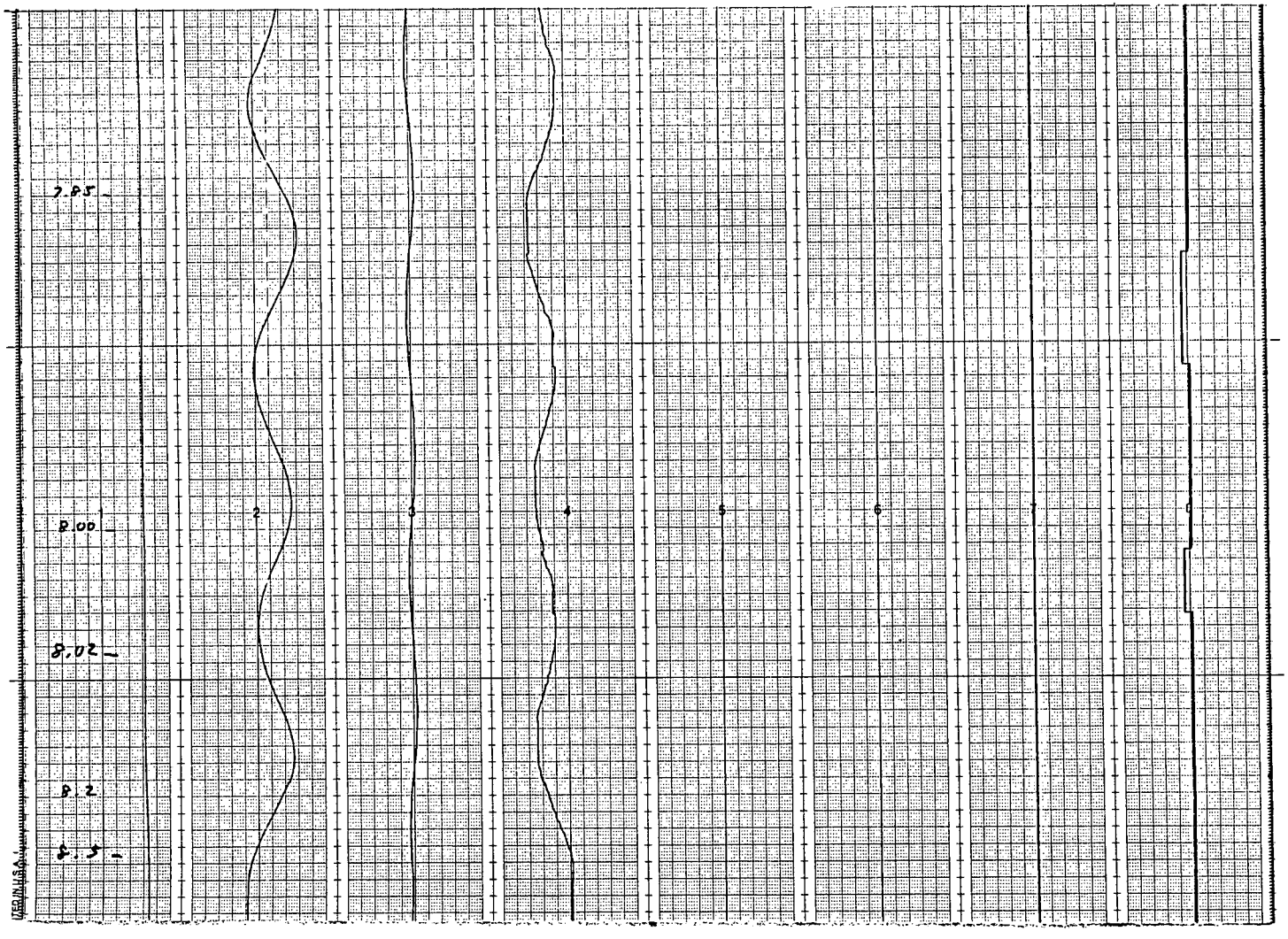

Figure 3-5. Caged Spin-Up to 0.59 rad/sec (34 deg/sec)

CHANNEL	1	2	3	4
	ω_z	ω_x	ω_y	θ
	2 DEG/ SEC	0.1 DEG/ SEC	0.1 DEG/ SEC	0.05 DEG

TIME SCALE 1 SEC PER DIVISION

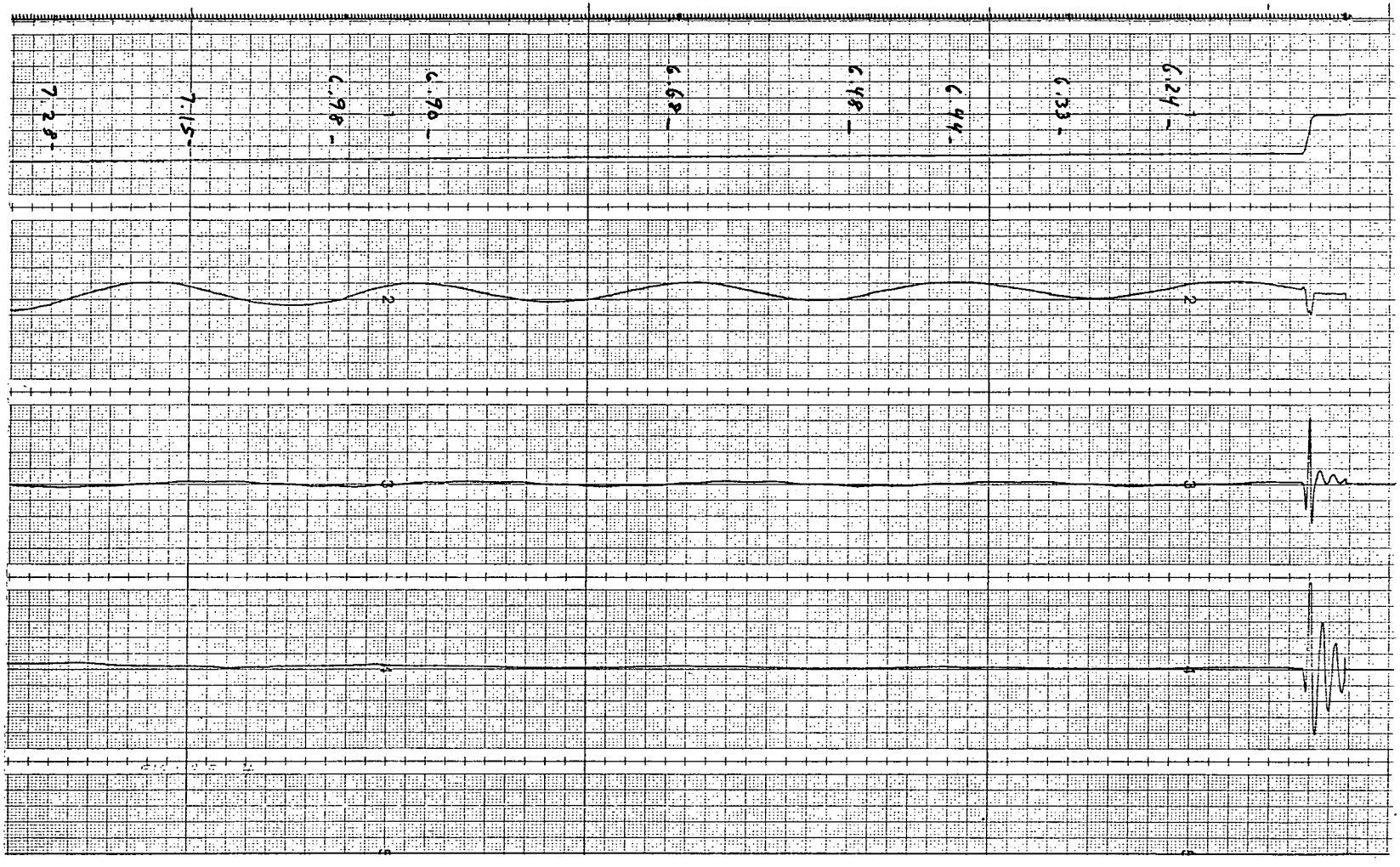

Figure 3-6. Caged Spin-Up to 0.51 Rad/Sec (29.1 Deg/Sec)

FOLDOUT FRAME 1

FOLDOUT FRAME 2

CR71

CHANNEL	1	2	3	4	5	6	7	8
	ω_z	ω_x	ω_y	θ	ACTM	DM		
PER DIVISION	2 DEG/ SEC	0.2 DEG/ SEC	0.05 DEG/ SEC	LOCKED	0.1 IN.	0.1 IN.		

TIME SCALE 1 SEC/DIVISION

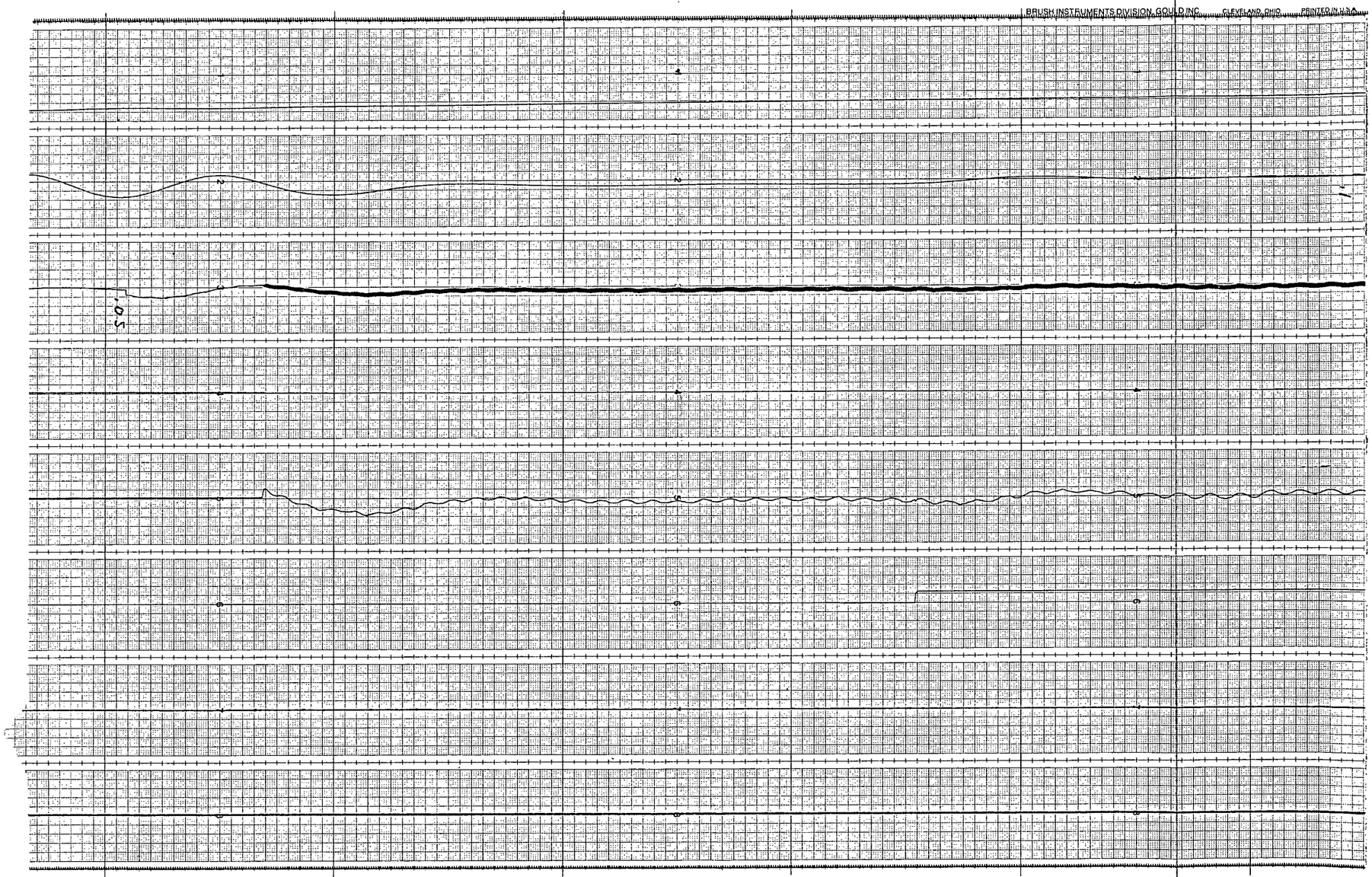

Figure 3-7. Rigid Body Active Mass Balance Runs

3.4 ACTIVE MASS BALANCE WOBBLE DAMPER WITH FLEXIBLE BOOMS

Figure 3-8 presents simulation results obtained with the active mass balance system when the booms are free. The model was spun up to 0.57 rad/sec (33 deg/sec) and released. In a few minutes the RCS wobble damper and spin-up jets were turned off and the active mass system turned on. It damped the initial motion in about one and a half cycles. The disturbance mass system was then commanded to move 2 inches. The oscillation was again damped in one and a half cycles. The limit cycle oscillation of the active masses was excited by the operation of the disturbance mass system causing a broadening of the ω_Y trace. It will be noted that much longer nutation periods (120 sec) occur in this record. This suggests that the limit cycle acts as a dither to the booms relieving the stiction in the pivots.

3.5 CMG WOBBLE DAMPER

Figure 3-9 shows simulation results obtained with the CMG wobble damper with the booms locked (rigid body) for configuration 2. The action is at an average spin rate of about 0.558 rad/sec (32 deg/sec). The model was spun-up with the Z RCS and then allowed to coast and the amplitude of the nutation angular velocities observed. The CMG wobble damper was then turned on and damped the oscillation in approximately two cycles. Channels 5 and 6 record sine α_1 and the tracking error with scales of 0.01 radians per division. The broad traces are due to a relatively high-frequency, low-amplitude limit cycle in the CMG gimbal loops, which has a negligible effect on the performance of the system.

3.6 CMG WOBBLE DAMPER WITH FLEXIBLE BOOMS

Figures 3-10 and 3-11 present configuration 2 simulation results obtained with the CMG wobble damper and flexible booms. The initial oscillations were observed while the model was coasting. The CMG controller was switched on when the spin rate was 0.471 rad/sec (27 deg/sec). The oscillation was damped in about one-fourth of a cycle. This result is in agreement with theoretical predictions that an increased damping ratio is to be expected with flexible booms.

FOLDOUT FRAME 1

FOLDOUT FRAME 2

CR71

CHANNEL	1	2	3	4	5	6	7	8
	ω_z	ω_x	ω_y	θ	ACTM	DM	XRCS	ZRCS
SCALE	2 DEG/S	0.2 DEG/S	0.05 DEG/S	0.05 DEG	0.1 IN.	0.1 IN.		

TIME SCALE 1 SEC/DIVISION

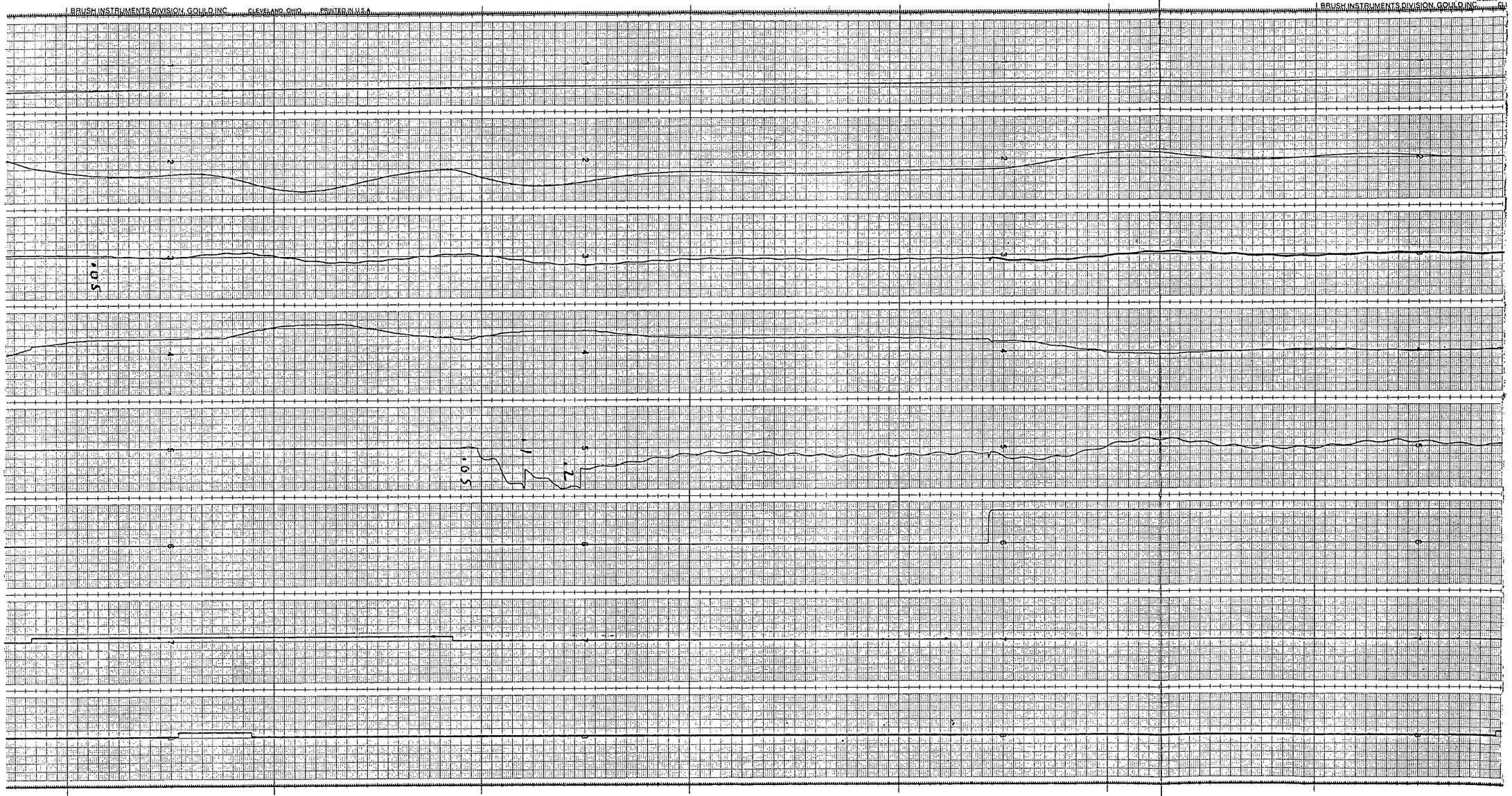

Figure 3-8. Active Mass Balance Wobble Damper With Flexible Booms

CR71

CHANNEL	1	2	3	4	5	6	7	8
	ω_Z	ω_X	ω_Y	θ	Sa_1	TER	XRCS	ZRCS
PER DIVISION	2 DEG/SEC	0.1 DEG/SEC	0.1 DEG/SEC	LOCKED	.01 RAD	.01 RAD		

TIME SCALE 1 SEC/DIVISION

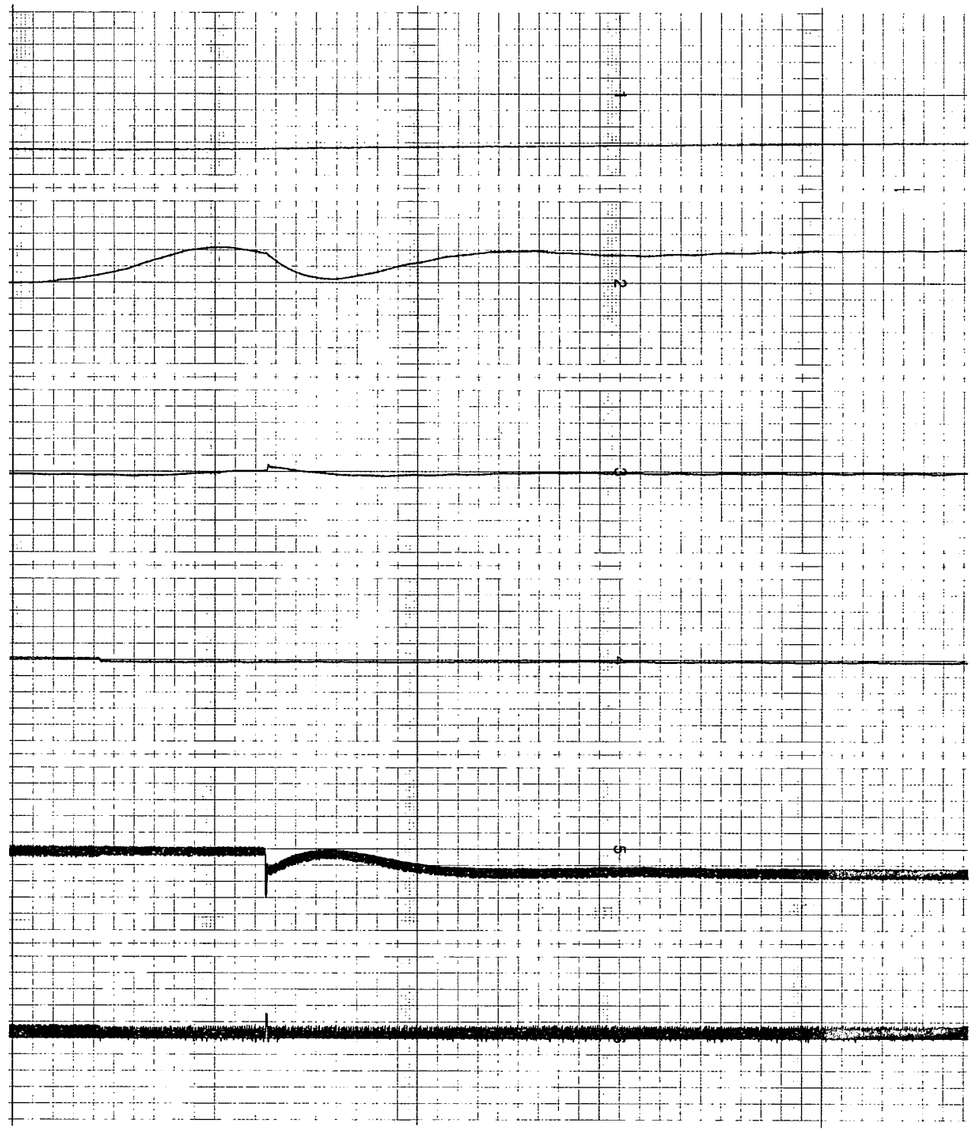

Figure 3-9. Rigid CMG Wobble Damper—Configuration 2

CR71

CHANNEL	1	2	3	4	5
	ω_Z	ω_X	ω_Y	θ	sa_Z
PER DIVISION	2 DEG/SEC	0.1 DEG/SEC	0.1 DEG/SEC	0.05 DEG	0.01 RAD

TIME SCALE 1 SEC/DIVISION

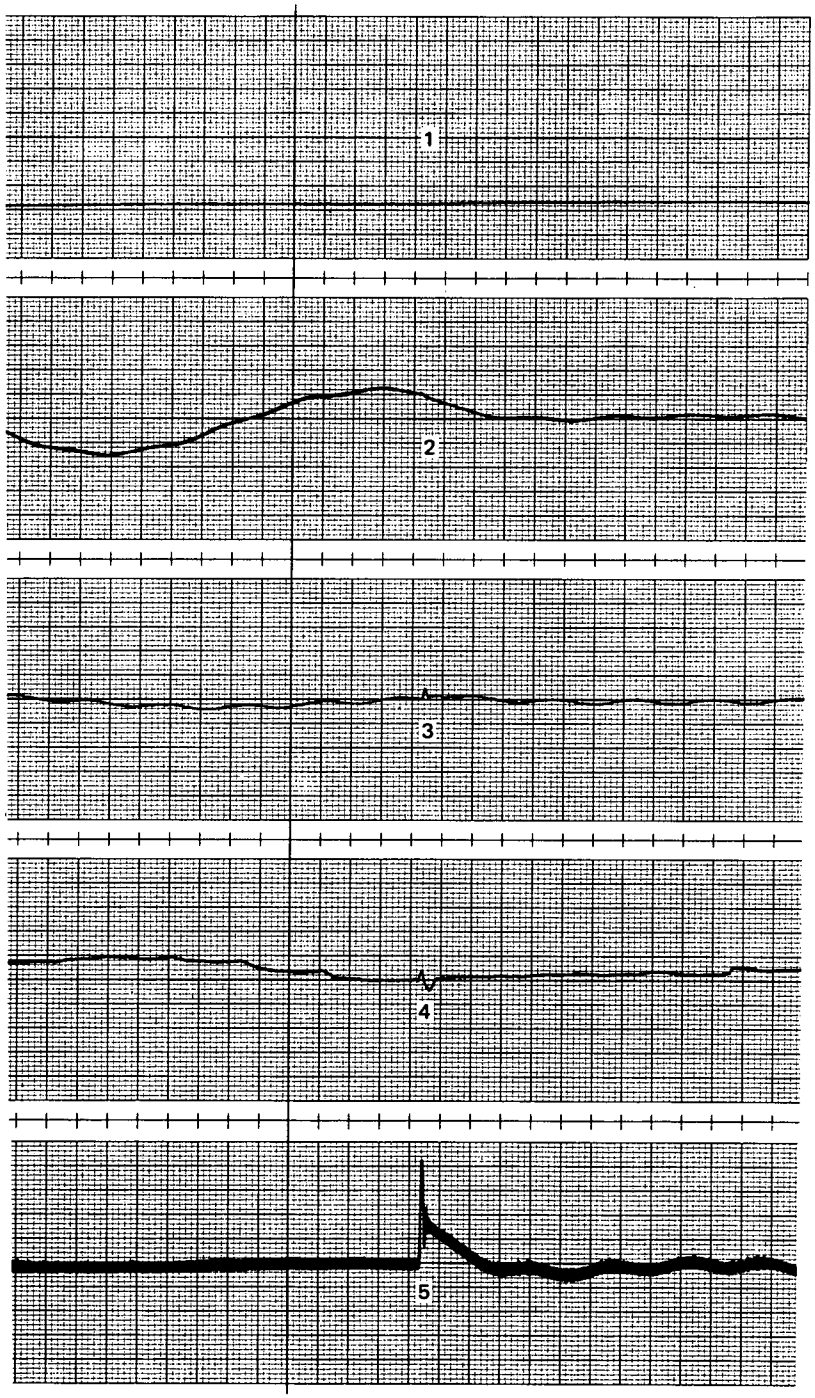

Figure 3-10. CMG Wobble Damper with Flexible Booms—Configuration 2

F

CHANNEL	1	2	3	4	5	6
	ω_X	ω_Y	ω_Z	β_1	β_2	β_3
PER DIVISION	0.2 DEG/SEC	0.2 DEG/SEC	2 DEG/SEC	1 DEG	1 DEG	5 DEG

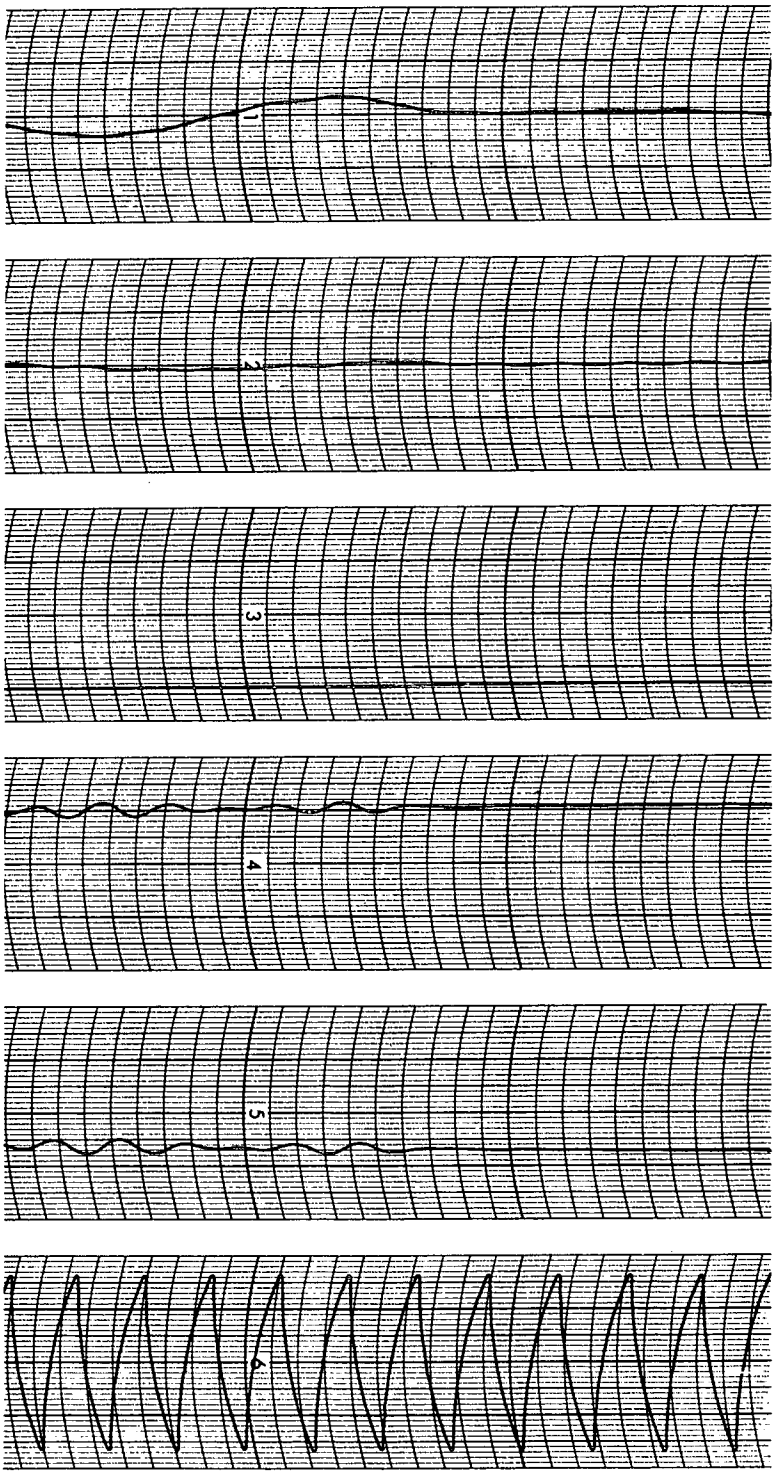

Figure 3-11. CMG Wobble Damper with Flexible Booms—Configuration 2

Section 4
DISCUSSION OF RESULTS

The system with flexible booms tended to exhibit the rigid-body nutation period. A number of runs were made with configuration 2 at various spin speeds, and the nutation periods were measured to investigate the phenomenon in greater detail. The results are presented in Figure 4-1. The upper curve is the flexible-body nutation period and the lower curve is the rigid-body nutation period. The crosses are experimentally determined points. It will be noted that the observed points generally fall between the two curves. At 0.419 rad/sec (24 deg/sec) the experimentally observed points lie close to the rigid-body curve. The points deverge from the rigid-body curve as the spin rate is increased. Near the stability boundary, the points jump up closer to the flexible body curve. The dashed lines indicate the general trend. It is believed that the observed behavior is caused by slip-stick friction in the boom pivot bearings. The simulation run records show that the boom angle tends to move in small pumps as is typical of slip-stick friction. At the lower spin-rates where only small boom amplitudes occur, the system tends to behave as a rigid body. At the higher spin-rates where large boom amplitudes tend to occur, the system behaves more nearly according to flexible-body predictions.

In view of the foregoing, it is somewhat difficult to assess the influence of the flexible booms on the active and disturbance mass systems. The charateristics of the active mass balance system are C = 16m/rad/sec (53 ft/rad/sec), m_c = 0.777 kg (1.72 lb) each, r_X = 0.254 m (0.833 ft), λ = 0.148. For the conditions (configuration 1) of the rigid active mass balance run (Figure 3-7), Ω = 0.628 rad/sec (36 deg/sec), yield ζ = 0.5, according to Equation (2-20); and this appears to agree with the experimental result. Computed on a rigid-body basis we would expect ζ = 0.37 to be observed in the flexible boom run (Figure 3-8) since the spin speed is lower, 0.489 rad/sec (28 deg/sec). Actually the damping appears nearly the same

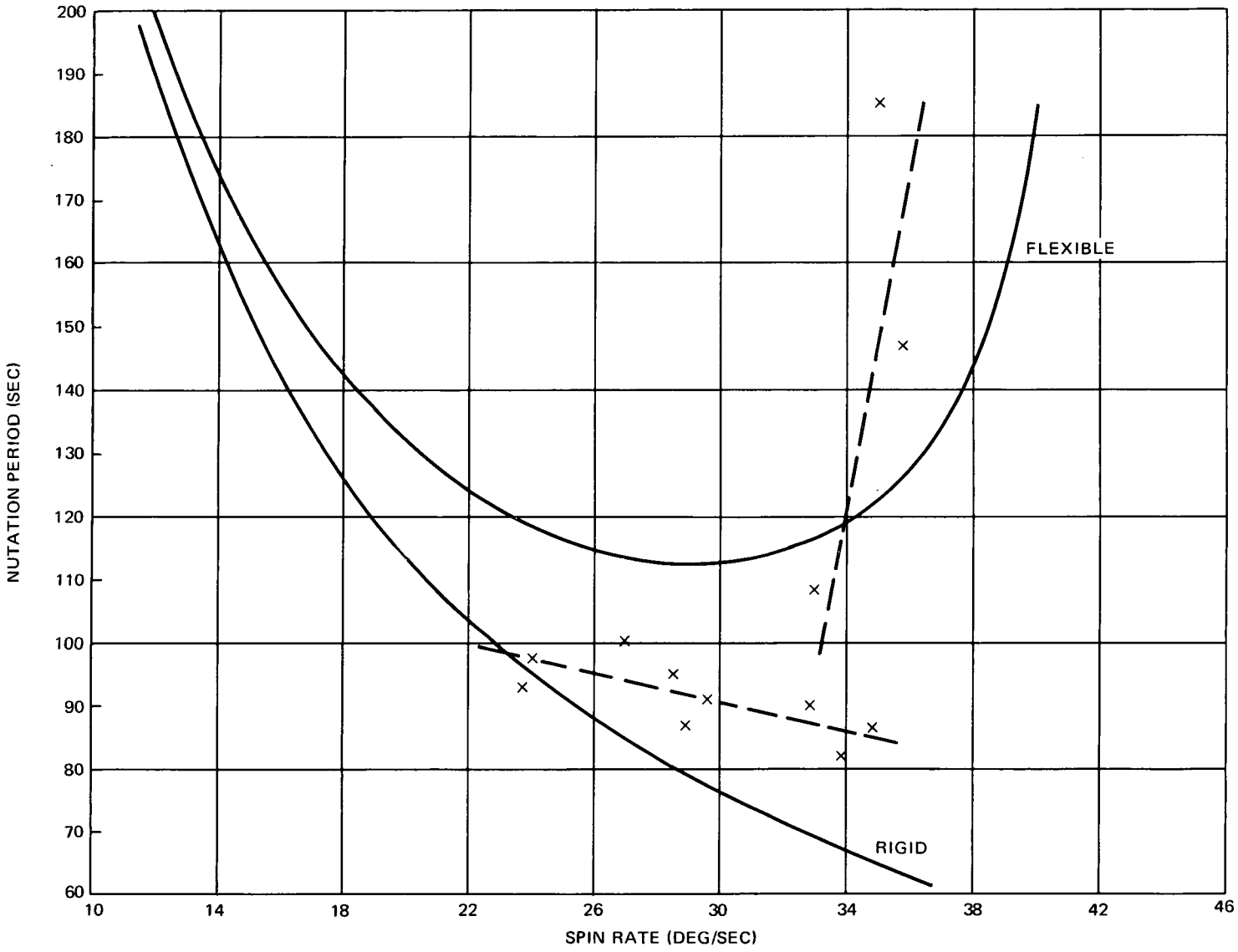

Figure 4-1. Nutation Period vs Spin Rate—Configuration 2

in both runs. If we compute the damping for the flexible boom case by using the reduced inertia we obtain $\zeta = 0.55$. This indicates that on this run, the flexible effects are acting according to theory. The nutation period observed on this record, 120 sec, is closer to the theoretical flexible boom value of 128 sec and distant from the rigid body value of 87 sec. A somewhat similar result is obtained with the CMG wobble damper (configuration 2). The angular momentum of the two CMG's is 0.922 kg m^2/sec (0.68 slug ft^2/sec), and the input gain is 6 (dimensionless). On a rigid body basis, Equation (2-14), these parameters would produce a damping ratio, $\zeta = 0.7$, which is about the value obtained in the simulation run (Figure 3-9). The flexible boom CMG run yields more nearly critical damping (Figure 3-10). If the CMG damping for the flexible run is computed from the reduced inertias (Figure 2-9), a damping ratio, $\zeta = 0.9$, is obtained in reasonable agreement with the observed value.

Figures 4-2 through 4-8 present the results of a digital computer simulation using the data of configuration 1 and a boom viscous damping ratio $\zeta = 0.06$ for the flexible booms at a spin rate of 0.628 rad/sec (36 deg/sec). This run exhibits the theoretical nutation period of 122 sec. Figures 4-9 through 4-15 present digital simulation results for configuration 1 with RCS wobble damping. The wobble damping dead zone was 0.00524 rad/sec (0.3 deg/sec) and the pair of on jets developed a moment of 0.149 Nm (0.11 ft lb). Figures 4-16 through 4-23 give digital simulation results for configuration 2 with the CMG wobble damper. The gimbal angle command was $\alpha_c = 10\omega_x$. The integral of the gimbal angle with a time constant of 400 sec was subtracted from the gimbal angle command to cause the gimbal angle to slowly return to its nominal position.

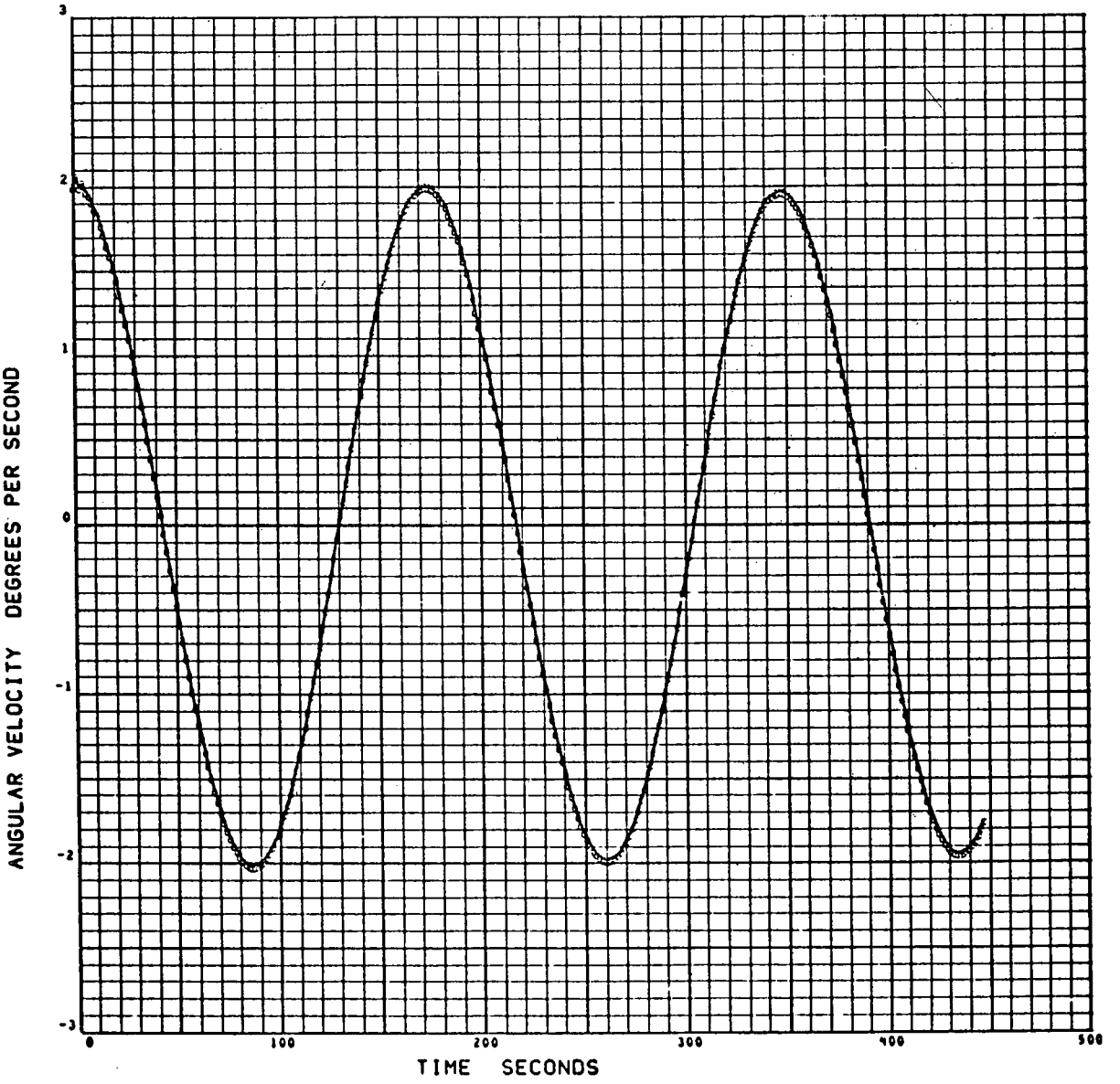

Figure 4-2. Configuration 1 Flexible Booms – X Component of Angular Velocity

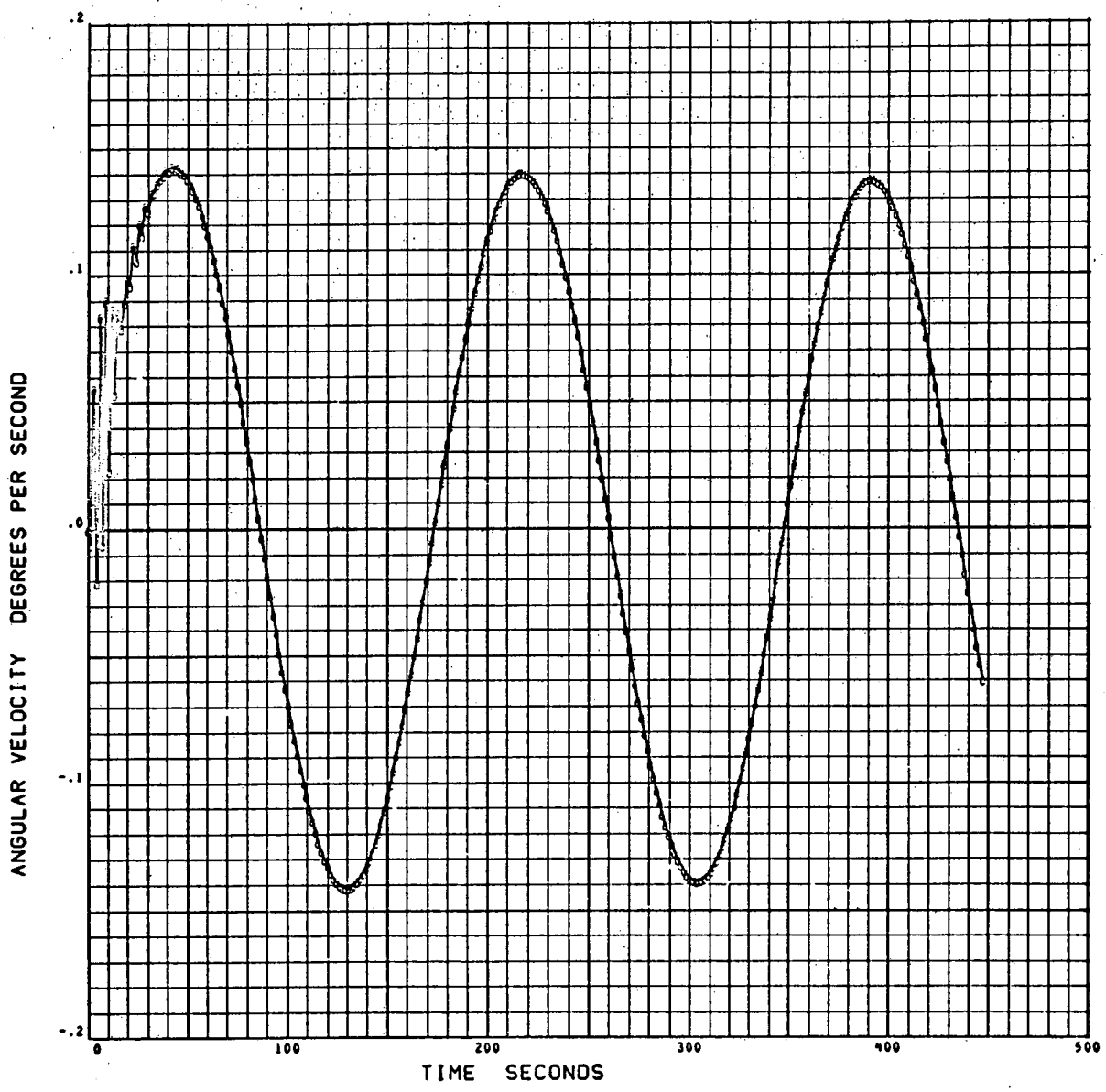

Figure 4-3. Configuration 1 Flexible Booms – Y Component of Angular Velocity

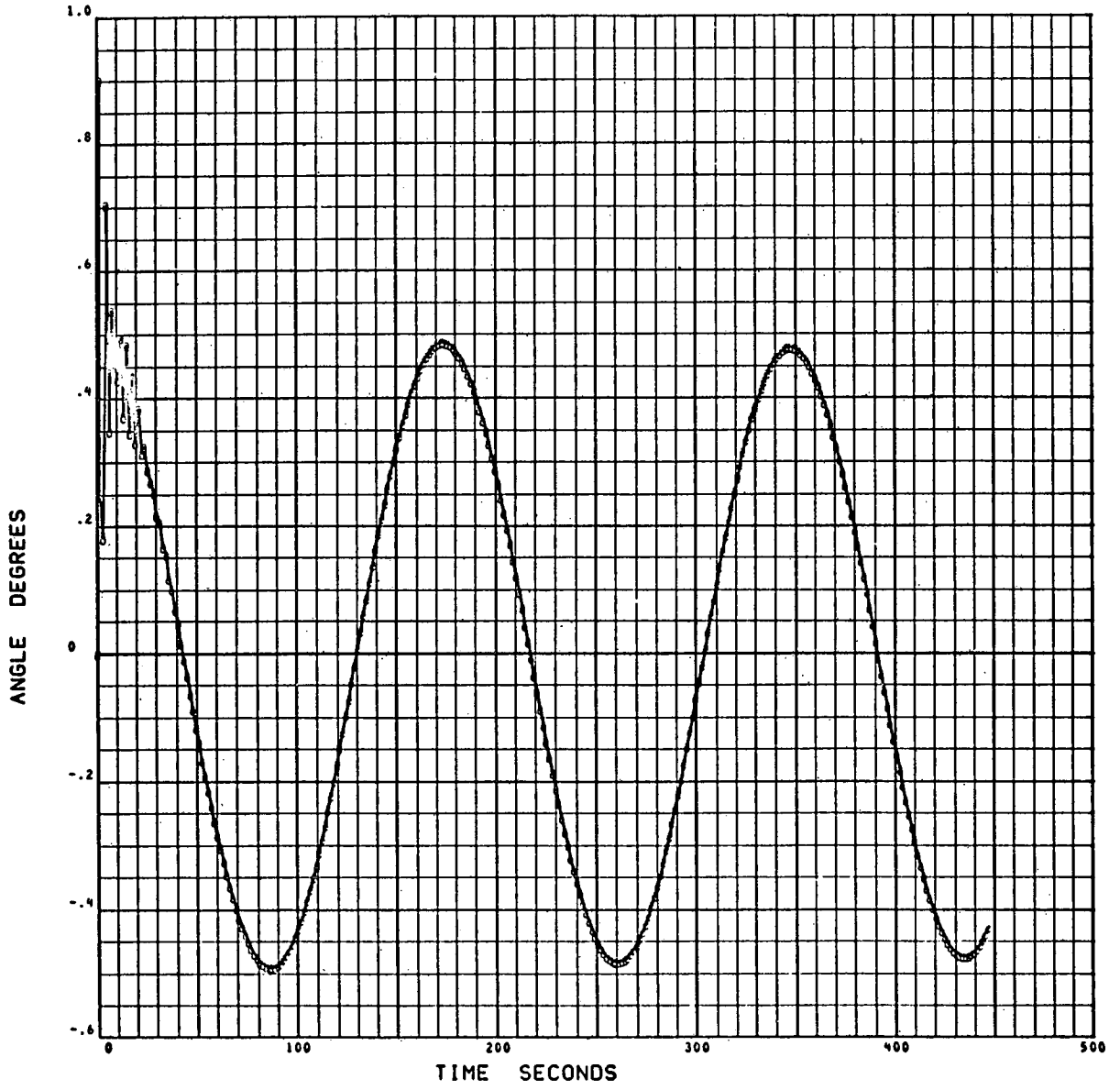

Figure 4-4. Configuration 1 Flexible Booms – Boom Angle Theta

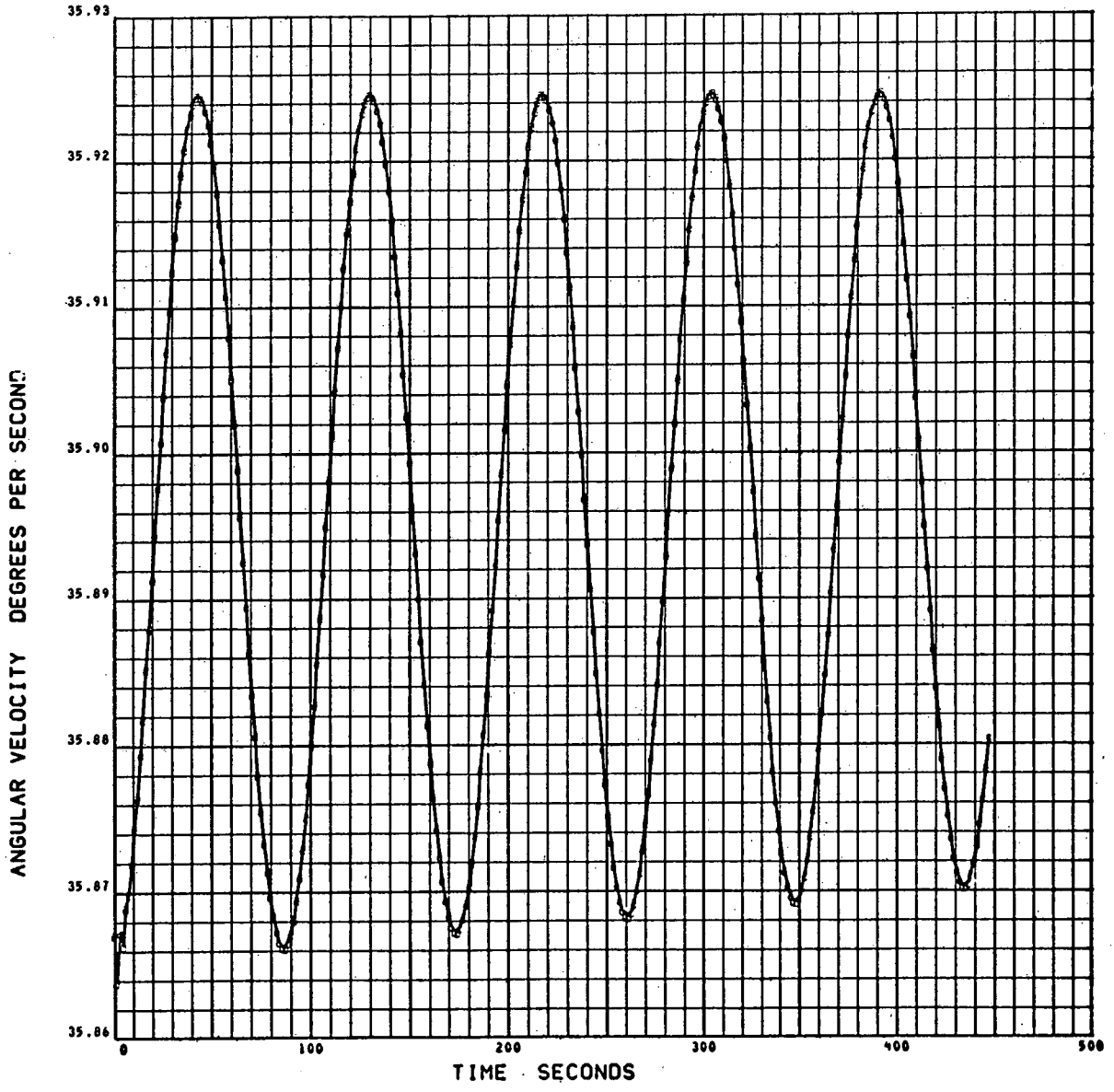

Figure 4-5. Configuration 1 Flexible Booms – Z Component of Angular Velocity

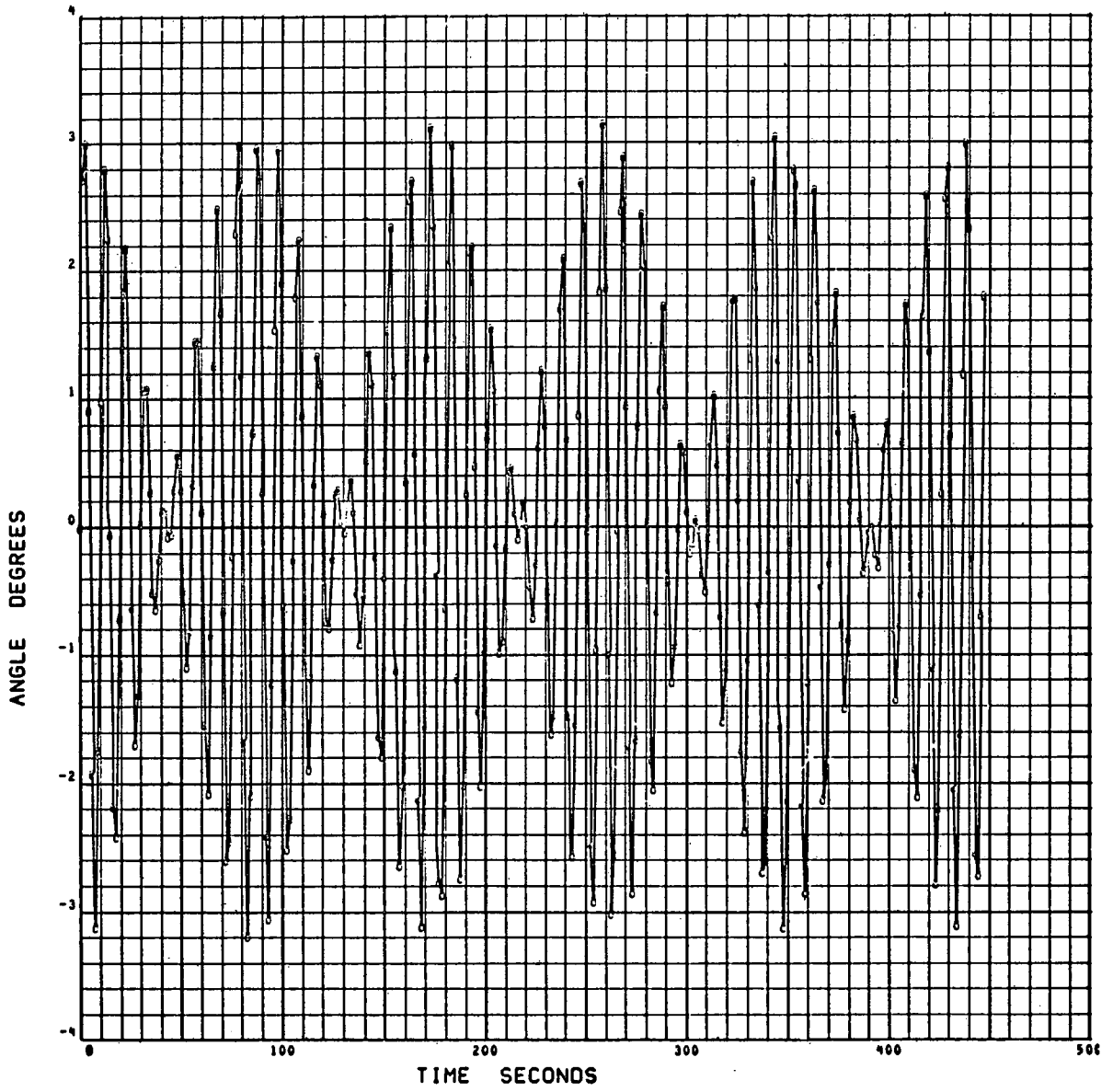

Figure 4-6. Configuration 1 Flexible Booms – Euler Angle Beta 1

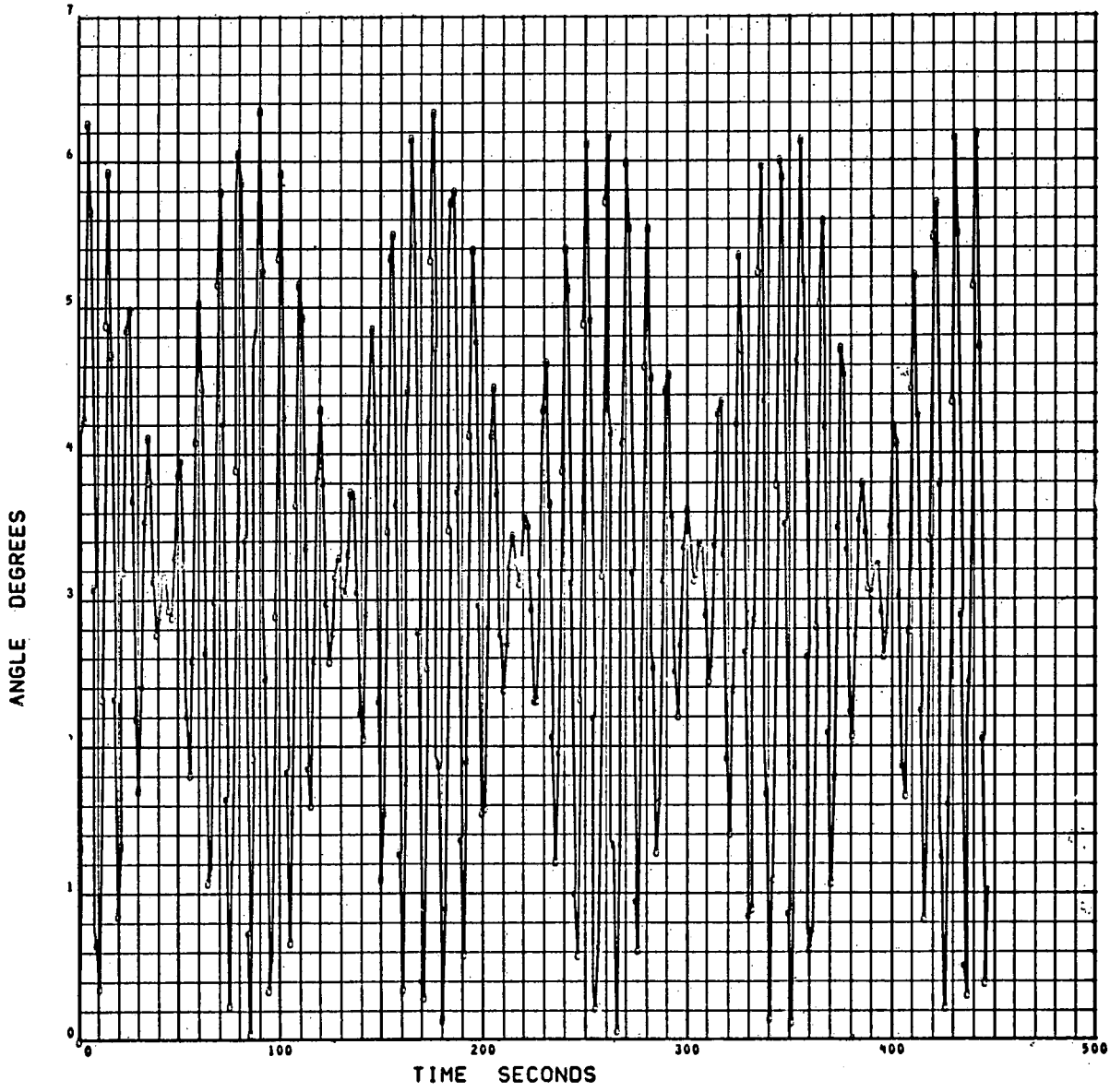

Figure 4-7. Configuration 1 Flexible Booms – Euler Angle Beta 2

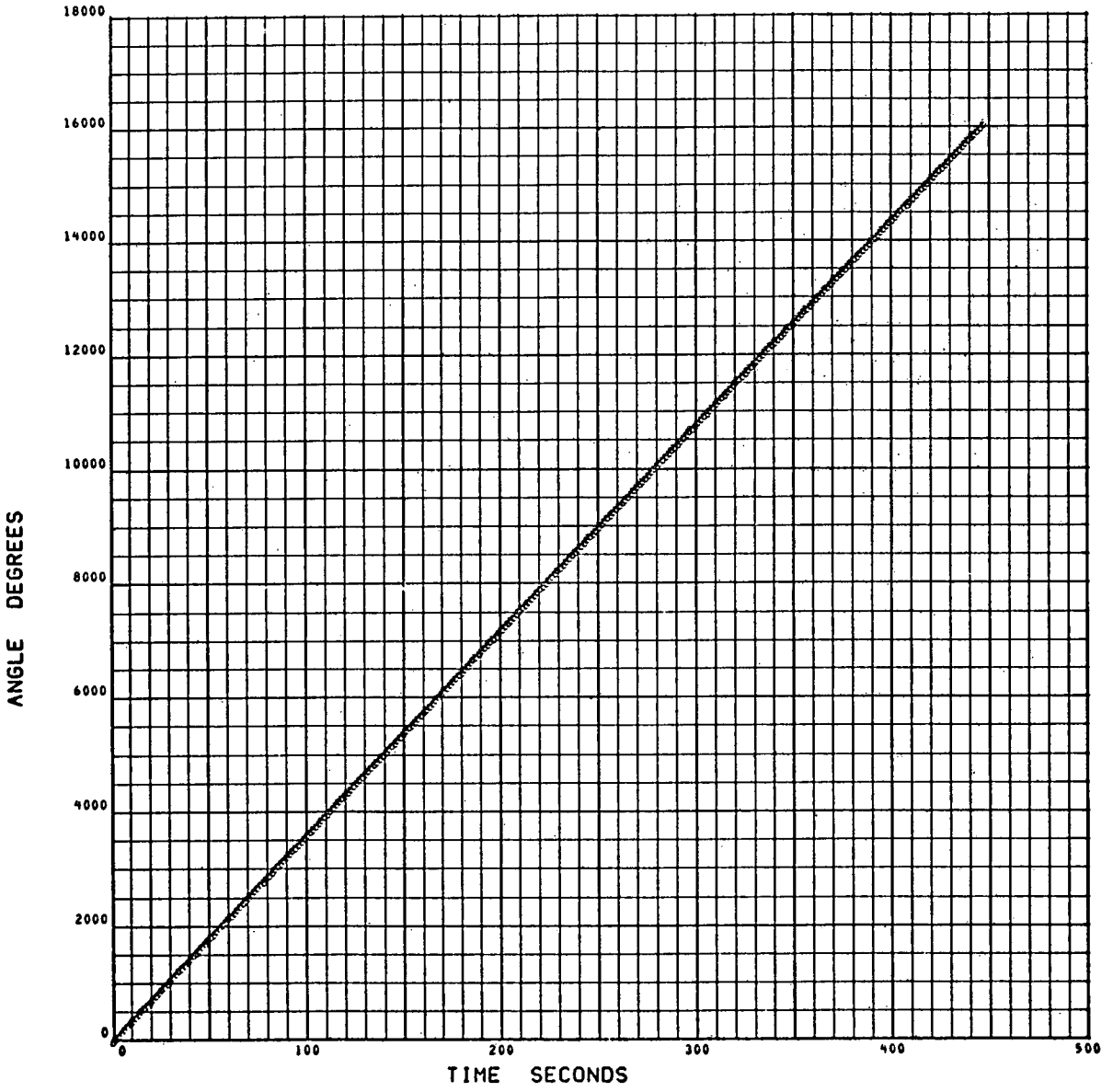

Figure 4-8. Configuration 1 Flexible Booms – Euler Angle Beta 3

B

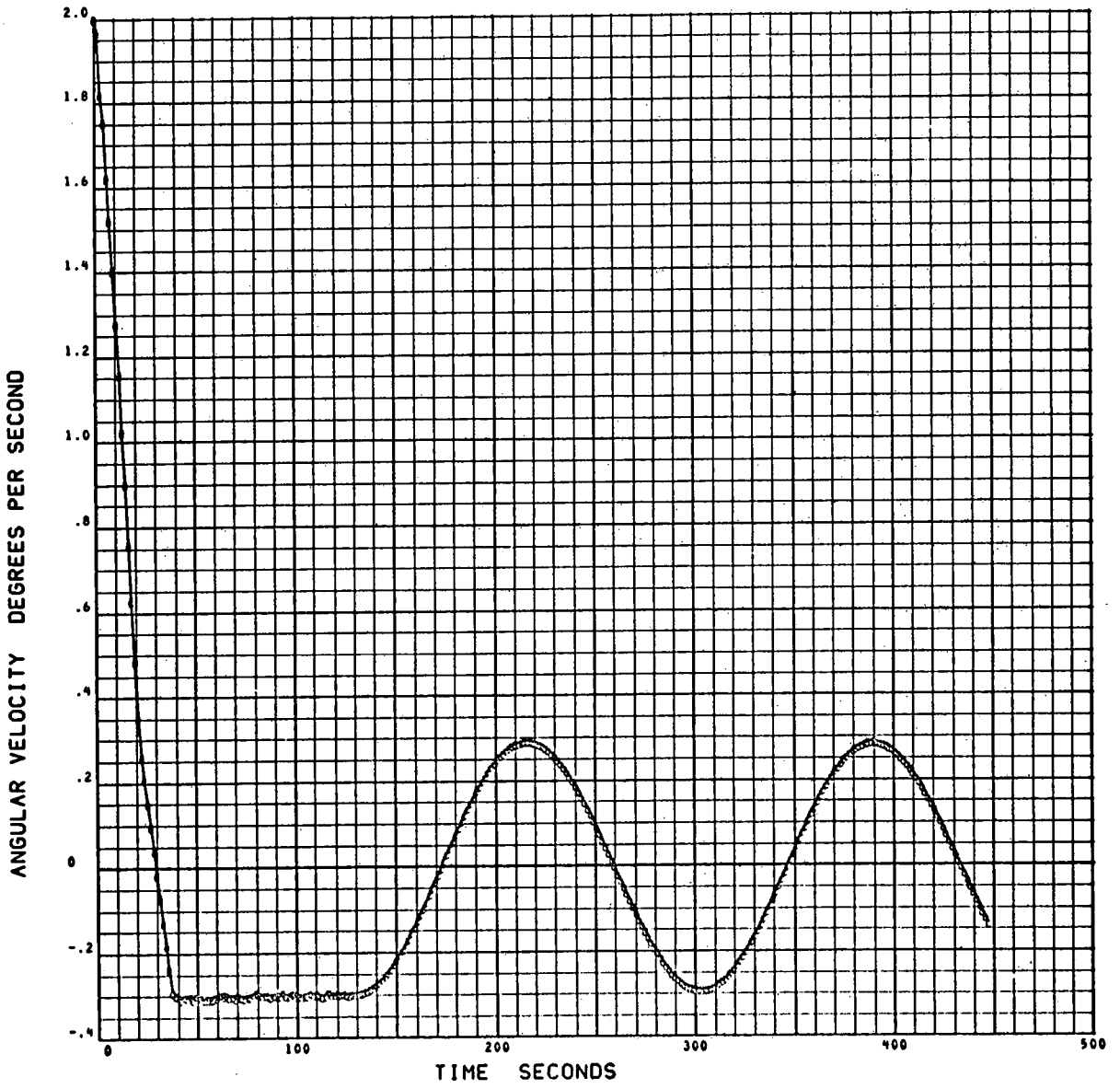

Figure 4-9. Configuration 1 RCS Wobble Damping – X Component of Angular Velocity

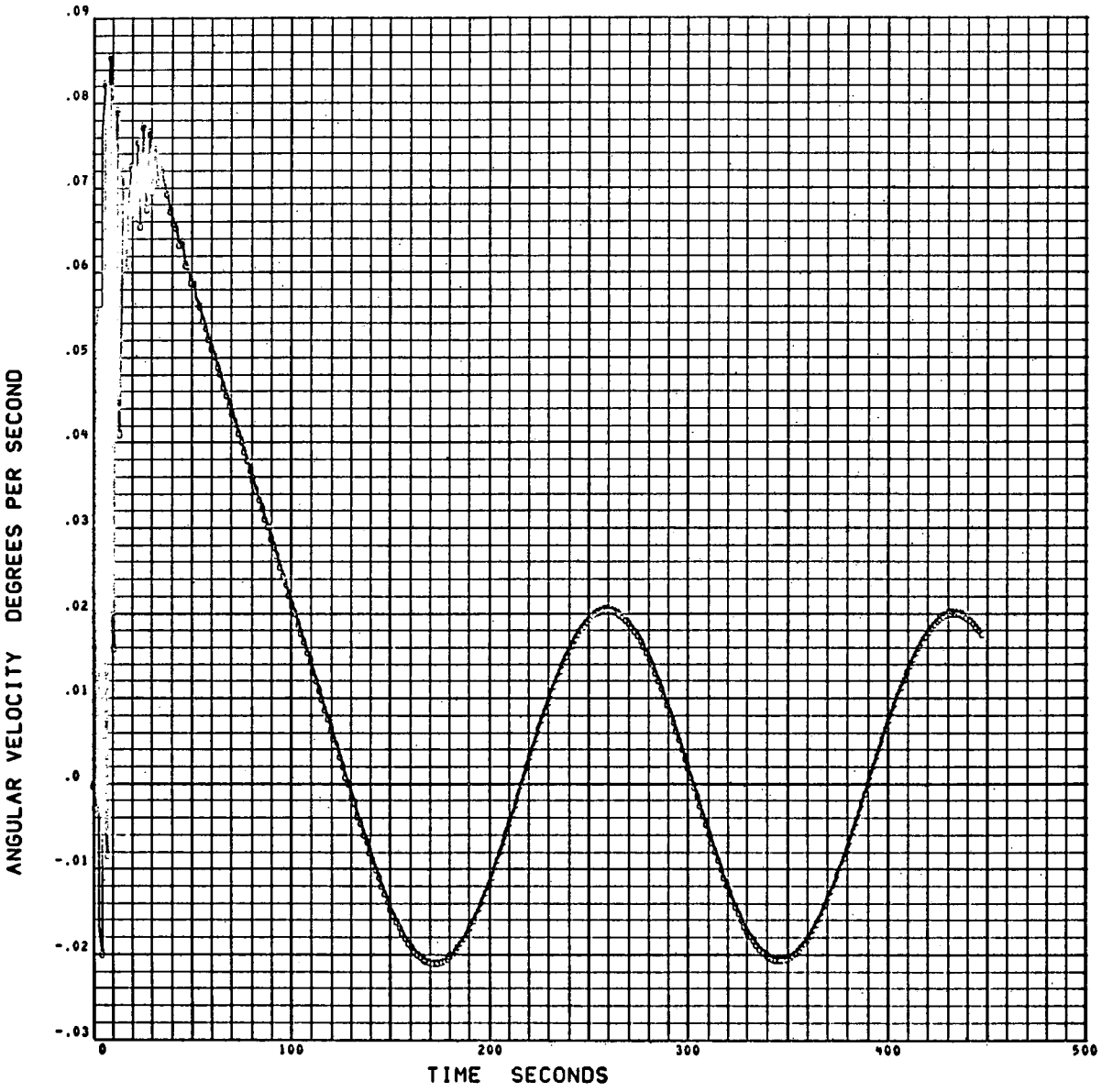

Figure 4-10. Configuration 1 RCS – Y Component of Angular Velocity

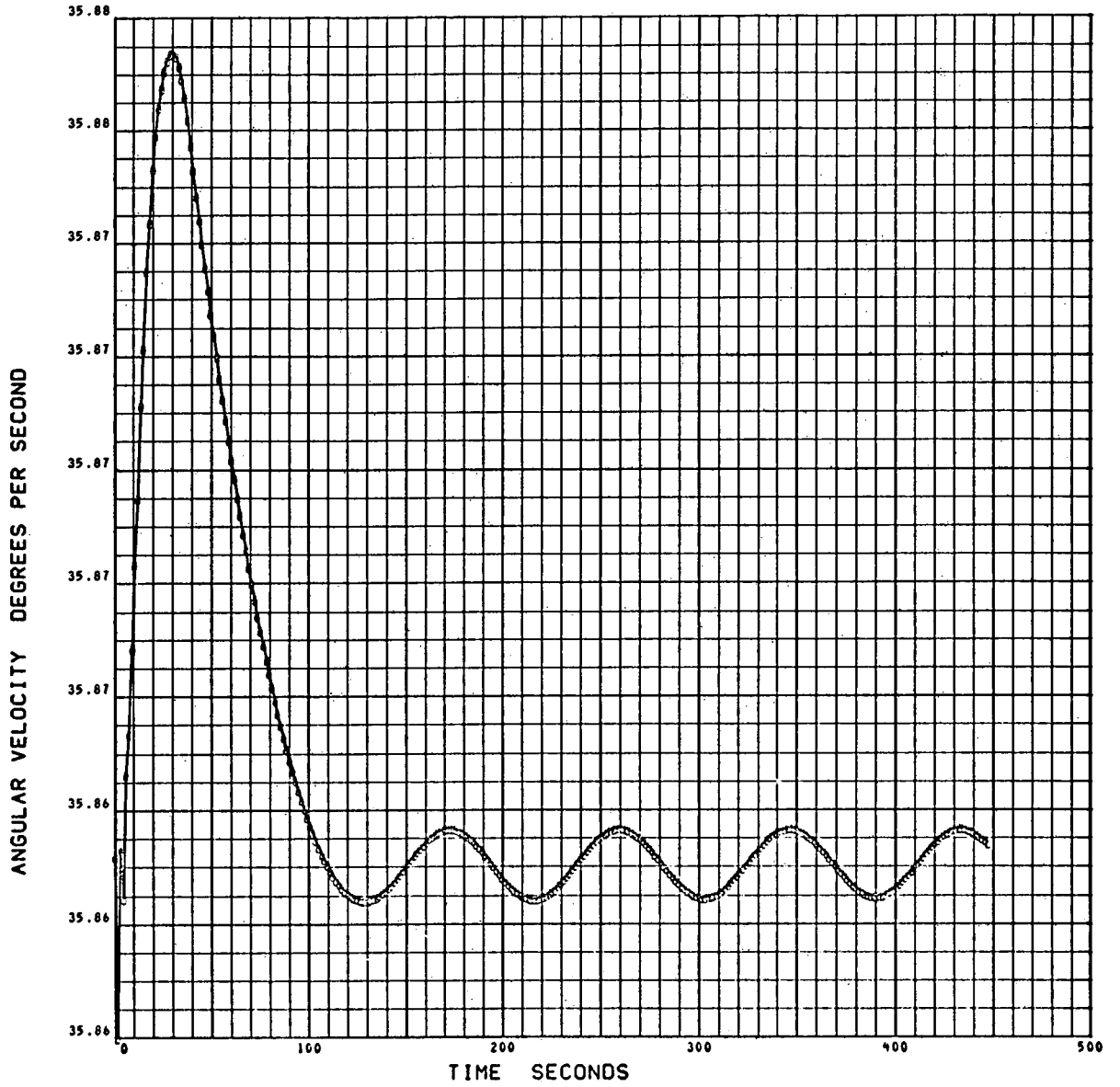

Figure 4-11. Configuration 1 RCS – Z Component of Angular Velocity

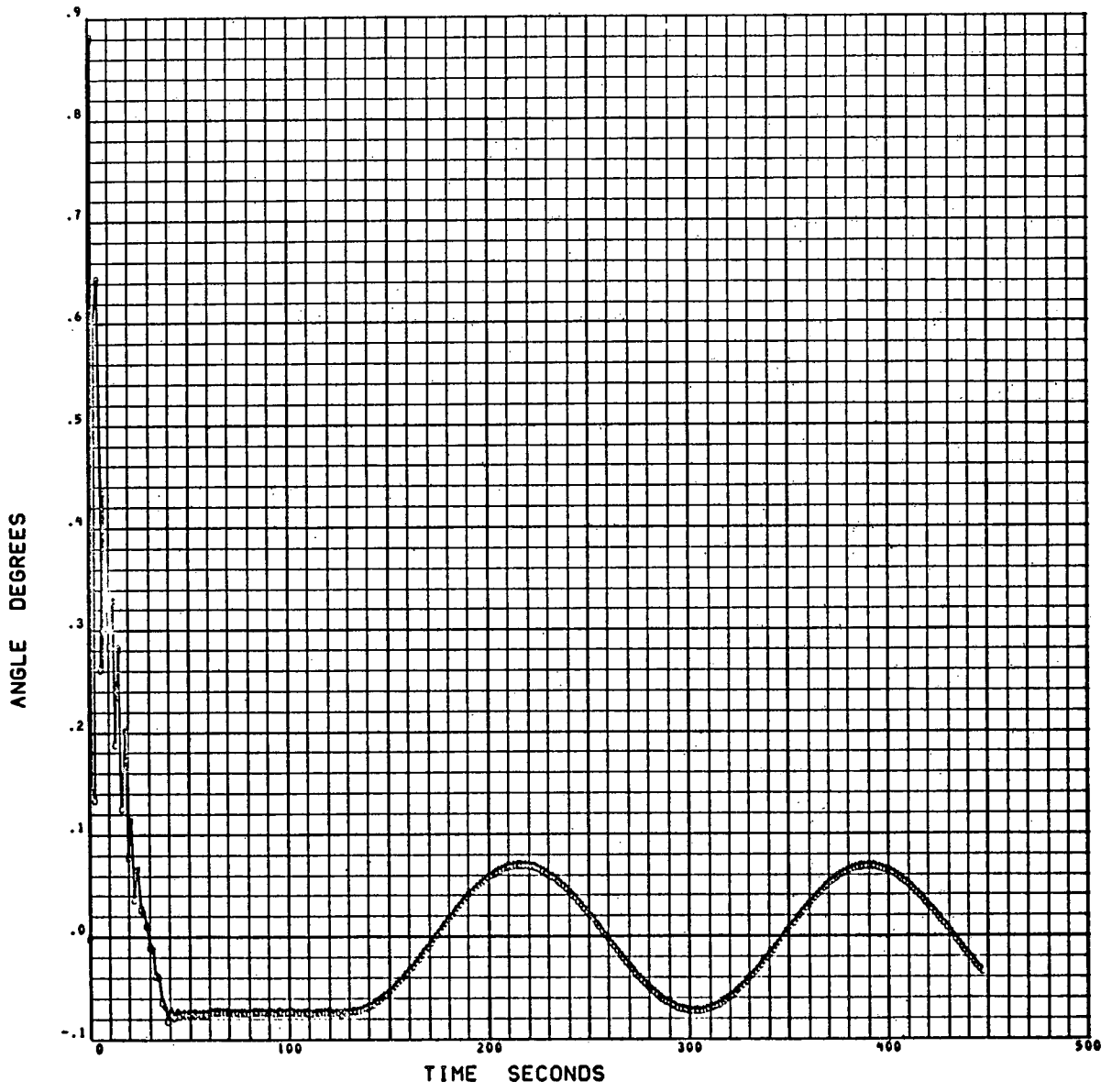

Figure 4-12. Configuration 1 RCS Damping – Boom Angle Theta

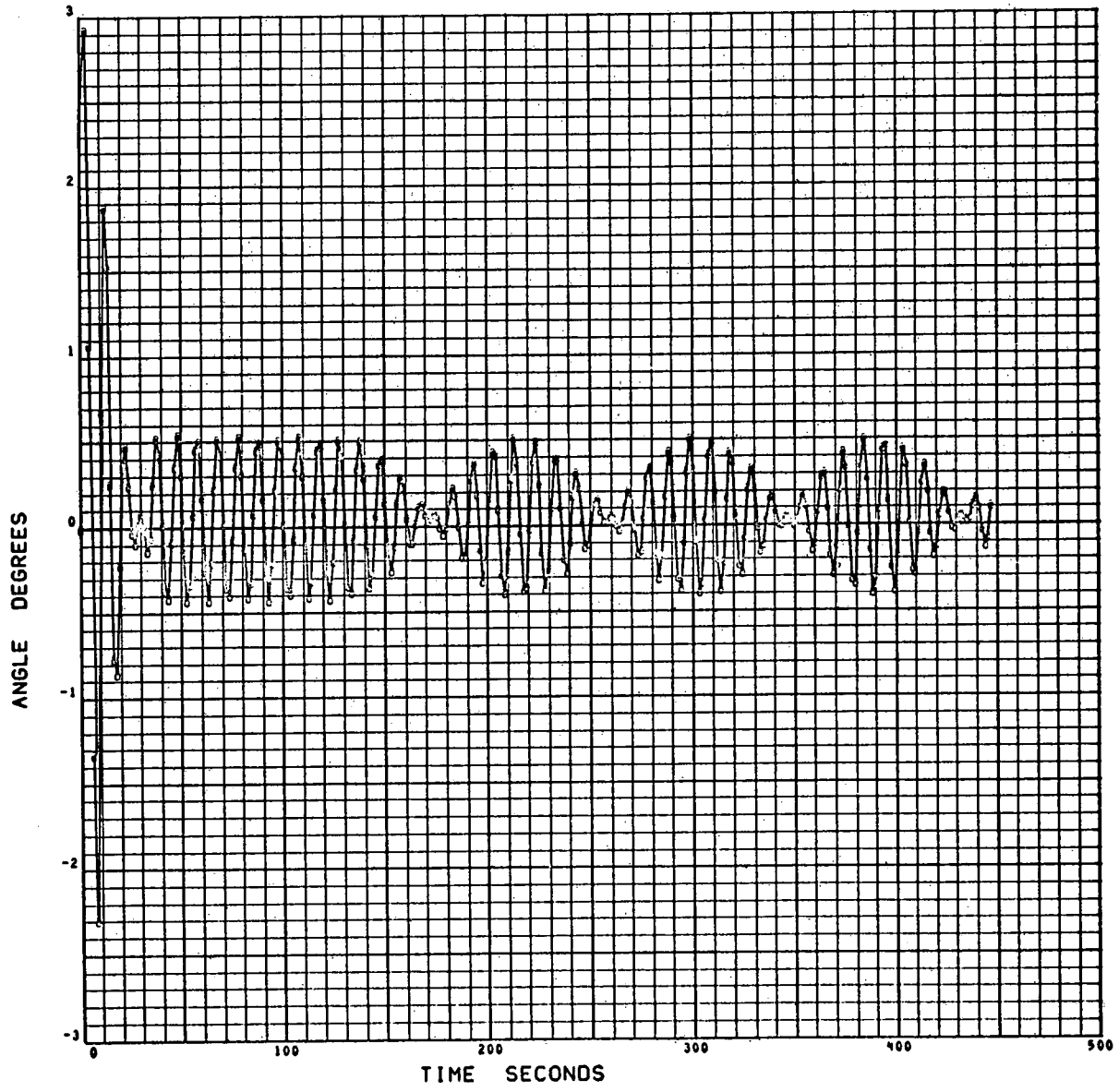

Figure 4-13. Configuration 1 RCS Damping – Euler Angle Beta 1

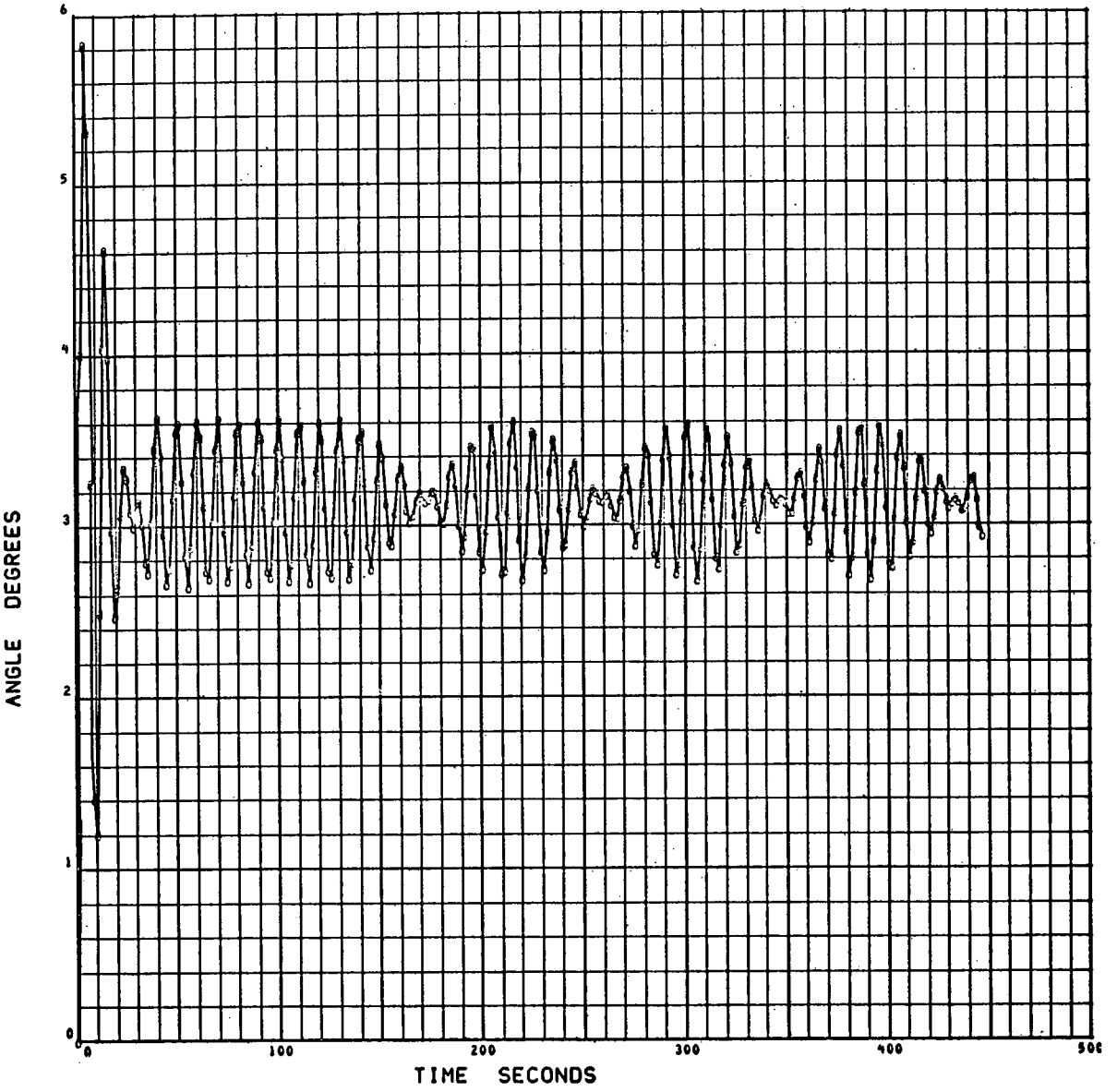

Figure 4-14. Configuration 1 RCS Damping — Euler Angle Beta 2

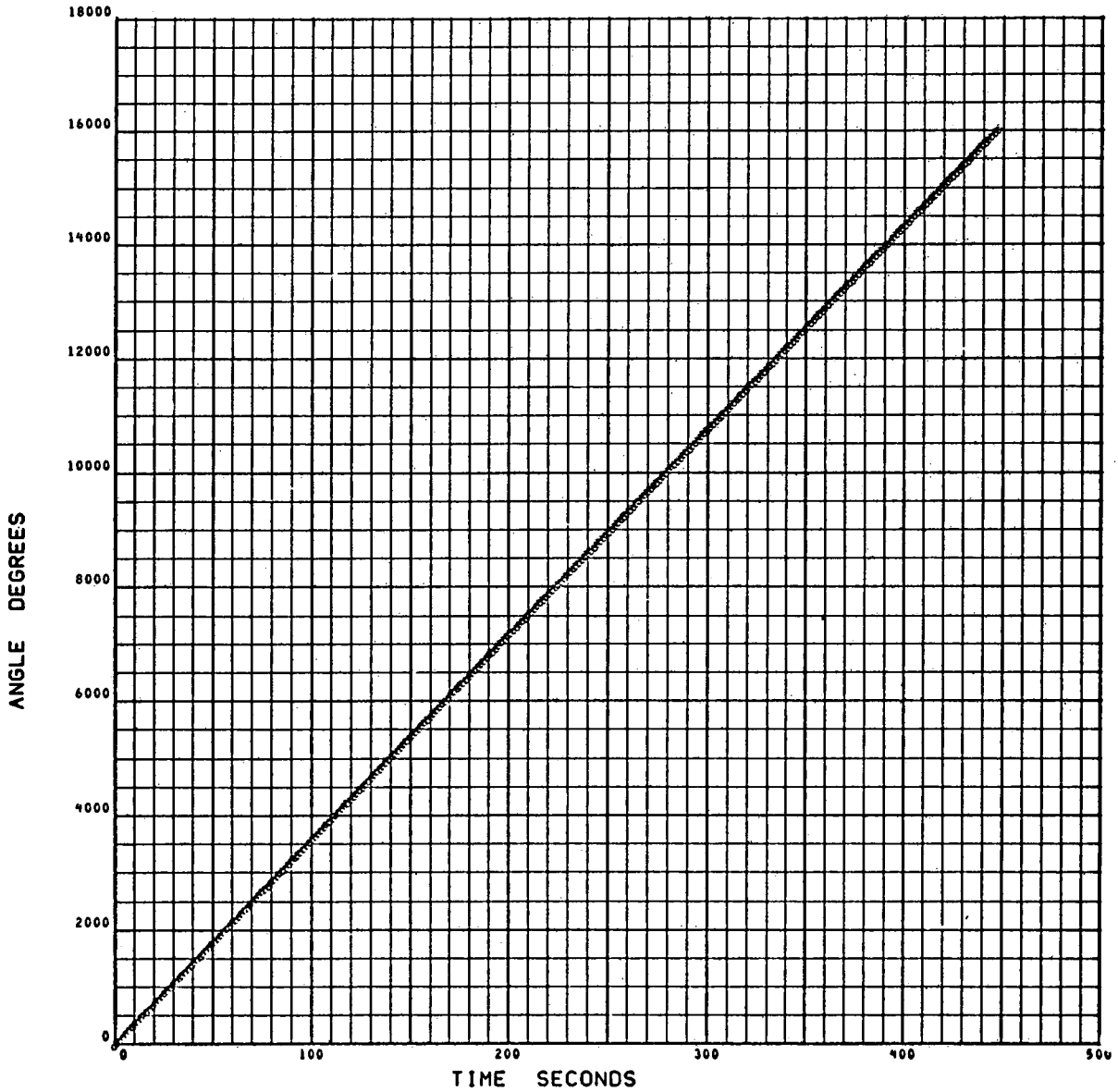

Figure 4-15. Configuration 1 RCS Damping – Euler Angle Beta 3

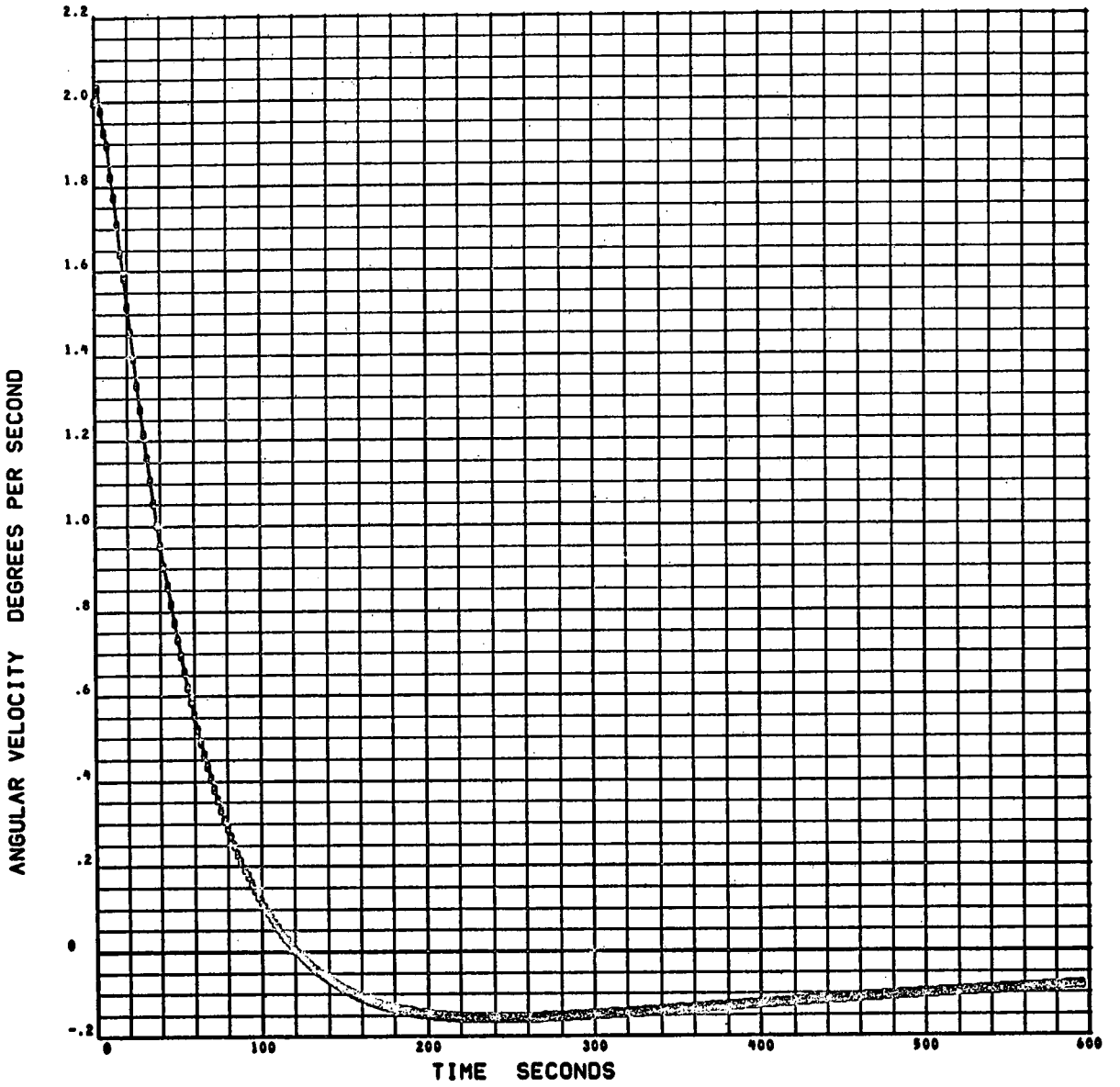

Figure 4-16. Configuration 2 CMG Damping – X Component of Angular Velocity

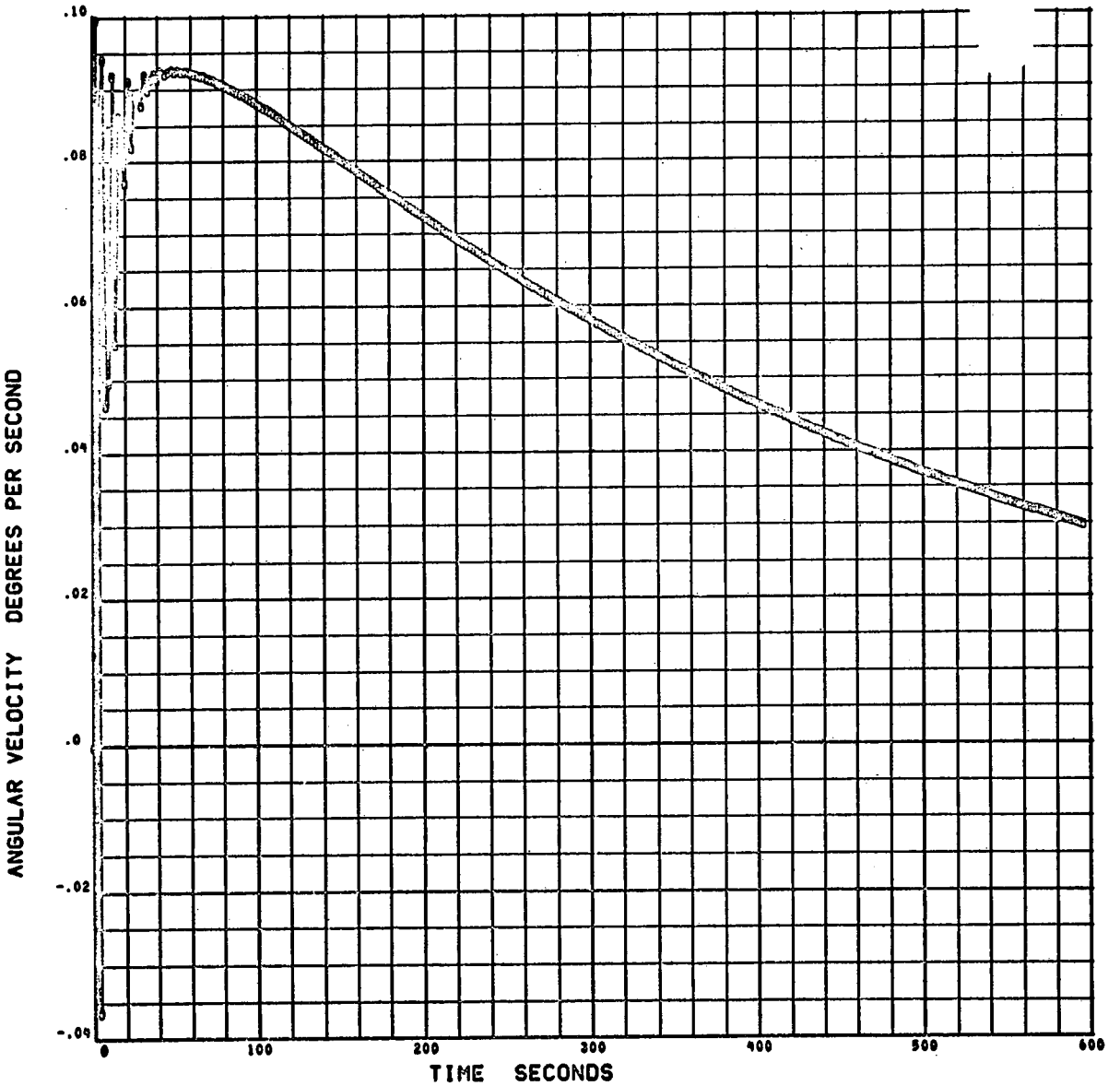

Figure 4-17. Configuration 2 CMG Damping – Y Component of Angular Velocity

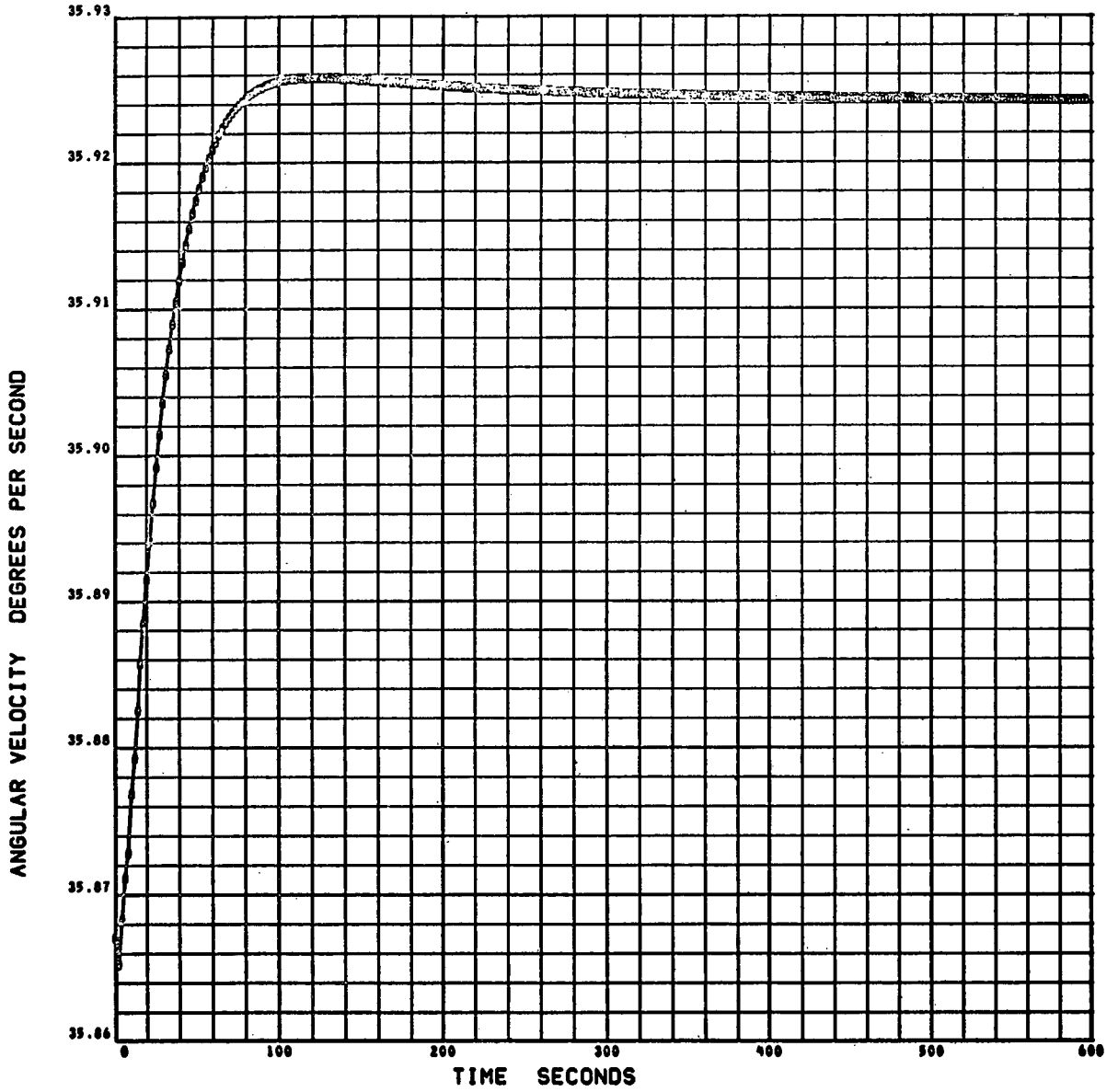

Figure 4-18. Configuration 2 CMG – Z Component of Angular Velocity

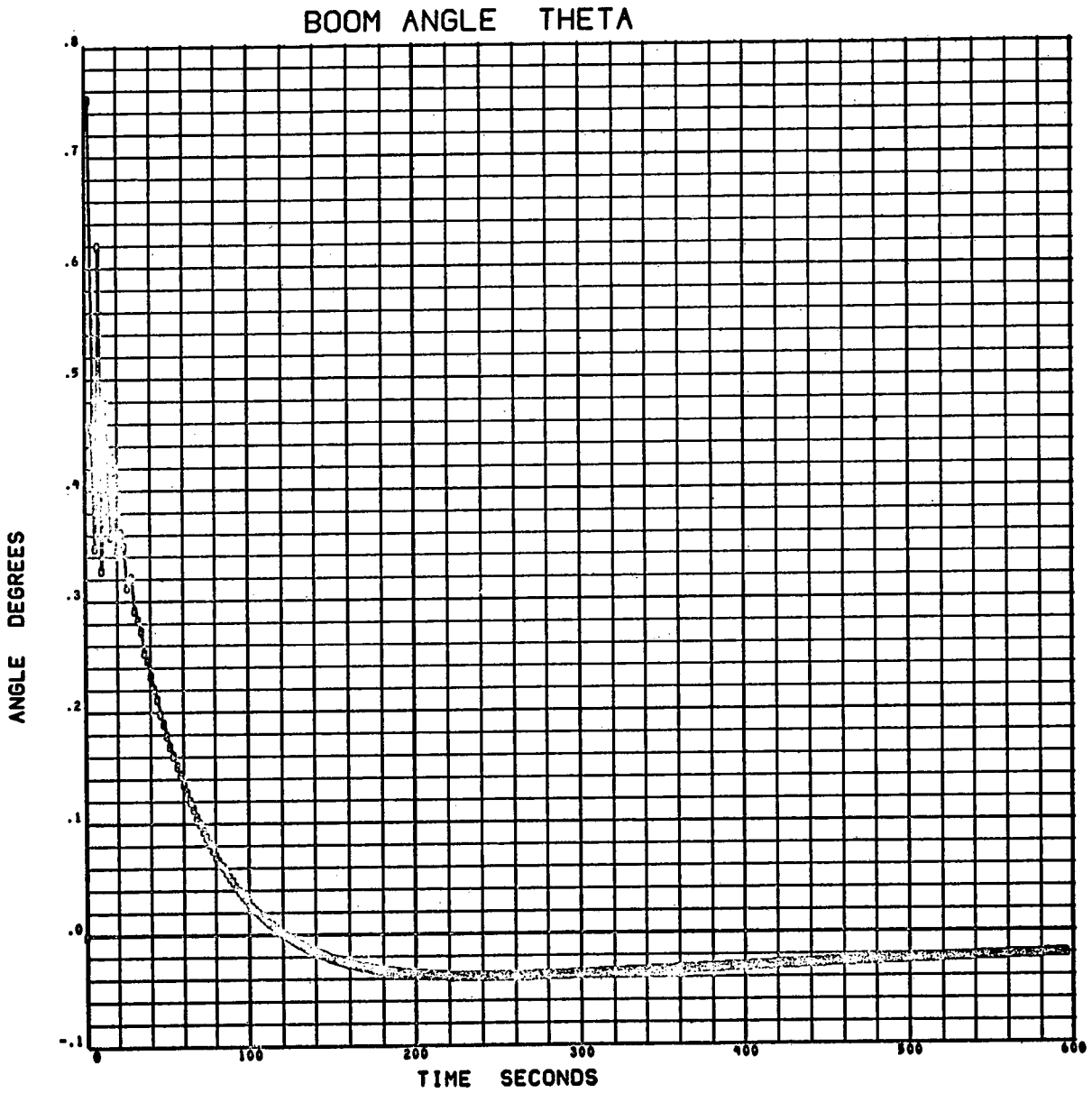

Figure 4-19. Configuration 2 CMG – Boom Angle Theta

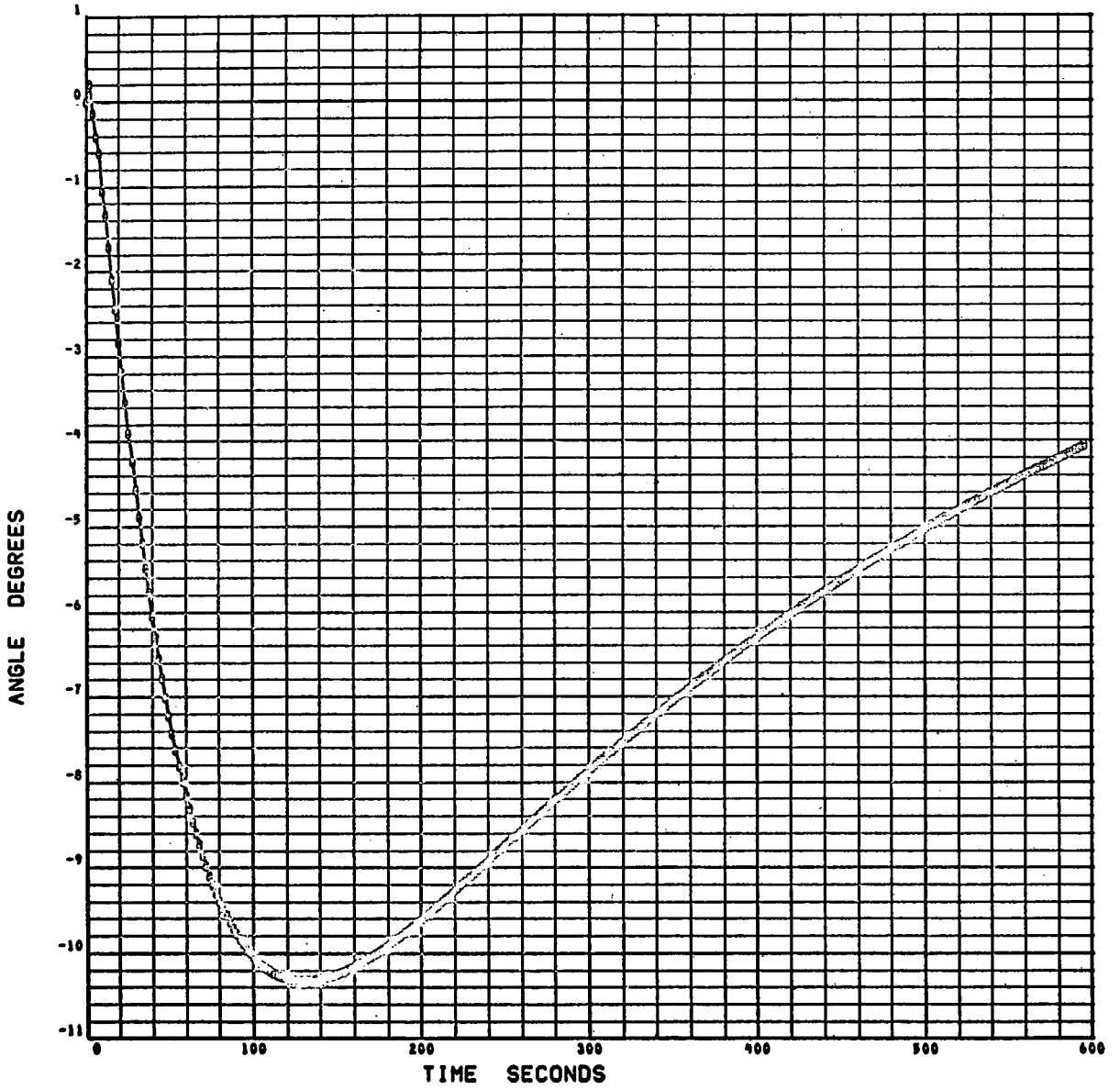

Figure 4-20. Configuration 2 CMG – Gimbal Angle

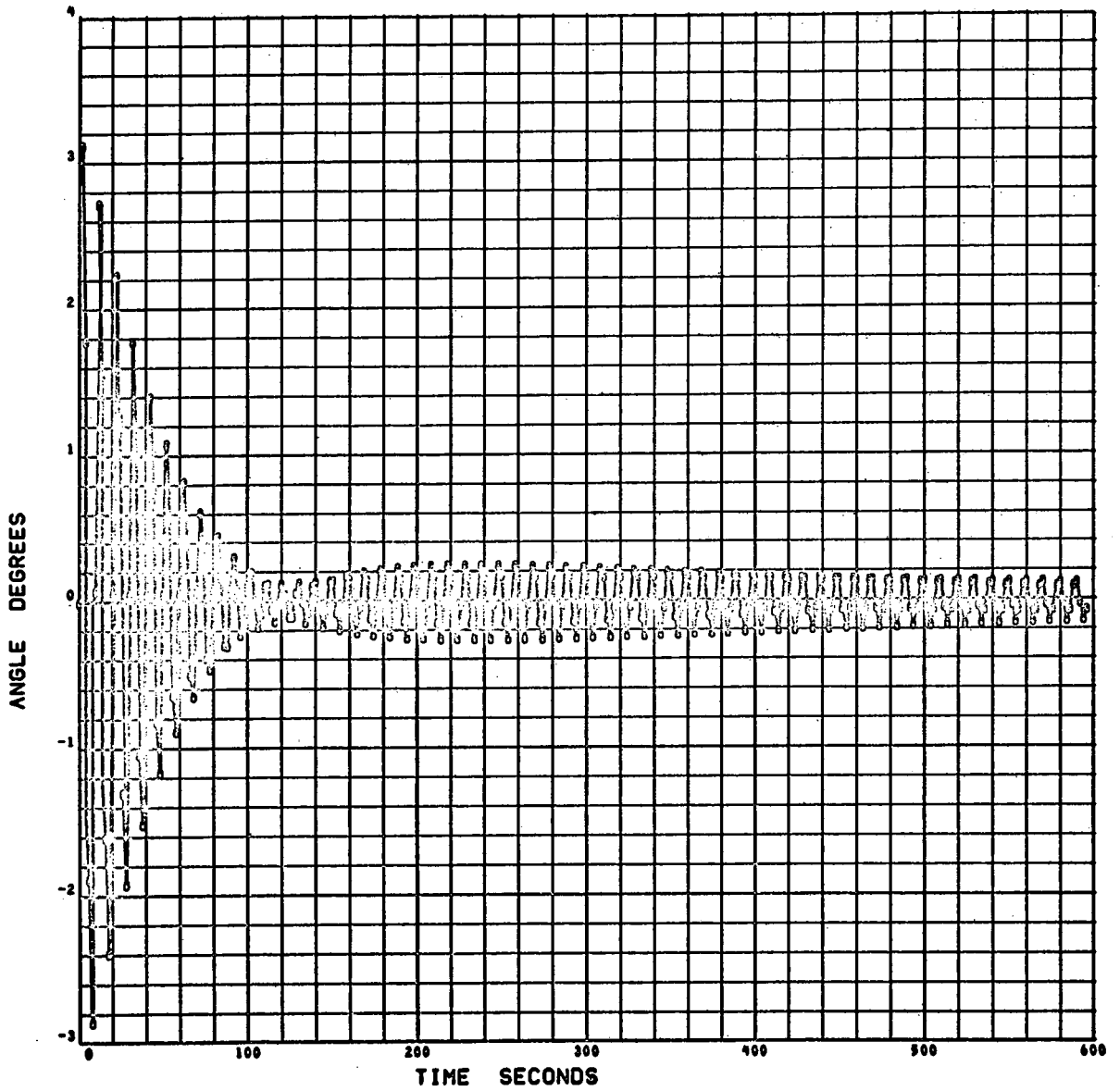

Figure 4-21. Configuration 2 CMG — Euler Angle Beta 1

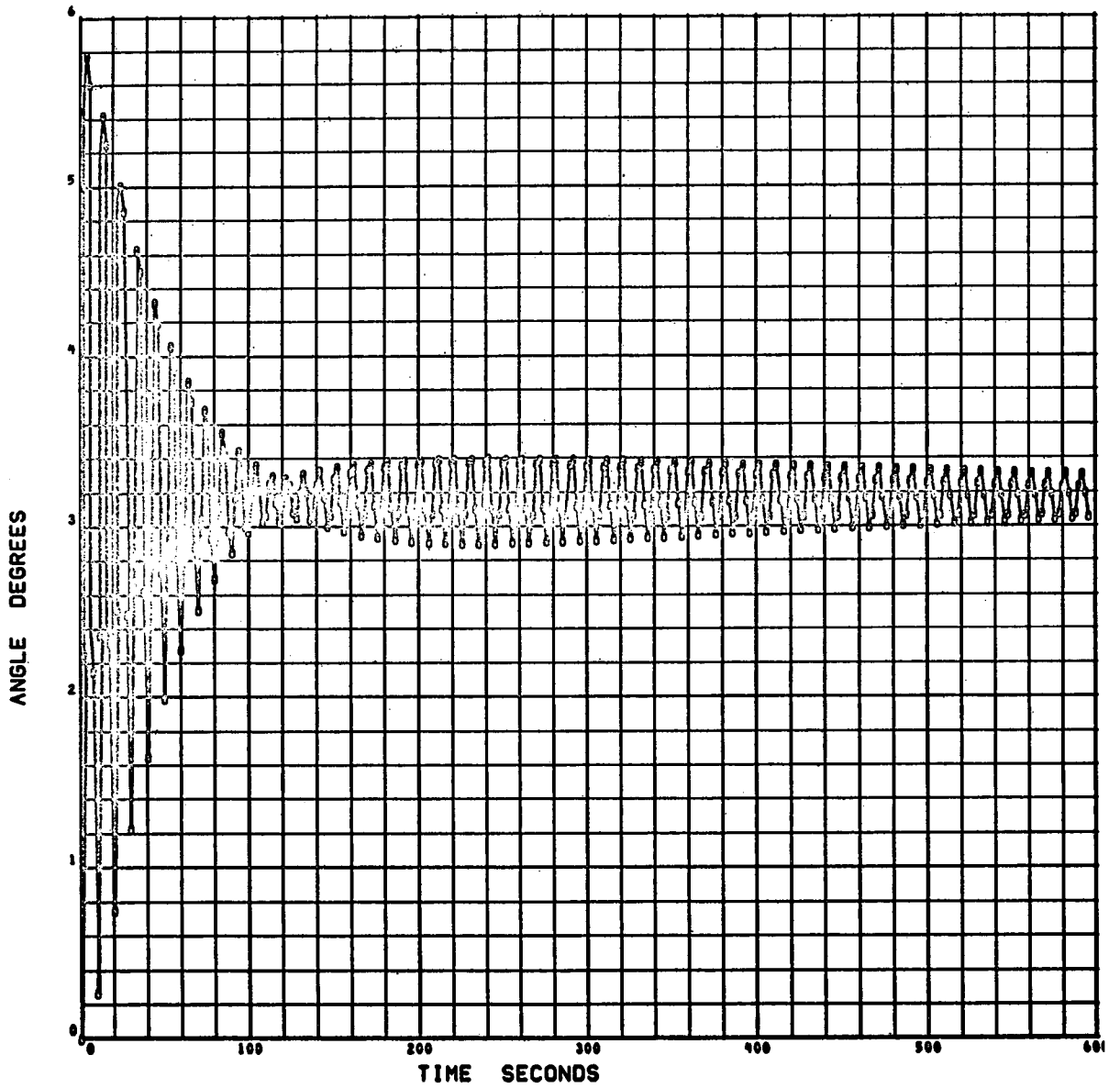

Figure 4-22. Configuration 2 CMG — Euler Angle Beta 2

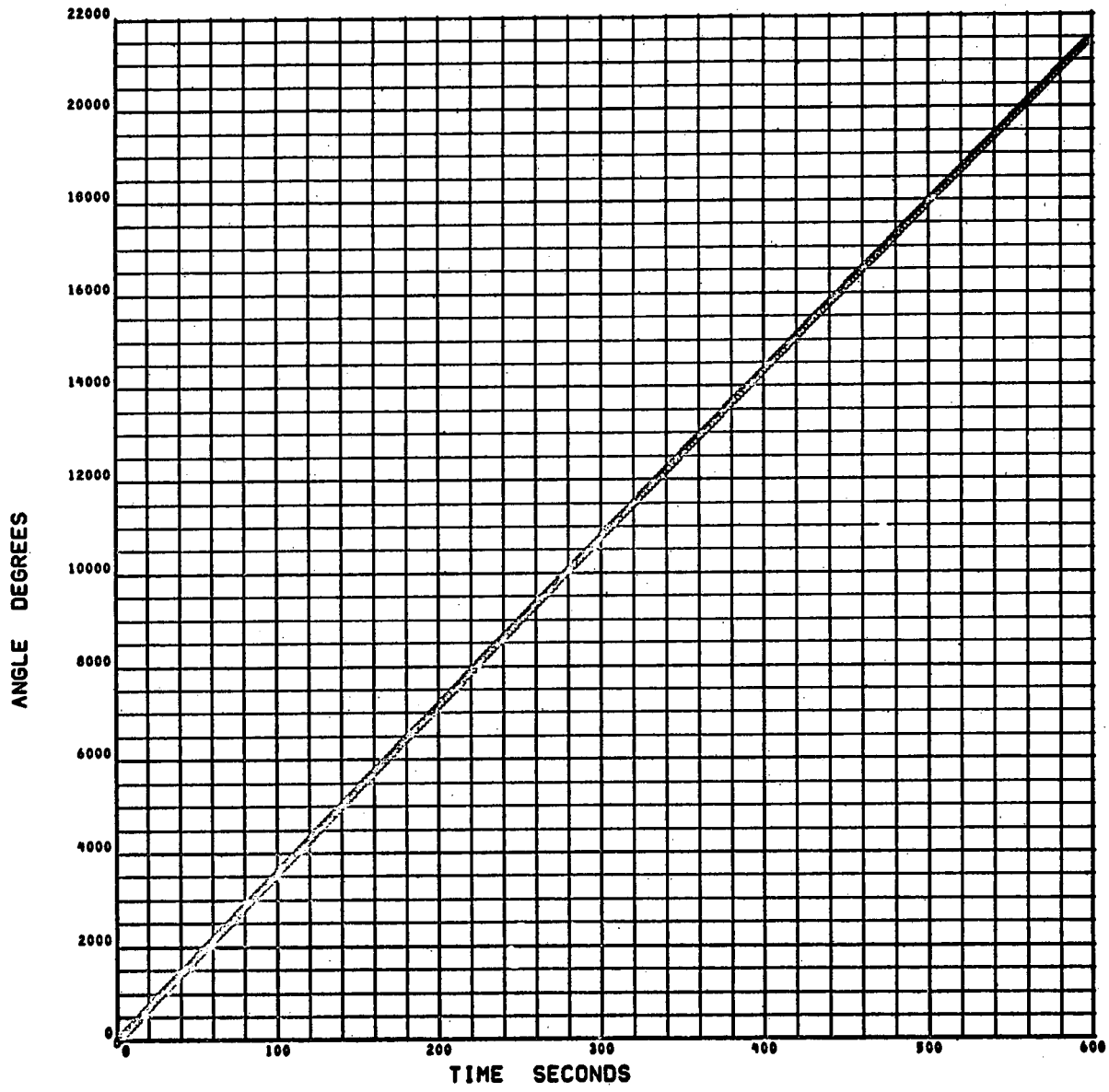

Figure 4-23. Configuration 2 CMG – Euler Angle Beta 3

Section 5
CONCLUSIONS

The rigid body behavior of the simulation system was in good agreement with theoretical expectations. The flexible boom system results were in good agreement with the predicted stability boundary and in reasonable agreement as to predicted nutation frequency when operating near the stability boundary. The RCS wobble damper functioned very well under all conditions simulated. The spin-up RCS functioned satisfactorily but was not as well aligned as is desirable. The disturbance mass and active mass systems performed excellently. The active mass system showed itself as a simple and effective wobble damper under both rigid and flexible body conditions. Simulation runs with the CMB wobble damper exhibited the increased damping ratio predicted for operation with the flexible booms as did the active mass wobble damper.

On the whole the air-bearing simulation model appears to be a very effective tool for the investigation of the interaction of control systems with spinning vehicles with flexible booms. The pressure of time and funds did not allow as much effort to be devoted to precise adjustment of the model as is desirable to exploit its full potential as a simulation tool.

Movement of center of gravity with use of RCS gas upset the static balance and resulted in the model being operated in a less well-balanced condition than would otherwise be necessary. The small misalignments in the spin-up thrustors tended to obscure the phenomena under observation. In addition these extraneous moments often, but not consistently, appear similar experimentally to product of inertia disturbances and interfere with precisely dynamically balancing the model.

It is recommended that additional effort be devoted to

A. Improving the model static and dynamic balance, a straightforward but time-consuming task.

B. Change the boom pivot bearings to flexural pivots which would then exhibit structural rather than friction damping.

C. Devise means to eliminate the small amplitude high-frequency oscillation of the active mass system.

Appendix A
DERIVATION OF EQUATIONS OF MOTION

Figure A-1 illustrates the configuration under consideration. A rigid central body of mass M and principal moments of inertia I_x, I_y, I_z is spinning with angular velocities ω_x, ω_y and $\omega_z' = \Omega + \omega_z$ where Ω is much greater than ω_x, ω_y, and ω_z. Stability augmentation booms with tip masses m_1 and m_2 and of length ℓ are hinged at the points of connection to the central body a distance d from its center of gravity. The hinges restrict motion of the booms to the x-z plane, such motion being opposed by a torsion spring of constant K_H at the hinge so that in the unperturbed state the booms are aligned with the x principal axis of the center body. The x, y, z axes form an orthogonal coordinate system with axes parallel to the principal axis of the center body and origin at the center of gravity of the system. The small displacements q_1 and q_2 of the tip masses are thus restricted to be parallel to the z axis. (It may

CR71

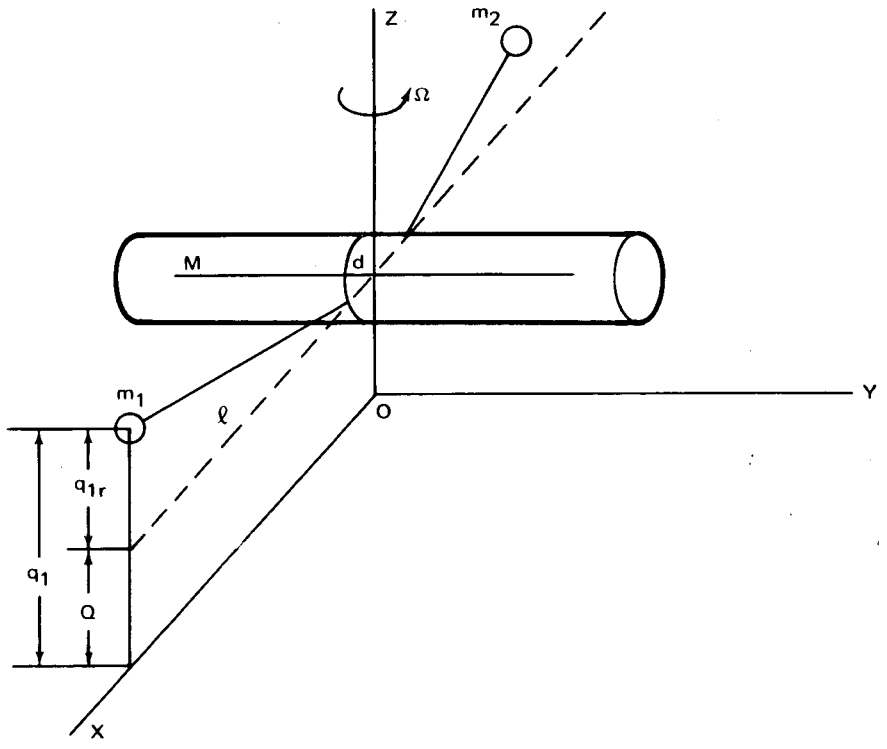

Figure A-1. Rotating Body with Flexible Stability Augmentation Booms

be shown that in-plane motions produce only second-order attitude effects.) The center body small displacement from equilibrium is Q. The displacements of the tip masses relative to the center body are q_{1r} and q_{2r}.

Although the equations of motion are developed for hinged booms, it will be subsequently shown that with minor modifications the same equations apply to tip masses supported by elastic cantilever beams.

For each of the three masses, one can write

$$m_i \vec{a}_i = \vec{F}_i \tag{A-1}$$

Where $\vec{a}_i$ is the inertial acceleration of m_i and $\vec{F}_i$ is the sum of the internal connection forces and external forces. In terms of quantities defined in the rotating coordinate system xyz,

$$\vec{a}_i = \vec{A}_o + \vec{\omega}x\vec{r}_i + 2\vec{\omega}x\dot{\vec{r}}_i + \vec{\omega}x\vec{\omega}x\vec{r}_i + \ddot{\vec{r}}_i , \tag{A-2}$$

where $\vec{A}_o$ is the acceleration of the origin o (system CG) expressed in xyz components, $\vec{\omega}$ is the inertial angular velocity vector of the center body in the xyz system, and r_i is the position vector of body i relative to o. The components of the position vectors of the bodies are;

$$\begin{aligned} \text{body } m_1,\ \vec{r}_1 &= \left[d + \ell,\ o,\ q_1 \right] \\ m_2,\ \vec{r}_2 &= \left[-(d + \ell),\ o,\ q_2 \right] \\ M,\ \vec{r} &= \left[Q_x,\ Q_y,\ Q_z \right] \end{aligned} \tag{A-3}$$

Inserting Equation (A-3) in Equation (A-2) and neglecting second-order terms gives the component equations, where the subscript e denotes external forces, for m_1

$$m_1 a_{1x} = m_1 A_{ox} - m_1 (d + \ell)\Omega^2 = F_{ix} + F_{iex} \tag{A-4}$$

$$m_1 a_{1y} = m_1 A_{oy} + m_1(d + \ell)\dot{\omega}_z = F_{1y} + F_{1ey} \tag{A-5}$$

$$m_1 a_{1z} = m_1 A_{oz} - m_1(d + \ell)\dot{\omega}_y + m_1(d + \ell)\Omega\omega_x + m_1\ddot{q}_1$$

$$= F_{1z} + F_{1ez} \tag{A-6}$$

for m_2

$$m_2 a_{ax} = m_2 A_{ox} + m_2(d + \ell)\Omega^2 = F_{2x} + F_{2ex} \tag{A-7}$$

$$m_2 a_{2y} = m_2 A_{oy} - m_2(d + \ell)\dot{\omega}_z = F_{2y} + F_{2ey} \tag{A-8}$$

$$m_2 a_{2z} = m_2 A_{oz} + m_2(d + \ell)\dot{\omega}_y - m_2(d + \ell)\Omega\omega_x + m_2\ddot{q}_2$$

$$= F_{2z} + F_{2ez} \tag{A-9}$$

for M

$$M\ddot{Q}_x + MA_{ox} = -F_{1x} - F_{2x} + F_{Mex} \tag{A-10}$$

$$M\ddot{Q}_y + MA_{oy} = -F_{1y} - F_{2y} + F_{Mey} \tag{A-11}$$

$$M\ddot{Q}_z + MA_{oz} = -F_{1z} - F_{2z} + F_{Mez} \tag{A-12}$$

If we let $m_1 = m_2 = m$ and add the corresponding component equations we obtain for the x direction,

$$M\ddot{Q}_x + (M + 2m) A_{ox} = \Sigma F_{ex} \tag{A-13}$$

Since M + 2m is the total mass of the system and A_{ox} is the x component of acceleration of the center of gravity, the second term of Equation (A-13) is equal to the right-hand side and therefore $Q_x = 0$.

Similarly for the y direction, we obtain

$$Q_y = 0$$

In the z direction, the result is

$$M\ddot{Q}_Z + m\ddot{q}_1 + m\ddot{q}_2 + (M + 2m)\, A_{oz} = \Sigma F_{ez} \qquad \text{(A-14)}$$

Reasoning as above, Equation (A-14) becomes

$$M\ddot{Q}_z + m\ddot{q}_1 + m\ddot{q}_2 = 0 \qquad \text{(A-15)}$$

Equation (A-15) implies

$$q_1 + q_2 = -\frac{M}{m} Q_z \qquad \text{(A-16)}$$

In the following, it will be assumed that no external forces are present (i.e., $\vec{F}_{Me}$, $\vec{F}_{1e}$, $\vec{F}_{2e}$, = 0), so that $A_{oz} = 0$. The internal connection forces can be expressed in terms of the small deflections of the boom relative to the center body. Figure A-2 illustrates the forces acting on a mass and the corresponding reaction forces on the boom.

CR71

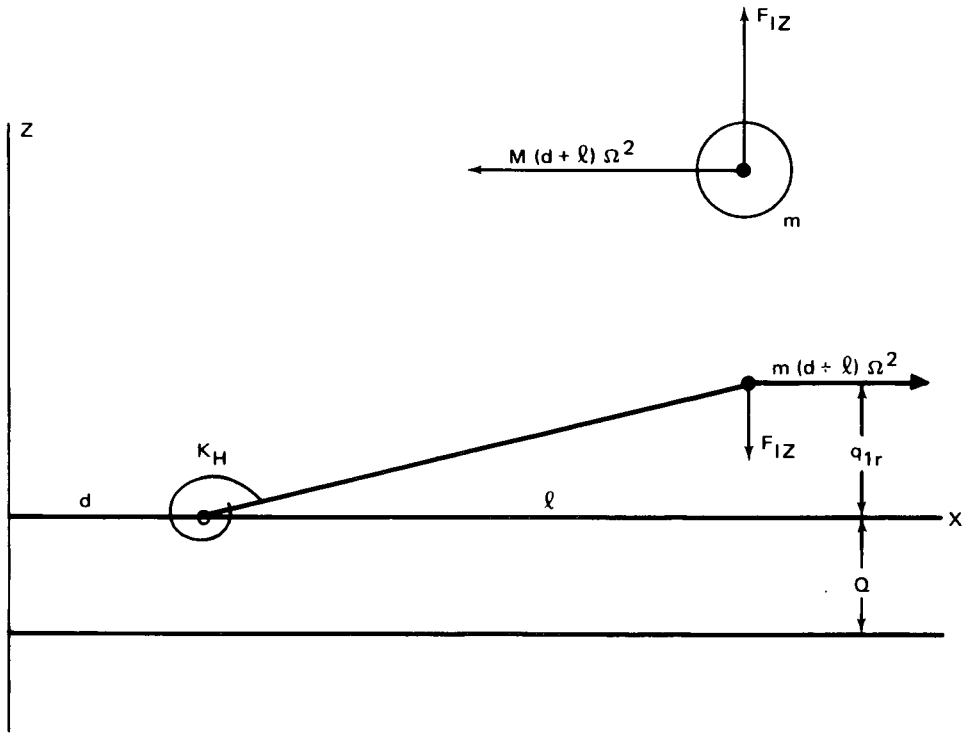

Figure A-2. Forces Acting on Mass and Boom

Summing moments about the hinge point and solving for F_{1z} we obtain,

$$F_{1z} = -\left[\frac{K_H}{\ell} + m(d + \ell)\Omega^2\right]\frac{q_{1r}}{\ell} \tag{A-17}$$

and similarly

$$F_{2z} = -\left[\frac{K_H}{\ell} + m(d + \ell)\Omega^2\right]\frac{q_{2r}}{\ell} \tag{A-18}$$

From the geometry we have, letting $Q_z = Q$,

$$q_1 = q_{1r} + Q$$

$$q_2 = q_{2r} + Q\,. \tag{A-19}$$

Inserting Equations (A-17) and (A-18) in Equation (A-12) and making use of Equations (A-16) and (A-19) yields

$$\ddot{Q}_z + \left(\frac{M + 2m}{Mm}\right)\left[m\frac{(d + \ell)}{\ell}\Omega^2 + \frac{K_H}{\ell^2}\right] Q = 0\,. \tag{A-20}$$

Now

$$\omega_s = \left[\frac{(d + \ell)}{\ell}\Omega^2 + \frac{K_H}{m\ell^2}\right]^{\frac{1}{2}}$$

is the spinning vibration frequency of the booms if they were attached to a rigid spinning shaft, thus Equation (A-20) can be written,

$$\ddot{Q} + \left(\frac{M + 2m}{M}\right)\omega_s^2 Q = 0 \tag{A-21}$$

Equation (A-21) indicates that the system can perform vibrations parallel to the z axis with m_1 and m_2 moving in the same phase and opposite in phase to M with frequency given by

$$\omega = \omega_s\left(\frac{M + 2m}{M}\right)^{\frac{1}{2}} \tag{A-22}$$

The absence of attitude variables in Equation (A-21) indicates that this translational vibration is uncoupled with the attitude motion of the system.

To arrive at the equations of angular motion of the system, we can equate the rate of change of angular momentum $\vec{H}$ to the torque $\vec{\tau}$ acting for each of the bodies.

$$\vec{H} = m_i \vec{r}_i x \vec{a}_i \quad \text{and} \quad \vec{\tau}_i = \vec{r}_i x \vec{F}_i \tag{A-23}$$

The component equations are, for m_1

$$\dot{H}_{1x} = 0 = \tau_{ix} \tag{A-24}$$

$$\dot{H}_{1y} = -m(d + \ell)\Omega^2 q_1 - m(d + \ell)\ddot{q}_1 + m(d + \ell)^2 \dot{\omega}_y$$

$$- m(d + \ell)\Omega\omega_x = \tau_{1y} \tag{A-25}$$

$$\tau_{1y} = -m(d + \ell)^2 \Omega^2 q_1 + (d + \ell)\left[\frac{K_H q_{1r}}{\ell^2} + \frac{m(d + \ell)}{\ell} \Omega^2 q_{1r}\right] \tag{A-26}$$

or

$$\tau_{1y} = m(d + \ell)\left[(\omega_s^2 - \Omega^2) q_{1r} - \Omega^2 Q\right] \tag{A-27}$$

$$\dot{H}_{1z} = m(d + \ell)^2 \dot{\omega}_z = \tau_{1z} \tag{A-28}$$

Similarly for mass 2,

$$\dot{H}_{2x} = 0 = \tau_{2x} \tag{A-29}$$

$$\dot{H}_{2y} = m(d + \ell)\Omega^2 q_2 + m(d + \ell)\ddot{q}_2 + m(d + \ell)^2 \dot{\omega}_y$$

$$- m(d + \ell)^2 \Omega\omega_x = \tau_{2y} \tag{A-30}$$

$$\tau_{2y} = -m(d + \ell)\left[\left(\omega_s^2 - \Omega^2\right)q_{2r} - \Omega^2 Q\right] \tag{A-31}$$

$$\dot{H}_{2z} = m(d + \ell)^2 \dot{\omega}_z = \tau_{2z} \tag{A-32}$$

For the center body, the corresponding $\dot{H}$ equations are the usual Euler equations for $\Omega \gg \omega_x$, ω_y

$$I_x\dot{\omega}_x + (I_z - I_y)\Omega\omega_y = -\tau_{1x} - \tau_{2x} \tag{A-33}$$

$$I_y\dot{\omega}_y + (I_x - I_z)\Omega\omega_x = -\tau_{1y} - \tau_{2y} = -M_c \tag{A-34}$$

$$I_z\dot{\omega}_z = -\tau_{1z} - \tau_{2z} \tag{A-35}$$

where τ appears with a negative sign since the connection moments occur in equal and opposite pairs.

Adding Equations (A-25) and (A-30), the equation of motion for the booms is obtained

$$m(d + \ell)\Omega^2(q_2 - q_1) + m(d + \ell)(\ddot{q}_2 - \ddot{q}_1) + 2m(d + \ell)^2 \dot{\omega}_y$$

$$- 2m(d + \ell)^2\Omega\omega_x = M_c \tag{A-36}$$

$$M_c = -m(d + \ell)(\omega_s^2 - \Omega^2)(q_{2r} - q_{1r}) \tag{A-37}$$

Equation (A-19) shows that $(q_{2r} - q_{1r}) = q_2 - q_1$, if we let

$$q_2 - q_1 = 2\ell\theta \tag{A-38}$$

Equation (A-36) may be written

$$2m\ell(d + \ell)\ddot{\theta} + 2m(d + \ell)^2 \dot{\omega}_y + 2m\ell(d + \ell)\Omega^2\theta - 2m(d + \ell)^2\Omega\omega_x$$

$$= M_c = -2m\ell(d + \ell)(\omega_s^2 - \Omega^2)\theta \tag{A-39}$$

D

dividing through by the coefficient of the first term Equation (A-39) can be written

$$\ddot{\theta} + \omega_s^2 \theta + \frac{d + \ell}{\ell} \dot{\omega}_y - \frac{d + \ell}{\ell} \Omega \omega_x = 0 \qquad \text{(A-40)}$$

Inserting the appropriate expressions for τ, Equations (A-33) through (A-35) become

$$I_x \dot{\omega}_x + (I_z - I_y)\Omega \omega_y = 0 \qquad \text{(A-41)}$$

$$I_y \dot{\omega}_y + (I_x - I_z)\Omega \omega_x = 2m\ell(d + \ell)(\omega_s^2 - \Omega^2)\theta \qquad \text{(A-42)}$$

$$I_z \dot{\omega}_z = -2m(d + \ell)^2 \dot{\omega}_z \qquad \text{(A-43)}$$

Equations (A-40), (A-42), and (A-43) then are the equations of free motion of the system. (Equation (A-43) merely indicates that $\dot{\omega}_z = 0$.) It will be noted that M_c, the connection moment, occurs on the right side of Equations (A-39) and (A-42) (with opposite signs). In order to determine the equation of motion for a system with cantilever booms, it is necessary to insert the corresponding connection moment expression.

Figure A-3 illustrates a massless uniform beam of length ℓ mounted a distance d from the spin axis, (i.e., the portion d is rigid) with a concentrated mass m mounted at the tip and spinning with angular velocity Ω. The beam is subject to a deflecting force F and a tension $P = m(d + \ell)\Omega^2$.

The basic beam equation is

$$EI\, Y'' = M(x) \; . \qquad \text{(A-44)}$$

where EI is the flexural rigidity of the beam, $Y'' = d^2y/dx^2$, M(x) is the bending moment applied at point x (origin taken at d), and Y is the lateral deflection. The moment is given by

$$M(x) = F(\ell - x) - P\left[Y(\ell) - Y(x)\right] . \qquad \text{(A-45)}$$

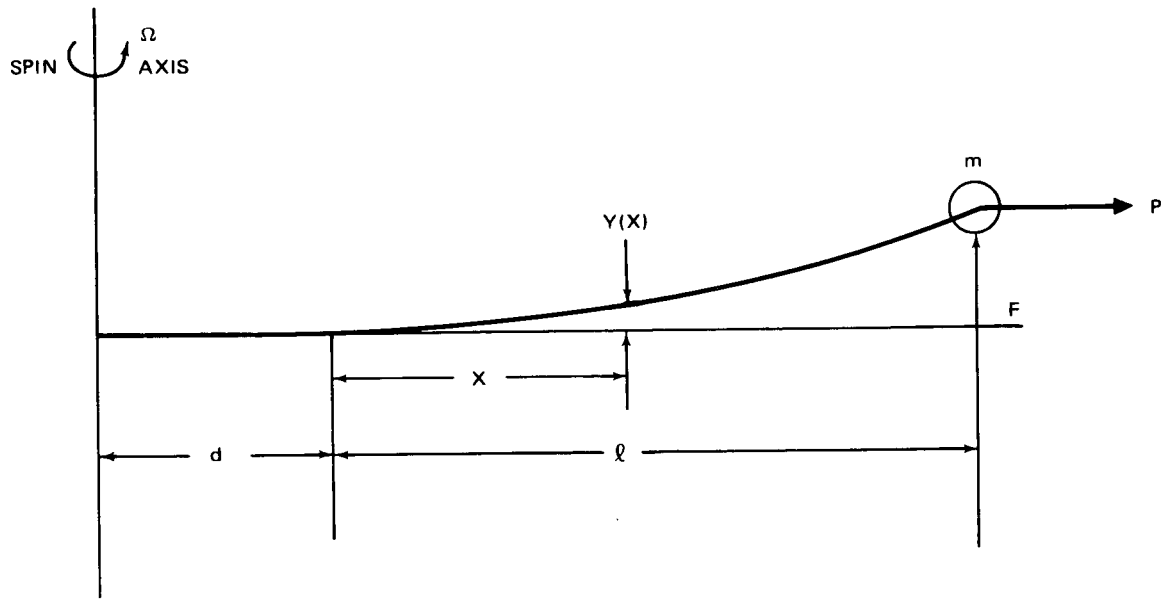

Figure A-3. Stiffness of a Spinning Boom

Differentiating and combining Equations (A-44) and (A-45) yields,

$$Y''' - \frac{P}{EI} Y' = - \frac{F}{EI} \tag{A-46}$$

with end conditions

$$Y(o) = Y'(o) = 0; \; Y''(\ell) = 0 \; . \tag{A-47}$$

Let $\alpha^2 = P/EI$. Laplace transforming Equation (A-46) and using the end conditions at x = 0 gives the transform of the solution as,

$$Y(S) = - \frac{F}{EI \, S^2 (S^2 - \alpha^2)} + \frac{Y''(o)}{S(S^2 - \alpha^2)} \; . \tag{A-48}$$

The inverse transform of Equation (A-48) is

$$Y(x) = - \frac{F}{EI\alpha^2} \left(\frac{1}{\alpha} \sinh \alpha x - x \right) + \frac{Y''(o)}{\alpha^2} (\cosh \alpha x - 1) \; . \tag{A-49}$$

Differentiating Equation (A-49) twice and using the condition that $Y''(\ell) = 0$ enables determination of $Y''(o)$ as

$$Y''(o) = \frac{F}{EI\alpha} \tanh \alpha\ell \ . \tag{A-50}$$

Inserting Equation (A-50) in Equation (A-49) produces the complete solution

$$Y(x) = \frac{F}{EI\alpha^3} \left[\alpha x - \sinh \alpha x + \tanh \alpha\ell \, (\cosh \alpha x - 1)\right] \ . \tag{A-51}$$

The tip deflection at $x = \ell$ is given by

$$Y(\ell) = \frac{F}{EI\alpha^3}(\alpha\ell - \tanh \alpha\ell) = \frac{F}{P} \left(\ell - \frac{1}{\alpha} \tanh \alpha\ell\right) \ . \tag{A-52}$$

The spring constant is given by

$$K = \frac{F}{Y} = \frac{P}{\ell - \frac{1}{\alpha} \tanh \alpha\ell} \ . \tag{A-53}$$

Vibration frequency of spinning cantilever. The spinning frequency ω_s, is given by

$$\omega_s^2 = \frac{K}{m} = \frac{P}{m(\ell - \frac{1}{\alpha} \tanh \alpha\ell)} \quad \frac{(d + \ell)}{\ell} \Omega^2 \quad \frac{1}{(1 - \frac{1}{\alpha\ell} \tanh \alpha\ell)} \tag{A-54}$$

This can be expanded in a series for purposes of comparison with the hinged boom solution as follows;

Let $\beta = \alpha\ell$ then Equation (A-54) can be written

$$\omega_s^2 = \frac{EI}{m\ell^3} \left(\frac{\beta^3}{\beta - \tanh \beta}\right) \tag{A-55}$$

Let

$$f = \frac{\beta^3}{\beta - \tanh\beta}, \text{ and } g = \frac{1}{f} = \frac{\beta - \tanh\beta}{\beta^3} \tag{A-56}$$

then using the series expansion for $\tanh\beta$

$$g = \frac{1}{3} - \frac{2}{15}\beta^2 + \frac{17}{315}\beta^4 - \frac{62}{2835}\beta^6 + \ldots \tag{A-57}$$

f can be expanded in a Taylor series in

$$f(\beta) = f(o) + f'(o)\beta + \frac{f''(o)\beta^2}{21} + \ldots \tag{A-58}$$

and

$$f(o) = \frac{1}{g(o)}, \quad f'(o) = -\frac{g'(o)}{g^2(o)}, \quad \text{etc}$$

as a result of these operations we obtain

$$f(\beta) = 3 + \frac{6}{5}\beta^2 - \frac{1}{175}\beta^4 + \ldots \tag{A-59}$$

and

$$\omega_s^2 = \frac{3EI}{m\ell^3} + \frac{6}{5}\frac{(d+\ell)}{\ell}\Omega^2 - \frac{1}{175}\frac{m\ell(d+\ell)^2\Omega^4}{EI} + \ldots \tag{A-60}$$

the first term is ω_B^2, the nonspinning natural frequency.

Accuracy of Approximation

If we use the first two terms of the series as an approximation, the accuracy can be estimated by a representative numerical example.

Let $\Omega = 0.63$ rad/sec, $\omega_B = 0.55$ rad/sec, $m = 189.17$ kg (13 slugs), $d = 0$, $\ell = 30.48$m (100 ft),

then

$$\alpha\ell = \frac{\Omega}{\omega_B}\left[\frac{3(d+\ell)}{\ell}\right]^{\frac{1}{2}} = 1.98393 \tag{A-61}$$

$$\omega_s = \left[\frac{d+\ell}{\ell}\,\frac{\Omega^2}{1-\frac{1}{\alpha\ell}\tanh\alpha\ell}\right]^{\frac{1}{2}} = 0.87817 \tag{A-62}$$

$$\omega_s = \left(\omega_B{}^2 + \frac{6}{5}\,\frac{(d+\ell)}{\ell}\,\Omega^2\right)^{\frac{1}{2}} = 0.88249 \text{ rad/sec}$$

the difference is 0.00432 rad/sec or 0.49 percent. The moment exerted on the central body about the cg is

$$M_c = F(d+\ell) - PY \tag{A-63}$$

Let $\theta = Y/\ell$ then since

$$\omega_s{}^2 = K/m = \frac{F}{Ym} = \frac{F}{m\ell\theta} \tag{A-65}$$

and

$$P = m(d+\ell)\Omega^2 \tag{A-65}$$

$$M_c = m\ell(d+\ell)\,(\omega_s{}^2 - \Omega^2)\theta \tag{A-66}$$

It will be noted that the expression for M_c in Equation (A-66) is identical to that in Equations (A-39) and (A-42) for hinged booms so that for equal values of ω_s the spinning boom frequency the equations of motion are identical. However, the expressions for ω_s are different functions of the spin rate Ω.

For comparison

$$\omega_s{}^2 \text{ cantilever} = \frac{(d+\ell)\,\Omega^2}{\ell(1-\frac{1}{\alpha\ell}\tanh\alpha\ell)} \approx \omega_B{}^2 + \frac{6}{5}\,\frac{(d+\ell)}{\ell}\Omega^2 \tag{A-67}$$

$$\omega_s^2 \text{ hinged} = \omega_B^2 + \frac{d + \ell}{\ell} \Omega^2 \qquad \text{(A-68)}$$

If $d + \ell/\ell$ hinged = $6/5\ (d + \ell)/\ell$ cantilever as for instance in a dynamic model correct tracking of ω_s with spin rate will be obtained.

Appendix B
COMPARISON WITH CANTILEVER BEAM EQUATIONS

Hinged boom vibration frequency with boom arm mass included

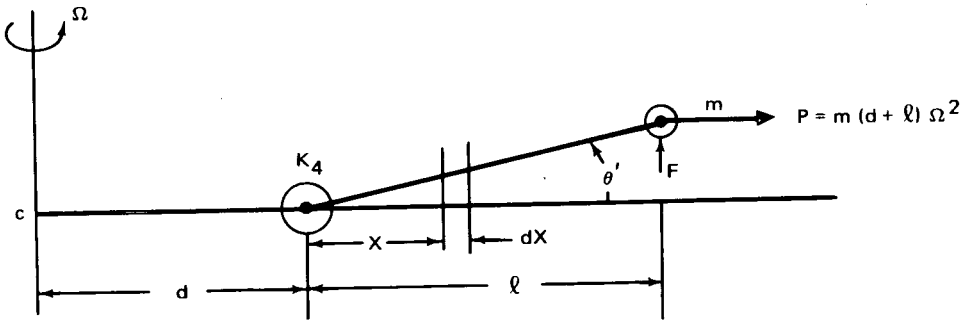

the potential and kinetic energy for a small displacement θ' are

$$2V = K_H\theta^2 + m\ell(d + \ell)\Omega^2\theta^2 + C\Omega^2\theta^2 \int_o^\ell x\,(d + x)\,dx \qquad (B\text{-}1)$$

$$2V = K_H\theta^2 + \ell\Omega^2\left[\left(m + \frac{m_B}{3}\right)(d + \ell) + \frac{m_B d}{6}\right]\theta^2 \qquad (B\text{-}2)$$

$$2T = m\left\{\left[(\ell\dot{\theta})^2 + (d + \ell)^2\Omega^2\right] + \int_o^\ell dm\left[x^2\dot{\theta}^2 + (d + x)^2\Omega^2\right]\right. \qquad (B\text{-}3)$$

where

c is the mass per unit length of the boom arm and $m_B = c\ell$ is the total mass of the boom arm

then

$$\frac{d}{dt}\left(\frac{\partial T}{\partial\dot{\theta}}\right) + \frac{\partial V}{\partial\theta} = \left(m + \frac{m_B}{3}\right)\ell^2\ddot{\theta} + \left\{K_H + \left[\left(m + \frac{m_B}{3}\right)(d + \ell) + \frac{m_B d}{6}\right]\Omega^2\ell\right\}\theta' = 0 \qquad (B\text{-}4)$$

whence

$$\omega_s^2 = \omega_B^2 + \frac{d + \ell}{\ell} \frac{\Omega^2}{R} \tag{B-5}$$

where

$$m' = m + \frac{m_B}{3} \left[\frac{3d + 2\ell}{2(d + \ell)}\right] \tag{B-6}$$

and

$$R = \frac{m + m_B/3}{m'} \tag{B-7}$$

where

$$\omega_B^2 = \frac{K_H}{\left(m + \frac{m_B}{3}\right)}$$

The moment applied to the center body about the cg is

$$M_c = F(d + \ell) - PY - C\Omega^2\theta \int_o^\ell (d + x)\, x\, dx$$

which can be put in the form

$$M_c = m' \frac{(d + \ell)^2 \ell}{d + \ell} \left[\omega_s^2 R - \Omega^2\right] \theta' \tag{B-8}$$

The object of this discussion is to demonstrate the relationship between the equations of motion and stability criteria for flexible cantilever booms and hinged booms on a rotating space station. It was shown in Appendix A that the angular equations of motion for the configuration under consideration are

$$I_1\dot{\omega}_1 + (I_3 - I_2)\Omega\omega_2 = 0 \tag{B-9}$$

$$I_2\dot{\omega}_2 + (I_1 - I_3)\Omega\omega_1 = 2\, M_c \tag{B-10}$$

$$2m\ell\,(d+\ell)\,\ddot{\theta} + 2m\,(d+\ell)^2\,\dot{\omega}_2 + 2m\,\ell(d+\ell)\,\Omega^2\theta - 2m\,(d+\ell)^2\Omega\omega_1$$

$$= -2M_c \tag{B-11}$$

where M_c is the internal connection moment between the central body and the two booms, I_1, I_2, I_3, ω_1, ω_2, Ω are the principal moments of inertia and angular velocities of the central body, m is the boom tip mass, and θ is the boom angle. It was shown that for massless hinged booms and a massless cantilever boom M_c is given by

$$M_c = m\,(d+\ell)^2\,\frac{\ell}{d+\ell}\,(\omega_s^2 - \Omega^2)\,\theta \tag{B-12}$$

and ω_s for the massless hinged boom is

$$\omega_s^2 = \omega_B^2 + \frac{(d+\ell)}{\ell}\,\Omega^2 \tag{B-13}$$

$$\omega_B^2 = \frac{K_H}{m\ell^2} \tag{B-14}$$

for the massless cantilever booms it was shown also

$$\omega_s^2 = \frac{(d+\ell)}{\ell}\,\frac{\Omega^2}{(1 - \frac{1}{\alpha\ell}\tanh\,\alpha\ell)} \tag{B-15}$$

or the approximation

$$\omega_s^2 \cong \omega_B^2 + \frac{6}{5}\,\frac{(d+\ell)}{\ell}\,\Omega^2 \tag{B-16}$$

where

$$\omega_B^2 = \frac{3\,EI}{m\ell^3} \text{ and } \alpha^2 = \frac{m(d+\ell)\,\Omega^2}{EI} \tag{B-17}$$

If the mass of the arm of the hinged boom is accounted for, it was shown that

$$M_c = m' (d + \ell)^2 \frac{\ell}{(d + \ell)} \left[\omega_s{}^2 R - \Omega^2\right] \theta' \tag{B-18}$$

and the spinning vibration frequency is

$$\omega_s{}^2 = \omega_B{}^2 + \frac{d + \ell}{\ell} \frac{\Omega^2}{R} \tag{B-19}$$

$$m' = m + \frac{m_B}{3} \left[\frac{3d + 2\ell}{2(d + \ell)}\right] \tag{B-20}$$

$$R = \frac{m + m_B/3}{m'} \tag{B-21}$$

Equation (B-11) takes a different form due to the distributed mass of the boom arms as follows;

$$\frac{dH}{dt} = \left[2m\ell (d + \ell) + 2c \int_o^\ell (d + x)\, x\, dx\right] \ddot{\theta}' + \left[2m (d + \ell)^2 + 2c \int_o^\ell (d + x)^2\, dx\right] \omega_2 + \left[2m\ell (d + \ell) + 2c \int_o^\ell (d + x)\, x\, dx\right] \Omega^2 \theta'$$

$$- \left[2m (d + \ell)^2 + 2c \int_o^\ell (d + x)^2\, dx\right] \Omega \omega_1 = -2 M_c \tag{B-22}$$

The integrals involved evaluate to

$$c \int_o^\ell (d + x)\, x\, dx = \frac{m_B}{3} \ell (d + \ell) \left[\frac{3d + 2\ell}{2(d + \ell)}\right] \tag{B-23}$$

and

$$c \int_o^\ell (d + x)^2\, dx = \frac{m_B}{3} (d + \ell)^2 \left[\frac{3d(d + \ell) + \ell^2}{(d + \ell)^2}\right] \tag{B-24}$$

The last expression is the moment of inertia of the boom arm about an axis through the center of the station (not including the tip mass).

The first and third bracketed expressions on the right-hand side of Equation (B-22) then become

$$2\ell\,(d+\ell)\left\{m + m_B/3\left[\frac{3d+2\ell}{2(d+\ell)}\right]\right\} = 2\ell\,(d+\ell)\,m' \qquad \text{(B-25)}$$

the second and fourth expressions become

$$2I_B \equiv 2m\,(d+\ell)^2 + 2\frac{m_B}{3}(d+\ell)^2\left[\frac{3d\,(d+\ell)+\ell^2}{(d+\ell)^2}\right] \qquad \text{(B-26)}$$

This last is the total moment of inertia of the boom (arm and tip mass) about an axis through the center of the station and would directly add to the total spin inertia if the booms were rigidly connected. Equation (B-22) can then be written

$$2\ell\,(d+\ell)\,m'\,\ddot{\theta}' + 2I_B\,\dot{\omega}_2 + 2\ell\,(d+\ell)\,m'\,\Omega^2\,\theta' - 2I_B\Omega\omega_1 = -2M_c \qquad \text{(B-27)}$$

with definitions

$$A = \frac{I_1 - I_3}{I_2} \quad , \quad B = \frac{I_3 - I_2}{I_1}$$

and

$$c' = 2m'\frac{(d+\ell)^2}{I_2}\left(R\omega_s^2 - \Omega^2\right) \qquad \text{(B-28)}$$

the equations of motion of a rotating space station with hinged massy booms are

$$\dot{\omega}_1 + B\Omega\omega_2 = 0 \qquad \text{(B-29)}$$

$$\dot{\omega}_2 + A\Omega\omega_1 - \frac{\ell}{d+\ell} c' \theta = 0 \tag{B-30}$$

$$\ddot{\theta}' + R\omega_s^2 \theta' + \frac{I_B}{\ell(d+\ell)m'} \dot{\omega}_2 - \frac{I_B \Omega}{\ell(d+\ell)m'} \omega_1 = 0 \tag{B-31}$$

The equations of motion of the system with cantilever booms with

$$c = 2m \frac{(d+\ell)^2}{I_2} (\omega_s^2 - \Omega^2) \tag{B-32}$$

are

$$\dot{\omega}_1 + B\Omega\omega_2 = 0 \tag{B-33}$$

$$\dot{\omega}_2 + A\Omega\omega_1 - \frac{\ell}{d+\ell} c\,\theta = 0 \tag{B-34}$$

$$\ddot{\theta} + \omega_s^2 \theta + \frac{d+\ell}{\ell} \dot{\omega}_2 - \frac{d+\ell}{\ell} \Omega\omega_1 = 0 \tag{B-35}$$

The simplest way to arrive at the characteristic equation for these systems is to differentiate the last two and use the first to eliminate $\dot{\omega}_1$. It should perhaps be noted at this point that $I_B/\ell(d+\ell)m' \cong d+\ell/\ell$ and $R \cong 1$ for the dynamic model, so that the two sets of equations have nearly equal coefficients as they stand. However to demonstrate the variations with spin rate Ω further discussion is advantageous.

Carrying out the suggested operations and inserting the associated values of ω_s, the spinning natural frequency, yields for the cantilever boom system,

$$\ddot{\omega}_2 - AB\Omega^2\omega_2 - \frac{2m\ell(d+\ell)}{I_2} \left[\omega_B^2 + (\frac{6}{5}\frac{d}{\ell} + \frac{1}{5})\Omega^2\right] \dot{\theta} = 0 \tag{B-36}$$

$$\dddot{\theta} + \left[\omega_B^2 + \frac{6}{5} \frac{(d+\ell)}{\ell} \Omega^2\right] \dot{\theta} + \frac{(d+\ell)}{\ell} \ddot{\omega}_2 + \frac{(d+\ell)}{\ell} \Omega^2 B\omega_2 = 0 \tag{B-37}$$

E

The associated determinant is

$$S^4 + (\omega_s^2 - AB\Omega^2 + c)S^2 + B\Omega^2(c - A\omega_s^2) = 0 \qquad \text{(B-38)}$$

It may be shown that for the type of spacecraft under consideration with $A < B < 1$ the requirement for stability is

$$c > A\omega_s^2 \qquad \text{(B-39)}$$

or

$$\frac{2m(d+\ell)^2}{I_1 - I_3} > \frac{\omega_s^2}{\omega_s^2 - \Omega^2} = \frac{\omega_B^2 + \frac{6}{5}\frac{(d+\ell)}{\ell}\Omega^2}{\omega_B^2 + (\frac{6}{5}\frac{d}{\ell} + \frac{1}{5})\Omega^2} \qquad \text{(B-40)}$$

for a boom geometry similar to Skylab $d = 0$ and Equations (B-36), (B-37) and inequality (B-40) become

$$\ddot{\omega}_2 - AB\Omega^2\omega_2 - \frac{2m\ell^2}{I_2}\left[\omega_B^2 + \frac{1}{5}\Omega^2\right]\theta = 0 \qquad \text{(B-41)}$$

$$\ddot{\theta} + \left[\omega_B^2 + \frac{6}{5}\Omega^2\right]\dot{\theta} + \ddot{\omega}_2 + \Omega^2 B\omega_2 = 0 \qquad \text{(B-42)}$$

$$\frac{2m\ell^2}{I_1 - I_3} > \frac{\omega_B^2 + \frac{6}{5}\Omega^2}{\omega_B^2 + \frac{1}{5}\Omega^2} \qquad \text{(B-43)}$$

For the massy hinged booms the equations corresponding to Equations (B-41) and (B-42) are

$$\ddot{\omega}_2 - AB\Omega^2\omega_2 - \frac{2m'\ell(d+\ell)}{I_2}(R\omega_B^2 + \frac{d}{\ell}\Omega^2)\dot{\theta}' \qquad \text{(B-44)}$$

$$\ddot{\theta}' + \left[R\omega_B^2 + \frac{d+\ell}{\ell}\Omega^2\right]\dot{\theta}' + \frac{I_B}{\ell(d+\ell)m'}\ddot{\omega}_2 + \frac{I_B}{\ell(d+\ell)m'}\Omega^2 B\omega_2 = 0 \qquad \text{(B-44)}$$

The corresponding characteristic equation is

$$S^4 + \left(R\omega_s^2 - AB\Omega^2 + \frac{I_B}{(d+\ell)^2 m'} C'\right) S^2 + B\Omega^2 \left[\frac{I_B}{(d+\ell)^2 m'} C' - AR\omega_s^2\right] = 0 \qquad \text{(B-45)}$$

The condition for gyroscopic stability is

$$\frac{2I_B}{I_1 - I_3} > \frac{R\omega_s^2}{R\omega_s^2 - \Omega^2} = \frac{R\omega_B^2 + \frac{d+\ell}{\ell}\Omega^2}{R\omega_B^2 + \frac{d}{\ell}\Omega^2} \qquad \text{(B-46)}$$

Comparing stability criteria Equations (B-43) and B-46), it was noted that I_B is the total moment of inertia of the hinged massy boom about an axis normal to the spin axis and therefore is directly analagous to $2m\ell^2$ of Equation (B-43).

If we choose

$$\omega'^2_B = R\omega_B^2 \text{ hinged} = \omega_B^2 \text{ cantilever} \qquad \text{(B-47)}$$

and

$$\frac{d}{\ell} = \frac{1}{5}, \quad \frac{d+\ell}{\ell} = 1 + \frac{d}{\ell} = \frac{6}{5} \qquad \text{(B-48)}$$

the stability conditions of the hinged boom model will be identical to those of a cantilever boom vehicle at all spin speeds.

The equations of motion of the massy hinged boom system Equations (B-44) and (B-45) would differ from Equations (B-41) and (B-42) of the cantilever system by the presence of the coefficients $I_B/\ell(d+\ell)m'$, in the last two terms of Equation (B-45) and a difference of the coefficient of the last term of

Equation (B-44). This condition can be corrected by making a linear transformation of the boom angle variable

$$\theta = \frac{\ell(d + \ell)m'}{I_B}\,\theta' \tag{B-49}$$

in Equations (B-44 and (B-45). Each term of Equation (B-45) will then contain the factor $I_B/\ell(d + \ell)m'$ as part of its coefficient, and can be cancelled out. Equations (B-44) and (B-45) then become

$$\ddot{\omega}_2 - AB\Omega^2\omega_2 - 2\frac{I_B}{I_2}\left[\omega'_B{}^2 + \frac{d}{\ell}\Omega^2\right]\theta \tag{B-50}$$

$$\ddot{\theta} + \left[\omega'_B{}^2 + \frac{d + \ell}{\ell}\right]\theta + \omega_2 + B\Omega^2\omega_2 = 0 \tag{B-51}$$

Thus with the appropriate choice of parameters, the coefficients of Equations (B-50) and (B-51) can be made identical to those of Equations (B-41) and (B-42). The stability criteria are unchanged by the transformation. The cantilever boom angle θ is obtained from the model boom angle θ' by means of relation (B-49).

The air bearing model parameters actually used result in the following

$$d = 0.1397 \text{ m } (0.4583 \text{ ft}),\quad \ell = 0.6604 \text{ m } (2.1667 \text{ ft})$$

$$m = 3.634 \text{ kg } (0.2491 \text{ Slugs}),\quad m_B = 0.9819 \text{ kg } (0.0673 \text{ Slugs})$$

$$m + m_B/3 = 3.9617 \text{ kg } (0.2715 \text{ Slugs})$$

$$m' = 3.9889 \text{ kg } (0.2734 \text{ Slugs})$$

$$R = \frac{m + m_B/3}{m'} = 0.9932$$

$$I_B = 2.5785 \text{ kg m}^2 \text{ } (1.9023 \text{ Slug ft}^2)$$

$$\frac{I_B}{\ell(d + \ell)m'} = 1.223 \qquad \frac{\ell(d + \ell)m'}{I_B} = 0.8177$$

$$\frac{d + \ell}{\ell} = 1.2115$$

Appendix C
SOLUTION TO EQUATIONS

The equations of free motion of the hinged boom model including the boom arm mass are;

$$\dot{\omega}_1 + B\Omega\omega_2 = 0 \tag{C-1}$$

$$\dot{\omega}_2 + A\Omega\omega_1 - \frac{2m'\ell(d+\ell)}{I_2}(R\omega_s^2 - \Omega^2)\theta = 0 \tag{C-2}$$

$$\ddot{\theta} + R\omega_s^2\,\theta + \frac{I_B}{m'\ell(d+\ell)}\dot{\omega}_2 - \frac{I_B}{m'\ell(d+\ell)}\Omega\omega_1 = 0 \tag{C-3}$$

where

$$A = \frac{I_1 - I_3}{I_2},\quad B = \frac{I_3 - I_2}{I_1},\quad m' = m + \frac{m_B}{3}\left[\frac{3d+2\ell}{2(d+\ell)}\right]$$

$$R = \frac{m + \frac{m_B}{3}}{m'},\quad \omega_s^2 = \omega_B^2 + \frac{d+\ell}{\ell}\frac{\Omega^2}{R} \tag{C-4}$$

To obtain the equations for the cantilever beam booms substitute;

$$\frac{d+\ell}{\ell} \text{ for } \frac{I_B}{m'\ell(d+\ell)},\ m \text{ for } m',\ \text{and } \omega_s^2 \text{ cantilever for } R\omega_s^2$$

where

$$\omega_s^2 \text{ cantilever} \cong \omega_B^2 + \frac{6}{5}\frac{(d+\ell)}{\ell}\Omega^2 \tag{C-5}$$

Some additional definitions are convenient.

Let

$$\frac{2I_B}{I_1 - I_3} = \overline{IM} \tag{C-6}$$

which may be called the inertia margin and

$$\frac{2I_B}{I_1 - I_3}\left(1 - \frac{\Omega^2}{R\omega_s^2}\right) = \overline{SF} \tag{C-7}$$

which may be called the stability factor, since the types of space stations under consideration ($I_1 > I_3 > I_2$), the requirement for gyroscopic stability is SF > 1.

Equation (C-2) may be solved for ω_1 and substituted in Equation (C-3) to eliminate ω_1, and Equation (C-2) may be differentiated and ω_1 substituted from Equation (C-1) to eliminate ω_1 from Equation (C-2). The resulting equations are;

$$\ddot{\theta} + R\omega_s^2 (1 - \overline{SF})\,\theta + \frac{I_2 \overline{IM}}{2m'\ell(d + \ell)}(1 + A)\,\dot{\omega}_2 = 0 \tag{C-8}$$

$$\dot{\omega}_2 - \gamma^2 \omega_2 - \frac{2m'\ell(d + \ell)}{I_2}(R\omega_s^2 - \Omega^2)\,\dot{\theta} = 0 \tag{C-9}$$

where

$$\gamma^2 = AB\Omega^2. \tag{C-10}$$

Taking the Laplace transform of Equations (C-8) and (C-9) we obtain in matrix form;

$$\begin{bmatrix} S\dfrac{I_2\, IM\,(1+A)}{2m'\ell\,(d+\ell)} & S^2 + R\omega_s^2\,(1 - SF) \\ S^2 - \gamma^2 & -\dfrac{2\,m'\ell\,(d+\ell)}{I_2}\,(R\omega_s^2 - \Omega^2)\,S \end{bmatrix} \begin{bmatrix} \omega_2\,(S) \\ \theta\,(S) \end{bmatrix}$$

$$= \begin{bmatrix} S\,\theta_o + \dot{\theta}_o + \dfrac{I_2\, IM\,(1+A)}{2\,m'\ell\,(d+\ell)}\,\omega_{2o} \\ S\,\omega_{2o} + \dot{\omega}_{2o} - \dfrac{2m'\ell\,(d+\ell)}{I_2}(R\omega_s^2 \quad \Omega^2)\,\theta_o \end{bmatrix} \qquad \text{(C-11)}$$

The terms on the right with zero subscript are initial conditions. The determinate Δ of these equations is

$$-\Delta = S^4 + S^2\left[R\omega_s^2\,(1 + \overline{SF}A) - \gamma^2\right] + R\omega_s^2\,(\overline{SF} - 1)\,\gamma^2 = 0 \qquad \text{(C-12)}$$

Equation (C-12) is quadratic in S^2 and can be written

$$-\Delta = (S^3 + a^2)(S^2 + b^2) \qquad \text{(C-13)}$$

where a^2 and b^2 are given by

$$a^2 = \frac{1}{2}\left[R\omega_s^2\,(1 + \overline{SF}A) - \gamma^2\right] - \left\{\frac{1}{4}\left[R\omega_s^2\,(1 + \overline{SF}A) - \gamma^2\right]^2 + R\omega_s^2\,(1 - \overline{SF})\,\gamma^2\right\}^{\frac{1}{2}} \qquad \text{(C-14)}$$

$$b^2 = 1/2\left[R\omega_s^2\,(1 + \overline{SF}A) - \gamma^2\right] + \left\{\frac{1}{4}\left[R\omega_s^2\,(1 + \overline{SF}A) - \gamma^2\right]^2 + R\omega_3^2\,(1 - \overline{SF})\,\gamma^2\right\}^{\frac{1}{2}} \qquad \text{(C-15)}$$

From Equation (C-14) it may be noted that in order that $a^2 > 0$ and real the requirement is for $SF > 1$, as noted earlier.

The solution to Equation (C-11) is

$$\begin{bmatrix} \omega_2(s) \\ \\ \theta(s) \end{bmatrix} = \frac{1}{\Delta} \begin{bmatrix} -s\,\dfrac{2m'\ell(d+\ell)}{I_2}(R\omega_s^2 - \Omega^2) - \left[s^2 + R\omega_s^2(1 - \bar{s}F)\right] & \\ \\ -(s^2 - \gamma^2) & \dfrac{S\,I_2\overline{IM}(1+A)}{2m'\ell(d+\ell)} \end{bmatrix}$$

$$\cdot \begin{bmatrix} s\theta_o + \dot{\theta}_o + \dfrac{I_2\overline{IM}(1+A)}{2m'\ell(d+\ell)}\,\omega_{2o} \\ \\ s\omega_{2o} + \dot{\omega}_{2o} - \dfrac{2m'\ell(d+\ell)}{I_2}(R\omega_s^2 - \Omega^2)\,\theta_o \end{bmatrix} \qquad \text{(C-16)}$$

With initial conditions $\theta_o = \dot{\theta}_o = \omega_{2o} = 0 \qquad \omega_{1o} = \omega_1(t = 0)$ (C-17)

From Equation (C-2), $\dot{\omega}_{2o} = -A\Omega\omega_{1o}$. Inserting in Equation (C-16) yields

$$\omega_2(s) = \frac{-\left[s^2 + R\omega_s^2(1 - \bar{s}F)\right]}{-(s^2 + a^2)(s^2 + b^2)}\dot{\omega}_{2o} = \frac{\left[s^2 + R\omega_s^2(1 - \bar{s}F)\right]A\Omega\omega_{1o}}{-(s^2 + a^2)(s^2 + b^2)} \qquad \text{(C-18)}$$

$$\theta(s) = \frac{s\dot{\omega}_{2o}}{(s^2 + a^2)(s^2 + b^2)}\,\frac{I_2\overline{IM}(1+A)}{2m'\ell(d+\ell)}$$

$$= + \frac{2I_b(1+A)\Omega\ s\omega_{1o}}{2m'\ell(d+\ell)\ (s^2 + a^2)(s^2 + b^2)} \qquad \text{(C-19)}$$

With the aid of the transform pair,

$$\mathcal{L}^{-1}\left\{\frac{s}{(s^2 + a^2)(s^2 + b^2)}\right\} = \frac{\cos at - \cos bt}{b^2 - a^2}\ , \qquad \text{(C-20)}$$

the time solution to Equation (C-19) is,

$$\theta(t) = \frac{I_B(1+A)\Omega\omega_{1o}}{m'\ell(d+\ell)(b^2 - a^2)}\,(\cos at - \cos bt) \qquad \text{(C-21)}$$

Equation (C-18) may be written

$$\omega_2(s) = \frac{\left[S^2 + R\omega_s{}^2 (1 - \overline{SF})\right] AB\Omega^2 \omega_{10}}{-(S^2 + a^2)(S^2 + b^2) B\Omega} . \tag{C-22}$$

Since $AB\Omega^2 = \gamma^2$ and $a^2b^2 = R\omega_s{}^2 (1 - SF)\gamma^2$ (C-23)

Equation (C-22) becomes

$$\omega_2(s) = \frac{(S^2\gamma^2 + a^2b^2)}{-(S^2 + a^2)(S^2 + b^2)} \quad \frac{\omega_{10}}{B\Omega} . \tag{C-24}$$

with transform pairs

$$\mathscr{L}^{-1}\left\{\frac{S^2}{(S^2 + a^2)(S^2 + b^2)}\right\} = -\frac{a \sin at + b \sin bt}{b^2 - a^2} \tag{C-25}$$

and

$$\mathscr{L}^{-1}\left\{\frac{1}{(S^2 + a^2)(S^2 + b^2)}\right\} = \frac{1}{b^2 - a^2}\left(\frac{1}{a} \sin at - \frac{1}{b} \sin bt\right) \tag{C-26}$$

the time solution to Equation (C-24) is

$$\omega_2(t) = \frac{\omega_{10}}{B\Omega (b^2 - a^2)}\left[a(\gamma^2 - b^2) \sin at + b(a^2 - \gamma^2) \sin bt\right] \tag{C-27}$$

With initial conditions $\theta_o = \theta_o = \omega_{10} = o$, $\omega_{20} = \omega_2(t = o)$

We obtain from Equation (C-16)

$$\omega_2(s) = \frac{S R\omega_s{}^2 \overline{SF} (1 + A) \omega_{20}}{(S^2 + a^2)(S^2 + b^2)} + \frac{S\left[S^2 + R\omega_s{}^2 (1 - \overline{SF})\right]\omega_{20}}{(S^2 + a^2)(S^2 + b^2)} \tag{C-28}$$

or

$$\omega_2(s) = \frac{S\left[R\omega_s^2 (1 + \overline{SF}A)\right] \omega_{20} + S^3\omega_{20}}{(S^2 + a^2)(S^2 + b^2)} \qquad (C-29)$$

since $a^2 + b^2 = R\omega_s^2 (1 + \overline{SF}A) - \gamma^2$ the time solution is

$$\omega_2(t) = \frac{\omega_{20}}{b^2 - a^2}\left[(b^2 + \gamma^2)\cos at - (a^2 + \gamma^2)\cos bt\right] \qquad (C-30)$$

The solution for initial conditions on both ω_1 and ω_2 is obtained by adding Equations (C-27) and (C-30) (superposition).

The transform of the boom angle θ to an initial condition on ω_2 only is given by Equation (A-16) as,

$$\theta(s) = -\frac{I_B (1 + A) B\Omega^2 \omega_{20}}{m'\ell(d + \ell)(S^2 + a^2)(S^2 + b^2)} \qquad (C-31)$$

with time solution,

$$\theta(t) = -\frac{I_B(1 + A) B\Omega^2 \omega_{20}}{m'\ell(d + \ell)(b^2 - a^2)} (\cos at - \cos bt) \qquad (C-32)$$

Equation (C-32) may be combined with Equation (C-21) to give the response to initial conditions on both ω_1 and ω_2.

$$\theta(t) = \frac{I_B(1 + A)\Omega}{m'\ell(d+\ell)(b^2 - a^2)} (\omega_{10} - B\Omega\omega_{20}) (\cos at - \cos bt) \qquad (C-33)$$

From Equation (C-1)

$$\omega_1(t) = \omega_{10} - B\Omega \int_o^t \omega_2(\tau)\, d\tau \qquad (C-34)$$

Inserting Equations (C-27) and (C-30) in Equation (C-34) and performing the indicated operations yields

$$\omega_1(t) = \frac{\omega_{10}}{b^2 - a^2}\left[(\gamma^2 - b^2)\cos at + (a^2 - \gamma^2)\cos bt\right]$$

$$-\frac{\omega_{20}\, B\Omega}{b^2 - a^2}\left[\left(\frac{b^2 + \gamma^2}{a}\right)\sin at - \left(\frac{a^2 + \gamma^2}{b}\right)\sin bt\right] \qquad \text{(C-35)}$$